

Pulse Dipolar Electron Spin Resonance: Distance Measurements

Peter P. Borbat and Jack H. Freed

Abstract In recent years electron spin resonance (ESR) has provided the means to obtain structural constraints in the field of structural biology on the nanoscale by measuring distances between paramagnetic species, which usually have been nitroxide spin-labels. These ESR methods enable the measurement of distances over the wide range from ca. 6–10 Å to nearly 90 Å. While cw methods may be used for the shortest distances, it is the pulse methods that enable this wide range, as well as determination of the distributions in distance. In this chapter we first describe the underlying theoretical concepts for understanding the principal pulse methods of double quantum coherence (DQC)-ESR and double-electron–electron-resonance (DEER), which we collectively refer to as Pulse-Dipolar ESR Spectroscopies (PDS). We then provide technical aspects of pulse ESR spectrometers required for high quality PDS studies. This is followed by an extensive description of sensitivity considerations in PDS, based largely upon our highly sensitive 17.3 GHz pulse spectrometer at ACERT. This description also includes a comparison of the effectiveness of the respective PDS pulse methods. In addition, the newer methods of 5-pulse DEER, which enables longer distances to be measured than by standard DEER, and 2D-DQC, which provides a convenient mapping for studying orientational coherence between spin labels and their interspin vector, are described.

Keywords ESR · PDS · DQC · DEER · Dipole-dipole · PELDOR · Spin-label

Contents

- 1 Introduction
- 2 Distance Measurements by ESR
 - 2.1 General Aspects, Electron Spin Dipolar Coupling
 - 2.2 cw ESR Method and Its Range

P.P. Borbat and J.H. Freed (✉)
Department of Chemistry and Chemical Biology, ACERT National Biomedical Center for
Advanced ESR Technology, Cornell University, Ithaca, NY 14853-1301, USA

- 2.3 Pulse Methods
- 2.4 Relaxation
- 2.5 Distance Ranges
- 2.6 Distance Distributions and Extracting Distance Information
- 2.7 Orientational Effects in PDS
- 2.8 Multi-spin Effects
- 3 Technical Aspects
 - 3.1 Spectrometers
- 4 Sensitivity Considerations
 - 4.1 Sensitivity in PDS Experiment
 - 4.2 Short Distances, Low Concentrations
 - 4.3 Long Distances
 - 4.4 Distances in the Optimal PDS Range
 - 4.5 Examples
- 5 Newer Aspects
 - 5.1 5-Pulse DEER
 - 5.2 More on Sensitivity: Method Comparison
 - 5.3 2D-DQC: Orientations
 - 5.4 Multifrequency
- 6 Summary and Perspectives
- Appendix
- Signals in 3,4,5-Pulse DEER Sequences
- References

Abbreviations

cw	Continuous-wave
DEER	Double electron–electron resonance
DQ, DQC	Double-quantum, double-quantum coherence
DQF	Double-quantum filtering
ESEEM	Electron spin-echo envelope modulation
ESR	Electron spin resonance
FID	Free induction decay
hf	Hyperfine
log	Natural logarithm
MEM	Maximum entropy method
MTSSL	Methane-thiosulfonate spin-label
mw	Microwave
PDS	Pulsed dipolar spectroscopy
PELDOR	Pulsed electron–electron double resonance
RPE	Refocused primary echo
SNR	Signal-to-noise ratio
SQ, SQC	Single-quantum, single-quantum coherence
SSPA	Solid-state power amplifier
TWTA	Traveling-wave tube amplifier

1 Introduction

Applications of pulse and continuous-wave (cw) electron spin resonance (ESR) in the field over the last decade [1–15] even surpass the more traditional study of molecular dynamics [16–19]. ESR has provided the means to obtain structural constraints on the nanoscale by measuring distances between paramagnetic species, which usually have been nitroxide spin-labels. Both, cw [8, 9] and pulsed [1–3, 5–7, 10–15, 20] ESR, have been useful in this regard. However, pulsed ESR methods are not limited to just nitroxides; all possible combinations amongst nitroxides, radical cofactors, and transition metal ions have been investigated [10, 21–28]. Taken together, cw and pulsed ESR enable the measurement of distances over the wide range from ca. 6–10 Å to nearly 90 Å, with only the shorter range of ESR-measurable distances readily accessible to cw ESR.

Distance measurement by pulsed double electron–electron resonance (DEER, also referred to as PELDOR) [29–32] was introduced as an alternative for isolating weak electron–electron dipolar couplings from electron-spin-echo decays, which are usually dominated by relaxation and nuclear modulation effects [33, 34]. Since then several other pulsed methods of distance measurements were introduced [15, 35–38] and most notable is double-quantum coherence ESR (DQC ESR or DQC for short) [15, 35]. Applications of the mainstream pulse methods of DEER and DQC to structural problems in biology have been growing rapidly over the past few years [2, 5, 11, 12, 39–42]; consequently, in this chapter the focus is on them. At ACERT, we intensively apply and actively develop all aspects for both methods. Therefore, we refer to them collectively as pulse dipolar ESR spectroscopy (PDS), since the inclusion of the term “dipolar” makes clear their function and removes any ambiguity with respect to classic ELDOR [43–45]. Continuing progress has been made over the last decade in new and improved pulse ESR methods and instrumentation. This includes the development of pulse spectrometers at several working frequencies [46–50]; resonators [51–57]; new pulse sequences [15, 36, 58–61]; methods of data analysis and structure modeling [1, 62–71]; and expanding the application base.

Even though, as we will demonstrate, our pulse spectrometers at ACERT have achieved high sensitivity permitting one to record very high quality data on samples with biomolecular concentrations in the low micromolar range, this is still insufficient to satisfy the ever-growing demand of related biomedical research. At ACERT this includes multiple collaborations and in-house research. The Center spectrometers, having been in continuous operation for several years, have provided measurements on several thousand samples, but the demand for measurements is increasing. This is caused largely by the rapidly growing interest in the distance information that PDS can uniquely provide, but also by the extensive progress made by biotechnology, which has greatly improved such aspects of biochemical engineering as protein expression and purification, enabling the production and spin labeling of mutated protein variants in large numbers. However, it is clear that in order to continue to attend to the needs of this rapidly expanding field, it will be primarily necessary to achieve greater sensitivity and higher throughput than modern state-of-the-art pulse

spectrometers can provide. This motivates new instrumentation developments and improvements to the existing methods. We show in this chapter examples directed to this goal.

There are several earlier reviews outlining the methods for distance measurements by ESR [17, 18, 30, 72–76]; however, we include in this chapter some background material and emphasize the methodology and the latest developments through examples taken from our laboratory.

2 Distance Measurements by ESR

In the following subsections we provide the background for PDS methods in general, starting with the descriptions of DEER (or PELDOR) and DQC for the ideal two-spin system. Then we will comment on additional essential aspects, such as relaxation, multi-spin systems, intermolecular effects, distance range and distributions, data processing, and orientations.

2.1 General Aspects, Electron Spin Dipolar Coupling

The ESR distance measurements described in this chapter are all conducted in low-temperature frozen solutions, typically using nitroxide spin labels. At the heart of the method is measuring the static dipole–dipole coupling between the spins of unpaired electrons localized in the case of nitroxides on the p - π orbitals of the NO groups.

The magnetic moments $\mathbf{m}_{1,2}$ of two electron spins 1 and 2, separated by the distance $r = |\mathbf{r}_{12}|$, interact through space via the electron spin dipole–dipole interaction

$$H_{\text{dd}} = \frac{1}{r^3} (\mathbf{m}_1 \cdot \mathbf{m}_2 - 3(\mathbf{m}_1 \cdot \mathbf{n}_{12})(\mathbf{m}_2 \cdot \mathbf{n}_{12})) \quad (1)$$

where $\mathbf{n}_{12} \equiv \mathbf{r}_{12}/r$. In a formal description, the electron spin magnetic moment \mathbf{m}_i is given by $\mathbf{m}_i = \gamma_e \hbar \mathbf{S}_i$ with γ_e the gyromagnetic ratio of an electron spin and \mathbf{S}_i the electron spin operator for the i th spin. Equation (1) for H_{dd} thus may be expressed (in angular frequency units) as:

$$H_{\text{dd}} \cong a(S_{1z}S_{2z} - \frac{1}{4}(S_{1+}S_{2-} + S_{1-}S_{2+})) \quad (2)$$

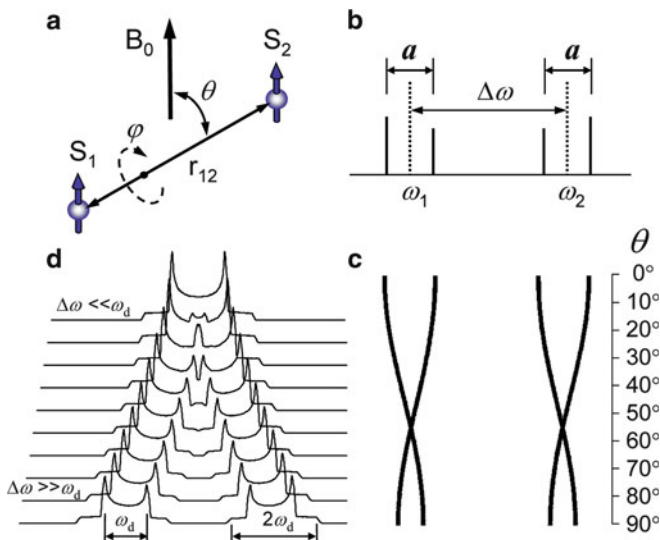


Fig. 1 (a) A pair of electron spins S_1 and S_2 coupled via the electron spin dipole–dipole interaction. Vector \mathbf{r}_{12} connecting the spins is directed along the z -axis in the molecular frame of reference. In this molecular frame the direction of the external magnetic field \mathbf{B}_0 is determined by Euler angles $\boldsymbol{\eta} = (0, \theta, \varphi)$. (b) Dipolar coupling $a = \omega_d(1 - 3 \cos^2 \theta)$ splits the spectrum of two electron spins resonating at ω_1 and ω_2 into doublets. (c) Angular dependence, $a(\theta)$, is shown as a roadmap. (d) In isotropic medium the lineshape, resulting from electron dipolar coupling and in the limit of weak coupling case ($\Delta\omega \equiv |\omega_1 - \omega_2| \ll \omega_d$) is the Pake doublet with the prominent splitting of ω_d . As $\Delta\omega$ decreases the lineshape becomes more complicated as the two spectra merge into a single spectrum at $\Delta\omega \cong \omega_d$, and finally in the limit of like spins for sufficiently strong coupling, $\Delta\omega \ll \omega_d$, the spectrum is again a Pake doublet with the splitting $3\omega_d/2$

Here the dependence on \mathbf{r}_{12} of the electron dipolar coupling, a , is given by

$$a(r, \theta) = \omega_d(1 - 3 \cos^2 \theta) \quad (3)$$

with

$$\omega_d \equiv 2\pi\nu_d = \gamma_e^2 \hbar / r^3 \quad (4)$$

We will call ω_d the “dipolar frequency” (ν_d is in Hz). In Eq. (3) the angle θ is between the direction of the external magnetic field \mathbf{B}_0 and \mathbf{r}_{12} as shown in Fig. 1a. Equation (2), limited to A (secular) and B (pseudosecular) terms of the “dipolar alphabet,” is valid in high magnetic fields, where the non-secular terms C to F (not shown) are unimportant [77]. The term in $S_{1z}S_{2z}$ in Eq. (2) is known as the secular term, and that in $S_{1\pm}S_{2\pm}$ the pseudosecular term.

One usually uses the point dipole approximation in employing Eq. (2), i.e., the electron spins are far enough apart that their distributions (in, e.g., nitroxide p - π orbitals) are unimportant, i.e., $r > 5 \text{ \AA}$ for nitroxides. An asymmetry parameter

may be necessary in the case of delocalized spin density, e.g., for closely situated spatially confined tyrosyl radicals, giving rise to a slightly rhombic spectral shape [78]. If in the absence of the dipolar coupling of Eq. (2), the two electron spins have resonance frequencies ω_1 and ω_2 , then, the case of unlike spins may be stated as $\omega_d \ll \Delta\omega$, where $\Delta\omega \equiv |\omega_1 - \omega_2|$. In this case, the resonant frequency of each spin is split into a doublet separated by $|\omega_d|$, as shown in Fig. 1b arising just from the secular term. The precise value of a thus depends on the angle θ , yielding a range of values of a from $-2\omega_d$ to $+\omega_d$. The dipolar spectrum from the PDS experiment provides this splitting, which in Fig. 1c is plotted for each doublet as a function of the angle θ .

The case of unlike spins requires considering only the secular term in Eq. (2) and dropping the pseudosecular term. In the opposite case of like spins, that is, $\omega_d \gg \Delta\omega$ then the pseudosecular term becomes important and the rhs of Eq. (4) becomes $3\gamma_e^2\hbar/2r^3$. Otherwise the results are equivalent. The intermediate case of $\omega_d \cong \Delta\omega$ is more complex. As $\Delta\omega$ decreases, the two spectra at $\Delta\omega \cong \omega_d$ start to fuse into a single spectrum (cf. Fig. 1d), whose shape is obtained by careful simulation using Eq. (2) including both secular and pseudosecular terms. In the case of nitroxide spin labels, the two nitroxide spins in a given molecule usually have their ω_1 and ω_2 substantially different. This arises from their different orientations with respect to the \mathbf{B}_0 field, so their effective hyperfine (hf) and g values (arising from their hf and g tensors) are typically different. In the centimeter range of ESR frequencies (9–17 GHz) and above this means that for nitroxide spins the unlike spin limit is reached for ca. 20 Å.

In a typical case of an isotropic frozen sample, one observes an average over θ , which contains the whole range of splitting, giving rise to a distinct dipolar spectrum, known as a Pake doublet [79], as depicted in Fig. 1d (top). For weak coupling it shows a prominent splitting of ω_d , corresponding to $\theta = 90^\circ$, and another splitting of $2\omega_d$, corresponding to $\theta = 0^\circ$ (Fig. 1d, bottom). As we can see, even when the two electron spins (e.g., of nitroxides) in a given bilabeled molecule resonate at two different frequencies, because of different orientations and/or nuclear magnetic quantum numbers, they still yield a single lineshape (Pake doublet), resulting from their common dipolar interaction. Assuming one knows the correct limit (i.e., of weak or strong coupling), the distance r is then immediately and accurately obtained from a measurement of ω_d . We do not illustrate in the figure the effects of electron exchange J for the following reason. In the case of weak dipolar coupling, J is typically too small and can produce only a small inward or outward shift of the Pake doublet branches, with an overall shape change that is difficult to assign to a finite J . When J becomes large enough to be measured, ω_d is in the range of strong coupling and the whole coupling spectrum becomes complex, especially because ω_d and J are usually distributed.

In cases when ω_d is sufficiently large, it can be determined directly from the static broadening of the nitroxide cw ESR (or FT ESR) spectrum [9], but this is also likely to fall into the regime where pseudo-secular terms are significant requiring careful spectral simulation. As a rule, in cw ESR the dipolar couplings have a small

effect on the spectrum and are masked by much larger broadenings caused by magnetic tensor anisotropy. Smaller couplings ω_d necessitate using pulse ESR methods, as we discuss below. The use of spin echoes in the pulse experiment cancels the effects of hyperfine and g -tensor interactions, but not of the dipolar tensor interaction, which produces a distinct temporal evolution of the spin echo, from which this contribution to the lineshape can be reconstructed. Thus, in all cases, accurate values of distances are produced from the measured dipolar couplings.

2.2 *cw ESR Method and Its Range*

Cw ESR has been most often applied to nitroxides, whose powder spectra are dominated by the (inhomogeneous) broadenings from nitrogen hf and g -tensors, and unresolved proton superhyperfine couplings. One has to extract what usually is a small broadening effect from ω_d to the nitroxide powder spectra, which is usually accomplished by spectral deconvolution [80] or a multiple-parameter fit [9, 81]. When the ω_d is large and the molecule has a rigid structure, fitting cw ESR spectra can provide such useful details of molecular geometry as nitroxide orientations in addition to distances [9, 81].

As the distance increases and dipolar broadening is no longer large, measuring ω_d from cw ESR spectrum broadening may require referencing with the spectra from singly labeled species to approximate background intermolecular dipolar broadening. This presents a complication and is not always an option. Incomplete spin labeling makes the task more complex [82]. Only for distances less than 15 Å, does the dipolar coupling compete with other inhomogeneous spectral broadenings and thus can be reliably inferred from cw ESR spectra. If spectral deconvolution is used, then it should be decided which limit (i.e., of weak or strong coupling) to use. The worst case error, however, is only $(3/2)^{1/3}$, i.e., ~ 2 Å for $r < 15$ Å, if the incorrect limit is assumed. When one is not sure, taking as the mean $\omega_d \cong (5/4)\gamma_c^2 \hbar^2 / r^3$ will result in a maximum error in r of ~ 1 Å.

The case of strong dipolar coupling has been extensively utilized in cw ESR both in establishing proximity and in providing quantitative distances [4, 8, 9, 80, 81, 83–85]. Cw ESR is practical for short distances of about 8 Å up to a maximum of approximately 15–20 Å, with the values for distances under 15 Å being more reliable [86]. Distances in the range of 15–20 Å can be measured, but this usually requires good referencing as well as the spin concentration closer to the millimolar range.

Since pulse techniques have progressed to the state where they give reliable distances over a much wider distance range, with the measurements conducted routinely on just tens of micromolar of protein (or even less at ACERT, see below), the focus has shifted almost entirely to pulse techniques [72–76]. In the case of a broad spectrum, such as is encountered for two Cu^{2+} ions, measuring distances by cw ESR is not feasible unless the ions are very close, but there is no such serious problem for PDS [87]. Ku band DEER and especially DQC ESR, for example, were successful with Cu^{2+} – Cu^{2+} pairs even for distances in the range of 30–50 Å (ACERT, unpublished).

2.3 Pulse Methods

Pulse ESR conducted on solids is based on detecting a spin-echo, wherein the inhomogeneous spectral broadening is canceled out [88]. Spin echo temporal evolution is governed by the weaker effects of spin relaxation, electron–electron spin dipolar and exchange couplings, and (pseudo-secular) electron-nuclear hyperfine and nuclear quadrupole couplings [89–92]. The electron dipolar and exchange couplings can be isolated from the others by means of a suitable pulse sequence. Several pulse sequences were designed to obtain the dipolar coupling: PELDOR or 3-pulse DEER, 4-pulse DEER, single-frequency techniques such as “2+1” [38] and several others [36], methods based on relaxation [37], and DQC [35]. Of these, only 4-pulse DEER and DQC are used often, and the reasons for this will be explained in this chapter. These pulse sequences, to a varying extent, also help to alleviate the problem caused by the presence of single-labeled molecules. Their direct signal is filtered out in DQC, but they do contribute to the background intermolecular dipolar signal, which is best suppressed by working at low concentrations in DQC, but cannot be avoided in single-frequency techniques and DEER. These methods of PDS are routinely used for distances longer than 15 Å [5, 12, 14, 42, 58, 73], and in DQC it works well down to ~10 Å [11] (cf. Sect. 4.2), thereby overlapping significantly with the cw ESR range. However, it is much less affected by inefficient labeling, operates in the low micromolar range, and can readily yield distance distributions!

2.3.1 Theoretical Background

Most known pulse ESR methods conducted on solids are based on detecting the spin echo signal. The significant outcome of a PDS experiment is the modulation, by the electron-spin dipolar coupling, of the spin-echo amplitude as the pulse sequence is stepped out. In this respect, it belongs to the general class of ESEEM experiments [89–92], wherein the pulse sequence is stepped out and a series of spin echoes is acquired in order to obtain the echo modulation, from which weak electron spin interactions with surrounding nuclei or electrons can be inferred. A suitable pulse sequence is applied to the spin system initially in thermal equilibrium, and its associated density matrix evolves under the action of propagators describing the effects of the microwave pulses, interspersed with free evolution periods. Finally, the relevant part of the density matrix associated with the transverse magnetization is selected by using phase cycling to remove the undesired or irrelevant contributions to the spin-echo signal. The density matrix in thermal equilibrium contains only diagonal elements, representing just the populations of the energy levels. The microwave pulses yield off-diagonal density-matrix elements (coherences) with characteristic phases. One can theoretically manipulate these coherences using a series of pulse and free evolution propagators to generate the echo of interest. Stepping out the pulses in their proper sequence produces the time-domain signal

record, whose shape is determined in part or entirely by the electron-spin dipolar coupling. The relevant part of the signal, depending on just the encoded dipolar coupling, is then separated from the rest of the signal and processed into the dipolar spectrum (e.g., Pake doublet). Then the distance information may be inferred, or else it may be used as input into distance reconstruction software. Understanding how this modulation is generated and controlled is thus essential for optimizing and further developing PDS. We give a relatively simple introduction. We will employ the density matrix and spin operator formalisms, which can be applied in different ways depending on the objectives.

The initial density operator in thermal equilibrium, ρ_0 for two electron spins $\mathbf{S}_{1,2}$, is described by the static spin-Hamiltonian \hat{H}_0 as:

$$\rho_0 = \frac{\exp(-\hat{H}_0/kT)}{\text{Tr}[\exp(-\hat{H}_0/kT)]} \propto \hat{S}_{1z} + \hat{S}_{2z}, \quad (5)$$

where the z -axis is defined to coincide with the direction of the external magnetic field, and the subscripts refer to the two interacting spins. First-order expansion of Eq. (5) is appropriate for nitroxide spin labels down to liquid helium temperatures for working frequency up to Ka-band. The time evolution of the spin density operator ρ is governed by the Liouville–von Neumann equation.

$$\frac{d\rho}{dt} = -\frac{i}{\hbar} H^\times \rho(t) - \Gamma(\rho(t) - \rho(0)) \quad (6)$$

Here, $H^\times \rho \equiv [\hat{H}, \rho]$ with ρ being the density matrix, \hbar is Plank's constant divided by 2π , Γ is the relaxation superoperator, $i^2 = -1$. In frozen solutions, when dynamic processes are characterized by correlation times τ_c long enough that $\omega_d \tau_c \gg 1$ it is appropriate to introduce relaxation phenomenologically. However, it should be noted that dynamic processes such as caused by a local acyl group and collective dynamics or molecular libration do persist down to liquid helium temperatures and do require careful treatment using Eq. (6). For the purpose of this section we factor out relaxation by dropping the relaxation superoperator (but see Sect. 2.4 where it is discussed). Leaving out the relaxation, the density matrix evolves, under the action of \hat{H} as:

$$\frac{d\rho}{dt} = -\frac{i}{\hbar} [\hat{H}(t), \rho(t)] \quad (7)$$

Thus after a period of time Δt for a time-independent \hat{H} , the density matrix $\rho(t)$ becomes:

$$\rho(t + \Delta t) = e^{-(i\hat{H}\Delta t/\hbar)} \rho(t) e^{i\hat{H}\Delta t/\hbar} \quad (8a)$$

Or by introducing superoperator notation

$$U\rho(t)\xrightarrow{\hat{H}(\Delta t)}\rho(t+\Delta t) \quad (8b)$$

The superoperator $U(\Delta t) = \exp(-iH\times\Delta t/\hbar)$ is unitary, implying time-reversal. It can correspond to free-evolution or to pulse excitation. The level of rigor with which Eq. (8a) is treated depends on the particular objective. In general, for an accurate description, Eq. (8b) requires numerical treatment. An example of a numerical implementation to compute the DQC ESR signal carried out in Hilbert space using a series of transformations of Eq. (8a) was described in [93] but is not discussed in this Chapter, thus limiting this subject to a more basic discussion based on the concept of coherences and spin operator techniques.

2.3.2 Coherences

A pulse ESR experiment is essentially based on creation and manipulation of electron-spin (and nuclear-spin) coherences. It is the time evolution of electron-spin coherences under the action of the electron–electron spin dipolar interaction that makes it possible to determine this coupling and then to infer the distance.

We already stated that for a quantum system in thermal equilibrium, only the diagonal density matrix elements are nonzero and they represent the populations of the corresponding energy levels. The absence of off-diagonal elements corresponds to the fundamental assumption of having random phases between any two states of the quantum system at thermal equilibrium. The diagonal elements are automatically independent of the spin phases. In modern parlance, these elements have a coherence order of 0. However, away from equilibrium a correlation between pairs of eigenstates may exist. For example, so-called dipolar order wherein the density matrix is (partially) represented by the operator $2S_{1z}S_{2z}$ connecting the two spins does not require any change in net population of these levels. Off-diagonal density matrix elements such as $S_{\pm}, S_{1\pm}S_{2z}$ have distinct phases, corresponding to a coherent superposition of eigenstates and therefore must vanish as the system approaches its equilibrium.

Finite off-diagonal elements of the density matrix with their distinct phases are often referred to as coherences. They can be produced by a coherent perturbation, such as a resonant mw pulse. The action of the pulse on an electron spin yields a coherent superposition between the states involved in the transition, represented by S_{\pm} in the operator expansion of the density matrix, which will persist until the system returns to thermal equilibrium. In magnetic resonance these are single spin ± 1 coherences which are the only coherences that are experimentally detectable. Any density operator ρ can be decomposed into a sum of operator components ρ_p . Each such operator component is associated with a coherence order, p ; i.e., under rotation about the z -axis it transforms as $\exp(i\varphi\hat{F}_z)\rho_p \exp(-i\varphi\hat{F}_z) = \rho_p \exp(ip\varphi)$, where $\hat{F}_z = \sum_k S_{kz}$ is the z -component of the total spin angular momentum.

As noted above, single-quantum coherences $S_{1\pm}$ correspond to an observable signal. All other coherences of order one and higher cannot be observed, since average transverse magnetization in such cases is always zero. For example, products such as $2S_{1+}S_{2z}$, $S_{1+}S_{2+}S_{3-}$ have coherence order +1 but they do not correspond to detectable signals. In particular, anti-phase coherence, $2S_{1+}S_{2z}$, involving two spins, with coherence order 1, does not correspond to a detectable signal. Higher order coherence has all spins in a fixed phase relationship with other spins leading to zero net magnetization. For example, a $2S_{1x}S_{2y}$ term describes second order coherence of the two spins, with spins at an angle of 90° in the rotating x,y -plane, pointing either along x and y or $-x$ and $-y$ to the same extent.

Even though anti-phase or multi-quantum coherences cannot be directly observed, they do form and can be detected indirectly. Both in-phase and anti-phase single-quantum coherences (SQC) and double-quantum coherences are very useful in describing the PDS experiment. Multiple-quantum transitions and coherences in general have been treated in detail in numerous studies in the field of NMR (see for example the following [94–97]). Here, we outline the basic concepts and definitions in a way that is appropriate for the PDS experiment.

2.3.3 Single-Quantum Coherences

Let us consider a system of two coupled spins of $1/2$. In Fig. 2 we have four allowed single-quantum transitions. These transitions are associated with the corresponding off-diagonal elements of the density matrix for the two spins defined in the product space $|m_1, m_2\rangle$.

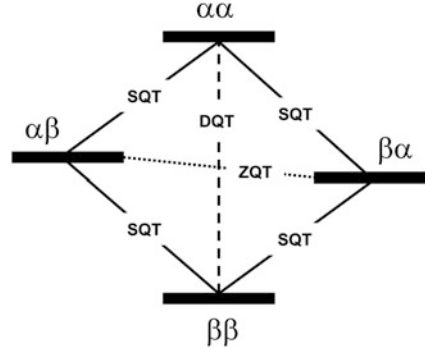
As noted above, one can conveniently express the density matrix as the expansion in a complete set of the spin operators, e.g., the density matrix for a single spin $S = 1/2$ is given as a linear combination of the Pauli spin matrices and the unit operator; for many-spin systems one may take the direct product.

Then the coherences can be conveniently expressed by the spin operators corresponding to the elements of the density matrix for two spins. Single quantum coherences are represented by the presence of spin operators $S_{1+}S_{2\alpha}$, $S_{1+}S_{2\beta}$, $S_{1-}S_{2\alpha}$, $S_{1-}S_{2\beta}$ constructed as an outer product in the operator expansion of the density matrix, as well as those obtained by permuting the spins 1 and 2 for a total of eight. Here, $S_{k\alpha} \equiv E_k/2 + S_{kz}$, $S_{k\beta} \equiv E_k/2 - S_{kz}$ and E_k is the 2×2 unit operator for the k th spin. We can rewrite these eight operators, which clearly imply single quantum transitions, which we call the single-quantum coherences (SQC), of which four are “in-phase” coherences, which have the form:

$$S_{1\pm}(S_{2\alpha} + S_{2\beta}) = S_{1\pm}E_2, (S_{1\alpha} + S_{1\beta})S_{2\pm} = E_1S_{2\pm} \quad (9)$$

Their existence in the density matrix expansion corresponds to the observable transverse magnetization with all spins having the same phase. The states of the two spins are distinct and not mixed. The other four SQC are the “anti-phase”

Fig. 2 Energy level diagram for the two-spin system showing single (SQT), double (DQT), and zero (ZQT) quantum transitions. The last two correspond respectively to simultaneous flip or flip-flop of the two spins. If the pulse acts only on one of the spins, DQT and ZQT are forbidden



coherences which cannot be directly detected. These correspond to coherent superposition among the four states of the two spins and they have the form:

$$S_{1\pm}(S_{2z} - S_{2\beta}) = 2S_{1\pm}S_{2z} \quad (10)$$

and the other two obtained by permuting the spins 1 and 2.

The anti-phase SQC can evolve into an observable in-phase SQC and back. The interconversion of these coherences can occur only due to spin coupling, e.g., it is caused by the dipolar part of the spin-Hamiltonian, and the interconversion rate depends on the strength of coupling. This property is used to produce modulation of the detected spin-echo signal. As anti-phase and in-phase coherences evolve, they can be manipulated by applying coherent pulses acting on one or both of the spins, e.g., refocusing them or changing the sense of interconversion. Note that independent of whether a coherence is detectable or not, if its coherence order is ± 1 , it can be refocused. This constitutes the basic idea of Pulse Dipolar ESR represented by the different flavors of PDS. This approach permits a relatively simple qualitative description of DEER pulse sequences (cf. Appendix).

We now show with a simple example of two electron spins in the weak coupling regime (cf. Fig. 1) how the evolution of SQC generates dipolar signals. That is in the next subsection we first show how we can derive the expressions for the dipolar signal in DQC and then we discuss DEER.

2.3.4 Double-Quantum Coherence

The double- and zero-quantum coherences (DQC and ZQC, respectively) are associated with the remaining two transitions in Fig. 2. DQC and ZQC correspond to transitions with simultaneous flips or flip-flops of both spins, respectively, and

are located on the anti-diagonal of the density matrix. DQC can be represented by terms in the operator expansion of the density matrix as follows¹ [94, 96]:

$$\begin{aligned} 2DQ_x &= S_{1-}S_{2-} + S_{1+}S_{2+} = 2S_{1x}S_{2x} - 2S_{1y}S_{2y} \\ 2DQ_y &= i(S_{1-}S_{2-} - S_{1+}S_{2+}) = 2S_{1x}S_{2y} + 2S_{1y}S_{2x}. \end{aligned} \quad (11)$$

ZQC looks similar but instead it contains the flip-flop terms $S_{1\pm}S_{2\mp}$. These coherences do not correspond to experimentally detectable observables and can only be detected indirectly in a pulse experiment.

The DQC experiment can be partitioned into four periods: *preparation*, *evolution*, *mixing*, and *detection* [94]. During the “preparation period” the in-phase SQC produced by the first pulse of the sequence evolves into an anti-phase SQC due to the coupling between the spins. Then this coherence is converted by another pulse into DQC, ZQC (and even higher orders of coherence depending on the total number of spins of the system, but we assume only two spins). At this point our focus is on DQC, which then evolves during the “evolution period” (with more pulses being applied during this period, as needed to complete the sequence or enhance performance). Finally, during the “mixing” period these coherences can be converted, e.g., by an appropriate pulse into anti-phase SQC, which then evolves into the observable in-phase SQC that at last is detected as an FID or a spin-echo. The incorporation of the evolution period for DQC into the pulse sequence enables double-quantum filtering. That is, only those coherence pathways that pass through DQC pathways are selected.

We illustrate these principles with examples and tools that are relevant to the pulse schemes currently employed in DQC pulsed ESR experiments, but also will help to explain DEER methods excluding subtle effects, such as phase shifts [98] etc. We assume, for clarity of presentation, that we have an isolated pair of weakly coupled spins of 1/2 and perfect, i.e., intense non-selective mw pulses. For a single pair of spins of 1/2 the highest order of coherence that can be produced is two. In this example we use the spin-Hamiltonian in the frame rotating with the mw field in which it becomes time-independent:

$$H_0 = \omega_1 S_{1z} + \omega_2 S_{2z} + a S_{1z} S_{2z} + b(S_{1+} S_{2-} + S_{1-} S_{2+})/2 \quad (12)$$

Here, $b = -a/2$, with $a = \omega_d(1 - 3 \cos^2 \theta)$ as in Eq. (3). [Electron exchange contribution is not included in Eq. (12).] We divide H_0 from Eq. (12) into two parts: H'_0 and H_{dd} . The first part contains resonant offset terms

$$H'_0 = \omega_1 S_{1z} + \omega_2 S_{2z} \quad (13)$$

¹ Note the density matrix also contains on the main diagonal ZQ $S_{1z}S_{2z}$ terms (dipolar order), which can be generated by spin manipulation or in equilibrium at low temperatures. They will play no role in the ensuing analysis, unless explicitly mentioned.

Here ω_1 and ω_2 represent, for the spins 1 and 2, their respective resonant frequency offsets from the applied frequency, ω_{mw} , i.e., $\omega_k = \omega_{k0} - \omega_{\text{mw}}$, where ω_{k0} is the Larmor frequency. The second part is the coupling, which is taken in the weak-coupling limit to be:

$$H_{\text{dd}} = aS_{1z}S_{2z} \quad (14)$$

Here the pseudo-secular term [proportional to b in Eq. (12)] is neglected. At this introductory stage, this weak coupling assumption (cf. Fig. 1) is made to simplify the discussion.

Preparation

We describe the preparation of DQC by the use of two or three pulses. These pulse sequences are the standard preparation sequences in NMR [94] and were employed in the DQ ESR experiments by Borbat and Freed [15].

For the 2-pulse preparation sequence (cf. Fig. 3a) the first pulse acts on both spins at equilibrium creating transverse coherence that is proportional to in-phase SQC ($S_{1y} + S_{2y}$). Since S_{1y} and S_{2y} will yield equivalent results (but with subscripts permuted) we need to only follow S_{1y} below. We shall employ, at this introductory stage, the standard Product Operator method [95, 99]. It can be implemented in different flavors, and some are more efficient. Here, we will purposely start with the Cartesian representation, which yields a more lengthy description but is straightforward and transparent. Here the pulses are taken as ideal $\pi/2$ or π pulses and the resonant offset terms in H'_0 commute with the dipolar coupling H_{dd} , allowing considering them independently. For example, we find using the Product Operator method that the effect of H_{dd} acting over a time t on S_{1x} and S_{1y} is:

$$\begin{aligned} S_{1x} &\xrightarrow{H_{\text{dd}}t} S_{1x} \cos(at/2) + (2S_{1y}S_{2z}) \sin(at/2) \\ S_{1y} &\xrightarrow{H_{\text{dd}}t} S_{1y} \cos(at/2) - (2S_{1x}S_{2z}) \sin(at/2). \end{aligned} \quad (15)$$

One can see from Eq. (15) that the action of a finite spin–spin coupling term a during the time interval t will cause the in-phase SQCs S_{1x} , S_{1y} to evolve as $\cos(at/2)$, whereas anti-phase SQCs $S_{1x}S_{2z}$, $S_{1y}S_{2z}$ evolve as $\sin(at/2)$. That is, there are “coherent oscillations” between these two coherences. When we include the resonance offset terms as well, we find:

$$\begin{aligned} S_{1y} &\xrightarrow{H'_0t} (S_{1y} \cos(\omega_1t) + S_{1x} \sin(\omega_1t)) \cos(at/2) \\ &\quad + 2 (S_{1x}S_{2z} \cos(\omega_1t) - S_{1y}S_{2z} \sin(\omega_1t)) \sin(at/2). \end{aligned} \quad (16)$$

That is, the respective coherences rotate with their angular frequencies in the rotating frame. At the end of the time interval $t = t_p$ the second $\pi/2$ -pulse converts the anti-phase coherence into the sum of DQC and ZQC.

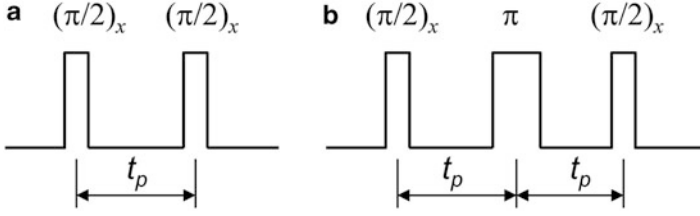


Fig. 3 Preparation of multiple-quantum coherence with two pulses (*left*) or a 3-pulse “sandwich” (*right*). These pulse propagators generate even coherence orders, i.e., 0 and 2 for two spins. If the last pulse is applied along the y -axis, odd coherence order will be produced

$$\begin{aligned}
 & 2S_{1x}S_{2z} \cos(\omega_1 t_p) \sin(at_p/2) \xrightarrow{(\pi/2)_x} \cos(\omega_1 t_p) \sin(at_p/2) \\
 & \times \left[\underbrace{(2S_{1x}S_{2y} + 2S_{1y}S_{2x})/2}_{2DQ_y} - \underbrace{(2S_{1y}S_{2z} - 2S_{1x}S_{2y})/2}_{2ZQ_y} \right] \quad (17)
 \end{aligned}$$

In this case the DQC and ZQC will be produced in equal amounts. In the case of $\omega_1 = \omega_2$ the ZQ_y term vanishes² when we consider the equivalent expression derived for S_{2y} . In Eq. (17) we do not consider any of the other terms on the rhs, since they will lead to unwanted coherence pathways that must be canceled out by “phase cycling” (cf. below).

With the preparation by the 3-pulse “sandwich,” considered next, we can obtain better conditions for generation of DQC. In this sequence, the first $(\pi/2)_x$ pulse again produces SQ coherence $S_{1y} + S_{2y}$. This coherence under the combined action of the spin–spin interaction, and the refocusing π -pulse, evolves into the sums of SQ in-phase $S_{1y} + S_{2y}$ and anti-phase $(S_{1x}S_{2z} + S_{1z}S_{2x})$ coherences:

$$\begin{aligned}
 (S_{1y} + S_{2y}) & \xrightarrow{H_0 t_p} \xrightarrow{(\pi)_x} \xrightarrow{H_0 t_p} (S_{1y} + S_{2y}) \cos(at_p) \\
 & + 2(S_{1x}S_{2z} + S_{2x}S_{1z}) \sin(at_p) . \quad (18)
 \end{aligned}$$

Here, the refocusing π -pulse removes any dependence upon the frequency offsets ω_1 and ω_2 . In Eq. (18) we see that the in-phase SQC appears as $(S_{1y} + S_{2y}) \cos(at_p)$. This will yield a primary echo at $2t_p$, whose intensity is modulated by the dipolar frequency, a . Then the last $(\pi/2)_x$ pulse turns anti-phase SQC into DQC:

$$2(S_{1x}S_{2z} + S_{2x}S_{1z}) \sin(at_p) \xrightarrow{(\pi/2)_x} 2(S_{1x}S_{2y} + S_{1y}S_{2x}) \sin(at_p) . \quad (19)$$

Thus all the anti-phase SQC is transformed into DQC when $\sin(at_p) = 1$. For this case, there is no ZQC. Note that if the last pulse in the sequence was applied

²This case, however, corresponds to strong coupling when the pseudosecular term cannot be neglected, necessitating replacing of a in Eq. (15) with $3a/2$.

along the y -axis, no DQC would be produced. Thus we see that in the case of nonselective pulses, and the preparation sequence of Fig. 3b, only DQ_y is generated.

Evolution of DQC Due to the Frequency Offsets

During the evolution period the DQC and ZQC evolve due to resonant frequency offsets and are invariant with respect to the dipolar part of the Hamiltonian:

$$\begin{aligned} DQ_{x(y)} &\xrightarrow{H_0 t} DQ_{x(y)} \cos(\omega_+ t) \pm DQ_{y(x)} \sin(\omega_+ t) \\ ZQ_{x(y)} &\xrightarrow{H_0 t} ZQ_{x(y)} \cos(\omega_- t) \pm ZQ_{y(x)} \sin(\omega_- t), \end{aligned} \quad (20)$$

with $\omega_{\pm} \equiv \omega_1 \pm \omega_2$. For the case of a typical ESR spectrum where there are wide spectral extents, signals are detected in the form of echoes, and the free-induction decay (FID) is too fast to be detected. To produce the maximum in-phase SQ echo at the final stage, the coherences in Eq. (20) should be refocused. The refocusing can be accomplished by a π -pulse placed at the middle of the DQC (or ZQC) pathway forming the sequence $t_{DQ} - \pi - t_{DQ}$. From Eq. (11) it follows that

$$DQ_y \xrightarrow{\pi_x} -DQ_y, \quad DQ_x \xrightarrow{\pi_x} DQ_x \quad (21)$$

Let us suppose that the second t_{DQ} interval is changed by an amount δt , then from Eqs. (20) and (21) one finds:

$$DQ_y(2t_1 + \delta t) = DQ_y(0) \cos(\omega_+ \delta t) - DQ_x(0) \sin(\omega_+ \delta t) \quad (22)$$

Let us assume for simplicity that both spins have identical ESR spectra of the form $g(\omega) = (2\pi\Delta\Omega^2)^{-1} \exp(-\omega^2/2\Delta\Omega^2)$ where $\Delta\Omega$ represents the spectral width. Then we can integrate Eq. (22) over the distribution for both spins to obtain the average signal for $DQ_y(2t_1 + \delta t)$. We find:

$$DQ_y(2t_1 + \delta t) = DQ_y(0) \exp(-\Delta\Omega^2 \delta t^2) \quad (23)$$

Note the same result holds for ZQC. The reader can see that Eq. (23) describes a virtual echo with maximum at $\delta t = 0$ and half width of $(\log 2)^{1/2} \Delta\Omega^{-1}$.

Mixing and Detection

At the end of the evolution period a $\pi/2$ pulse converts the refocused DQC (cf. previous Section) into SQ anti-phase coherence, which will then evolve into observable in-phase coherence. For the 6-pulse sequence described in Sect. 2.3.5 and Fig. 4, in addition another π pulse and evolution periods are used to evolve (mix) the coherences into detectable in-phase coherence. After the $\pi/2$ pulse we have:

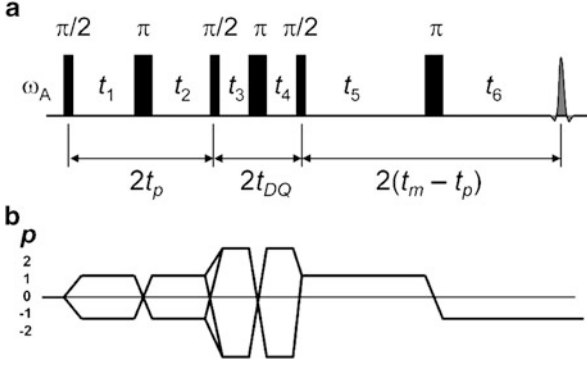


Fig. 4 In this diagram (a) shows the 6-pulse DQC sequence. The four desired coherence pathways starting with each spin in (b) correspond with the pulses shown in (a) in that a transition from one p state to another p state is generated by a pulse; the *horizontal lines* show coherence orders during the evolutions in the absence of a pulse. As for the timing between the various pulses the following is noted. The time interval $t_1 = t_2 = t_p$ is increased in equal steps, Δt_p , over a period of $t_m = t_p + t_5$. The time between the $t_3 = t_4 = t_{DQ}$ is kept fixed, $t_5 = t_6$ is stepped by $-\Delta t_p$ to maintain a constant evolution time, t_m , which is half the time from the first pulse to the echo, since usually $t_{DQ} \ll t_m$. The echo amplitude is recorded as a function of the time variable $t_\xi \equiv t_m - 2t_p$ over the range of $\pm t_m$ in steps of $2\Delta t_p$. The evolution time t_ξ starts from the initial time t_m and $t_\xi = 0$ when pulse separations are $t_1 = t_2 = t_5 = t_6$. Phase cycling isolates the dipolar signal, given by the four coherence pathways shown in (b) from the other coherence pathways, yielding the DQC signal that is an even function of t_ξ , therefore only one half is usually recorded

$$\begin{aligned} \text{DQ}_y &= \frac{1}{2i}(S_{1+}S_{2+} - S_{1-}S_{2-}) \sin(at_p) \xrightarrow{(\pi/2)_x} \\ &- (S_{1+}S_{2z} + S_{2+}S_{1z} + S_{1-}S_{2z} + S_{2-}S_{1z}) \sin(at_p) = 2(S_{1x}S_{2z} + S_{2x}S_{1z}) \sin(at_p) \end{aligned} \quad (24)$$

This is essentially the reverse of Eq. (19). The anti-phase coherences evolve during the mixing time back into observable SQ coherences. That is:

$$\begin{aligned} &-\frac{1}{2}(2S_{1+}S_{2z} + 2S_{2+}S_{1z} + 2S_{1-}S_{2z} + 2S_{2-}S_{1z}) \sin(at_p) \xrightarrow{H_0 t} \xrightarrow{\pi} \xrightarrow{H_0 t_2} \\ &-\frac{1}{2i}[S_{1+} e^{-i\omega_1 \delta t_2} + S_{2+} e^{-i\omega_2 \delta t_2} - S_{1-} e^{i\omega_1 \delta t_2} - S_{2-} e^{i\omega_2 \delta t_2}] \sin(at_p) \sin(at + \delta t_2/2) \end{aligned} \quad (25)$$

where $\delta t_2 \equiv t_2 - t$ ($t \equiv t_m - t_p$, cf. Fig. 4). The π -pulse refocuses the SQC at $t_2 = t$. One of the two counter rotating components in the square brackets of Eq. (25) is sufficient for calculation of the signal. This follows because the observed signal is proportional to the processing magnetization defined as follows:

$$M(t_2) = -\frac{2 \operatorname{Im}[\operatorname{Tr}(\hat{\rho}(t_2)S_+)]}{\operatorname{Tr}(S_-S_+)} M_0, \quad (26)$$

where M_0 is the static magnetization of the sample and $S \equiv S_1 + S_2$. The signal that is refocused during DQ evolution period is singled out by appropriate phase cycling. The real part of the echo signal becomes:

$$M(t_2) = M_0(\cos(\omega_1\delta t_2) + \cos(\omega_2\delta t_2)) \sin(at_p) \sin(a(t + \delta t_2/2))/2. \quad (27)$$

The terms in the first set of brackets, after averaging over all resonance offsets, ω_1 and ω_2 , produce an echo shape, with the maximum near $\delta t_2 = 0$. The echo envelope is modulated by $\sin(a\delta t_2/2)$. We see that the signal amplitude (at $\delta t_2 = 0$) as a function of preparation and/or mixing times is modulated by $\sin(at_p)\sin(at)$. Fourier transformation of $\cos(a(t_p - t))$, that emerges from the above product of two sin-functions, produces the dipolar spectrum, which in the case of weak dipolar coupling has the shape of and width of $2/3$ of the classical Pake doublet [79].

The point of following a particular coherence pathway and “filtering out” the other “unwanted” coherence pathways is to select the one that best provides the desired information, in this case the coupling between the electron spins. As we will show, with a proper pulse phase cycling just the refocused DQC signal is selected. We call this DQ filtering (DQF).

2.3.5 Six-Pulse DQC Sequence

This pulse sequence for distance measurements was introduced in 1996 at Cornell University by Saxena and Freed [100] and was developed into a powerful tool for distance measurements by Borbat and Freed [11, 15]. Although more challenging to implement than DEER, it is superior to DEER in some respects, thereby expanding our capacity to perform distance measurements. It does require, however, more intense microwave pulses and sophisticated phase-cycling.

Its advantages include greater sensitivity, especially for low concentration samples, since (nearly) all the spins are excited; the near absence of orientational effects in its standard 1D versions (with the option of developing them in the 2D version); filtering out single quantum signals and other noise by the double quantum filter; and the ability to obtain good results for distances as short as 10 Å [11, 101]. It is also immune to phase and amplitude drifts that may be troublesome for DEER. We show in Fig. 4 the six pulse sequence used in DQC-ESR. It transforms the initial density matrix under the successive action of six pulses and six subsequent free evolutions.

The 6-pulse sequence of Fig. 4 contains the 3-pulse preparation sequence $(\pi/2)_x - t_p - \pi - t_p - (\pi/2)_x$ which generates DQ coherence that during the evolution is refocused by the $t_{\text{DQ}} - \pi - t_{\text{DQ}}$ sequence, as described in the previous section. The fifth pulse produces anti-phase coherences (cf. Eq. (24)),

which evolve into observable SQ coherences, and the sixth pulse refocuses them (cf. Eq. (25)) to form an echo. This sequence is used with fixed t_m , and t_p is varied. The signal envelope is recorded as a function of $t_\xi \equiv t_m - 2t_p$.

This 6 pulse sequence allows for “zero dead-time” signals, which result from refocusing of first-order coherences in the middle of the data acquisition interval. That is, for Fig. 4 when one steps out t_p in the range $0 \leq t_p \leq t_m$ keeping t_m fixed, this yields a signal vs. t_ξ which ranges from $-t_m \leq t_\xi \leq t_m$. Keeping t_m fixed also has the effect of canceling out the role of phase (or T_2) relaxation on the echo at $t_2 = t_m - t_p$, since the total duration of the pulse sequence is independent of t_p .³ Note that Fig. 4 shows the four coherence pathways in which both spins participate. It starts and ends with spin 1 and 2. Since if we start with either spin 1 or 2 and independently end with either, then the total number of pathways is $4 \times 4 = 16$.⁴ Note that in the DQ coherence state, the spins 1 and 2 are symmetric [cf. Eq. (11)], such that the coherence pathway starting and ending with 1(2) and the coherence transfer pathway starting from 1(2) and ending with 2(1) are possible [35].

Assuming that the matrix elements are known for time-independent pulse propagators $R_k = \exp(-i(H_0 + H_{1k})\Delta t_k)$, for all pulses, $k = 1, \dots, 6$, where H_0 is given by Eq. (12) and H_{1k} represents the interaction term of the spin with the k th pulse; a closed form expression for the DQ signal can be written. Such a full expression for the signal in the 6-pulse sequence can be found in [102]. It was obtained by tracking down the density matrix elements along the relevant coherence pathways using the complete dipolar spin-Hamiltonian Eq. (2) instead of the approximate form of Eq. (14), and employing finite pulses. As a result the expression is quite complex. It is suitable for setting up computations, but it does not provide insight into the sequence essentials.

Neglecting dipolar coupling during the pulse allows for writing the explicit form of R_k and consequently for more readily conducting a detailed analysis. Note that in this regard different levels of approximation can be used: (1) weak coupling, ideal pulses; (2) weak coupling, arbitrary pulses; and (3) stronger coupling, arbitrary pulses.

The simplest, Case 1 can be analyzed using a suitable form of the product operator technique [95] and after minor algebraic effort leads to the ideal-case signal where the terms from all 16 pathways add to give:

$$V_{\text{DQ}}(a, t_p) = -R_{\text{DQ}} \sin(at_p) \sin(a(t_m - t_p)) = R_{\text{DQ}}(\cos(at_m) - \cos(at_\xi))/2 \quad (28)$$

R_{DQ} was added to account for relaxation and it can be simply expressed as

$$R_{\text{DQ}} = \exp(-2(t_m/T_{2,\text{SQ}} + t_1/T_{2,\text{DQ}})). \quad (29)$$

³Relaxation will however modify the signal if the coupled spins have different relaxation times or relaxation is described by stretched exponentials (cf. Sect. 2.4).

⁴That is two such diagrams should be combined into a graph to give all of 16 contributions.

Here $T_{2,\text{SQ}}$ and $T_{2,\text{DQ}}$ refer to the T_2 decay constants characteristic of SQC and, DQC, respectively (T_1 processes are neglected in these expressions). However, in general, the two nitroxide electron spins are located in different local environments, hence their respective T_2 s may be different, etc. This approach to the treatment of relaxation is a simplified one, but is satisfactory for most distance measurements [35, 101].

The more involved Case 2 requires some modifications to be made to the product operator method to accommodate arbitrary (e.g., selective) pulses, thus algebraically it becomes more involved if accurate amplitude factors are of interest [35]. One may derive a simple expression for DQC-ESR by the product operator method modified for arbitrary pulses [35]. It also works well for DEER. In the weak-coupling limit by using this method for arbitrary pulses one finds that the 6-pulse DQC signal may be written in the following form (or in general as a sum of terms of this form):

$$\begin{aligned} V_{\text{DQ}}(\omega_1, \omega_2, a, t_p) &= G(\omega_1)H(\omega_2)F(a, t_p)R_{\text{DQ}} \\ F(a, t_p) &= -\sin(at_p) \sin(a(t_m - t_p)) = (\cos(at_m) - \cos(at_p))/2 \end{aligned} \quad (30)$$

This expression has the same factors $F(a, t)$ and R_{DQ} as in the ideal case, but adds amplitude factors G and H , determining the fraction of spins participating in the signal.⁵ In general, there is a sum of terms with different amplitude factors based on the fact that there are four distinct coherence pathways with each of them giving rise to eight terms, accounting for coherence-transfer pathways, as noted above. For like spins, such as a pair of nitroxide spin labels, G and H are nearly equal, being dominated by a product of the resonant offset dependent factors, $S_2(\theta)$, which give the probability, $p(\theta, \omega)$ (or $S_2(\theta)$ for short), for a spin at the resonance offset ω to be flipped by a pulse with $\omega_{1\text{mw}} = \gamma_e B_1$ and nominal rotation angle θ . They are expressed as:

$$p(\theta, \omega) = \frac{\omega_{1\text{mw}}^2}{\omega^2 + \omega_{1\text{mw}}^2} \sin^2\left(\frac{\theta_e}{2} \sqrt{1 + \omega^2/\omega_{1\text{mw}}^2}\right) \quad (31)$$

The dependence of G and H on $\omega_{1\text{mw}}$ for the case of nitroxides is further discussed in Sect. 3.1. Refocusing of anti-phase and DQ coherences by π -pulses then requires simultaneous flipping of both spins in order to produce the required signal, therefore each of the $G(\omega_k)$ and $H(\omega_k)$ contains the cube of $p(\theta, \omega_k)$, if all three refocusing pulses are equal. They usually are set equal, so we can denote $p(\theta, \omega)$ as $S_2(\pi)$, for π -pulses. G also includes the efficiency to create $S_{k\pm}$ starting

⁵Note that for both DQC and DEER, the expression for the signal contains as a minimum two terms, except for nonoverlapping spectra in DEER, i.e., it contains terms for the signal from spins 1 and 2, and in the general case they are not equal. But we show just one for brevity.

from equilibrium. The effect of the third and fifth $\pi/2$ pulses is much less frequency dependent and usually can be ignored.

In Case 3, when the condition $|\omega_1 - \omega_2| \gg |a|$ no longer holds, the weak-coupling approach should be revised by including the pseudo-secular term, i.e., using Eq. (12), notwithstanding whether the pulses are ideal or not. For nitroxides, this includes distances under ~ 15 Å for nonselective pulses, corresponding to a large coupling (or to exotic cases of mutual arrangement of the nitroxide moieties such that the magnetic axes substantially coincide, thereby leading to small frequency differences for a significant fraction of pairs).

We outlined [35] a suitable approach for obtaining compact expressions for the signals in this case. The only (weak) assumptions made were that the dipolar interaction during the pulse has only an insignificant effect on the signals and also the DQ filter is “ideal,” which implies, as noted above, that the combined effect of preparation and mixing $\pi/2$ pulses is frequency-independent. This is indeed the case for intense pulses ($B_1 \geq 30$ G) and longer distances, ≥ 12 Å [93]. The agreement between computations based on this approach and rigorous computations [93] was found to be very good, justifying their applicability for most practical purposes. The equation based on the form given by Borbat and Freed [35] used for computing 1D DQC signals [93] is given here. The echo amplitude, V , is a function of $t_\xi \equiv 2t_p - t_m$, and is given by

$$V(t_\xi) = G(\omega_1)H(\omega_2)F(a, t_\xi), \quad (32)$$

with $G(\omega_1)$ and $H(\omega_2)$ taken as $p(\pi, \omega_k)^3$. The time variables are defined in accordance with Fig. 4. The dipolar evolution is contained in $F(a, t_\xi)$ expressed as a product of $f(t_p)f(t_m - t_p)$ with $f(t)$ given by:

$$f(t) = (p^2 + q^2 \cos(Wt)) \sin(at) - q \sin(Wt) \cos(at). \quad (33)$$

In Eq. (33), $a = \omega_d(1 - 3 \cos^2 \theta)$ and $W = (\Delta\omega^2 + b^2)^{1/2}$, where $\Delta\omega = \omega_1 - \omega_2$ and $b = -a/2$ represent the secular, a and pseudosecular, b parts of the dipolar coupling. Also, $q = b/W$ and $p^2 = 1 - q^2$. In the two limiting cases, i.e., when $|\Delta\omega| \gg |a|$ or $|\Delta\omega| \ll |a|$ Eq. (33) reduces to the form of Eq. (30) with $3a/2$ replacing a in the second limit, as expected when pseudo-secular terms are important.

It is evident from Eqs. (32) and (33) that even in the limit of ideal nonselective pulses, the effects of the pseudosecular term do not go away, since the spectral extent is limited, and they could encode orientations, although their overall effect on the 1D signal is small for most practical cases. A rigorous computational analysis [93] has shown that one rarely needs to go to such lengths, and the form given in Eqs. (32) and (33) produces accurate results and in most practical cases Eq. (30) should be adequate (cf. Sect. 2.7). It is in general true about all PDS methods that there is always a trade-off between one’s desire to describe a dipolar signal as accurately as possible, and to be able to analyze a broad range of systems, since the experiments inevitably encompass a number of secondary undesired

effects, such as those due to strong dipolar coupling, nonideal or overlapping excitations, complexity in the case of high-spins, relaxation, and ESEEM. It is important to be aware of all these details since this could help one to learn how to reduce them, thereby minimizing the distortions in the dipolar signals.

In computing the DQC signal for a pair of nitroxides, the values of ω_1 and ω_2 depend on the orientation of \mathbf{r}_{12} in the lab frame and the orientations of the nitroxide magnetic tensors in the molecular frame, whose z -axis is taken to coincide with \mathbf{r}_{12} . (More on this is in Sect. 5.3.) We shall choose Euler angles $\boldsymbol{\lambda}_i \equiv (\alpha_i, \beta_i, \gamma_i)$, with α_i set to zero, to represent the transformation from the dipolar frame to the magnetic frame of the i th nitroxide fragment ($i = 1$ or 2), and Euler angles $\boldsymbol{\eta} \equiv (0, \theta, \varphi)$ to represent the transformation from the lab frame to the dipolar frame. Then $\omega_k = \omega_k(\boldsymbol{\lambda}_k, \boldsymbol{\eta})$ for each orientation in $\boldsymbol{\eta}$, determined for each set of nitroxide nuclei magnetic quantum numbers (M_1, M_2). For example $\omega_k(\boldsymbol{\lambda}_k, \boldsymbol{\eta})$ can be calculated based on a commonly used approximation given by Libertini and Griffith, adequate up to Q -band [103]. Then the $G(\omega_1)$ of Eq. (30) will depend upon $\boldsymbol{\lambda}_1$ and $\boldsymbol{\eta}$, while $H(\omega_2)$ depends upon $\boldsymbol{\lambda}_2$ and $\boldsymbol{\eta}$, and $F(a(\mathbf{r}_{12}), t_\xi)$ just depends upon $\boldsymbol{\eta}$ as well as the magnitude $|\mathbf{r}_{12}| \equiv r$. It is then necessary to average the signal over an appropriate distribution in these variables, which we represent by angular brackets as:

$$V(t_\xi) = \left\langle G(\omega_1(\boldsymbol{\lambda}_1, \boldsymbol{\eta}))H(\omega_2(\boldsymbol{\lambda}_2, \boldsymbol{\eta}))F(r, \boldsymbol{\eta}, t_\xi) \right\rangle_{r, \boldsymbol{\lambda}_1, \boldsymbol{\lambda}_2, \boldsymbol{\eta}} \quad (34)$$

The relaxation function $R_{\text{DQ}}(\omega_1, \omega_2, \boldsymbol{\lambda}_1, \boldsymbol{\lambda}_2, \boldsymbol{\eta})$, which has been dropped for convenience in Eq. (34) can be placed outside the angular brackets, since for nitroxides, which are the major application of our DQ methods, at the reduced temperatures used, T_2 s are not substantially dependent upon $\boldsymbol{\lambda}_1, \boldsymbol{\lambda}_2$ nor upon $\boldsymbol{\eta}$. It is easy to see that when there is no correlation between $\boldsymbol{\lambda}_i$ and $\boldsymbol{\eta}$, then Eq. (34) yields the expected simpler form:

$$\begin{aligned} V(t_\xi) &= \langle G(\omega_1(\boldsymbol{\lambda}_1, \boldsymbol{\eta})) \rangle_{\boldsymbol{\lambda}_1} \langle H(\omega_2(\boldsymbol{\lambda}_2, \boldsymbol{\eta})) \rangle_{\boldsymbol{\lambda}_2} \langle F(r, \boldsymbol{\eta}, t_\xi) \rangle_{r, \boldsymbol{\eta}} \\ &\equiv G^{\text{AV}} H^{\text{AV}} \langle F(r, \boldsymbol{\eta}, t_\xi) \rangle_{r, \boldsymbol{\eta}}. \end{aligned} \quad (35)$$

Thus one can simply integrate over the distribution of orientations and magnitudes of r in the sample. An FT with respect to t_ξ will then yield the familiar Pake doublets.

Another simple limiting case occurs for weak coupling when the pulses can be regarded as nonselective, so that

$$G(\omega_1) \rightarrow G^\infty \quad \text{and} \quad H(\omega_2) \rightarrow H^\infty \quad (36)$$

independent of ω_1, ω_2 , which follows immediately from the $B_1 \rightarrow \infty$ limiting forms of Eq. (30). Then Eq. (35) becomes:

$$V(t_\xi) = G^\infty H^\infty \langle F(r, \boldsymbol{\eta}, t_\xi) \rangle_{r, \boldsymbol{\eta}} \quad (37)$$

This ideal case corresponds to all the spins in the sample contributing to the signal, so both G^∞ and H^∞ have the asymptotic value of unity. Actual values of G^{AV} and H^{AV} monotonically approach unity as B_1 increases. In this ideal case of an isotropic sample and weak coupling, Eq. (37), after neglecting a small constant term in Eq. (30), takes the form

$$V(t_\xi) = \int_0^\infty P(r) dr \int_0^1 \cos(\omega_d t_\xi (1 - 3u^2)) du \quad (38)$$

where the probability to have separation r , $P(r)$ is given by $4\pi n(r)r^2$ with $n(r)$ being the spin density. $V(t_\xi)$ in case of $n(r) = \delta(r - r_0)$ can be expressed via Fresnel integrals.

Relaxation factor R_{DQ} is different for all four contributing pathways in the case of unlike spins; faster relaxation pathways could become attenuated. In the limit of one of the two spins relaxing much faster (spin 1) only 4 of 16 terms will survive, that is those involving just spin 2 in the preparation, evolution, and detection periods.

2.3.6 Pulsed ELDOR

The 3-pulse electron–electron double resonance sequence was developed at Novosibirsk in 1981 and later renamed PELDOR (pulsed ELDOR) by its inventors Milov et al. [29]. It is based on modifying the echo produced with a 2-pulse Hahn echo sequence $\pi/2 - \tau - \pi$ at the “observer” frequency, ω_a , by a π -pulse applied at a different frequency, ω_b , as shown in Fig. 5a in the next page.

The position of the π -pulse at the observer frequency is fixed, while the π -pulse at ω_b is applied after a variable delay, t , subsequent to the first observer frequency pulse ($\pi/2$) at the time $t = 0$, as shown in the lower part of Fig. 5a. The spins that give rise to the echo are referred to as “A-spins,” and the rest are “B-spins” [34]. Only a fraction of the B-spins are excited by the pump pulse and the A-spins should not be affected by this pulse.

The dipolar signal is obtained by recording the echo amplitude at the observer frequency as a function of variable t . Thus, the 3-pulse sequence is described as:

$$(\pi/2)_a \xrightarrow{H_0(t)} \pi_b \xrightarrow{H_0(\tau-t)} \pi_a \xrightarrow{H_0(\tau)} \text{echo}, \quad (39)$$

where subscripts a and b indicate which spin is acted upon by the pulse. Pulses acting on A spins have well-defined phases. They can be used to perform phase-cycling to isolate the spin-echo from the signal offsets of instrumental origin. The magnetic field component of the mw pulse at ω_b is in the frame rotating at ω_a , making rigorous analysis of PELDOR a challenge [104].

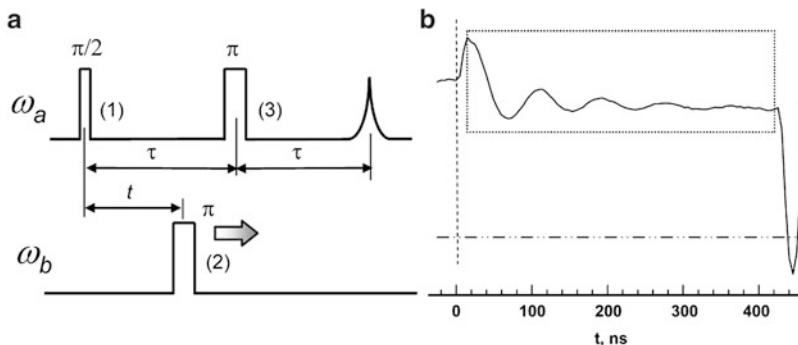


Fig. 5 (a) The original 3-pulse form of DEER (PELDOR) [29]. The primary echo is formed by the $\pi/2$ and π pulse sequence at the frequency of A-spins. The pumping pulse at ω_b is applied at a variable time t ranging from 0 to τ to probe the dipolar coupling between A and B spins. The spectral excitations at both frequencies should not overlap, thus the pulses are made selective. (b) 3-Pulse DEER for a 16.3 Å rigid biradical [35] in LC phase V, rapidly frozen from the isotropic phase; at -80°C . DEER was set up at 17.4 GHz with a 2 kW mw amplifier working in the linear regime at 10 dB below saturated output level. A low- Q dielectric resonator was used to accommodate the pulses at both DEER frequencies separated by ~ 100 MHz. The widths of $\pi/2$ and π pulses were 10 and 20 ns. The pumping pulse was positioned at the low-field portion of the nitroxide spectrum. The informative part of the signal trace is enclosed into the *dotted box*. The Bloch–Siegert phase shift of the signal [98] is clearly visible on the lhs and rhs of the box and can be eliminated by taking the magnitude of the signal obtained in quadrature. The *dash-dot line* corresponds to zero amplitude. The “dead-time” is about the width of the pump π -pulse. (b adapted from [101].)

A closed-form expression can be written for the primary echo in the presence of dipolar coupling if one ignores this dipolar coupling during the pulse, which would otherwise give rise to “forbidden” coherence pathways [102]. Assuming some simplifying conditions, it suffices to track the evolution of in-phase and anti-phase SQCs for arriving at the simple expression for PELDOR/DEER [105] that is satisfactory for most practical purposes. We have included such a derivation in the Appendix. When the dipolar coupling is large, or pulse excitations at the two frequencies overlap in spectral coverage, the spin dynamics becomes complicated and a closed-form expression cannot be written for the PELDOR pulse sequence, without making additional approximations, because the second pulse propagator is not time-independent in the frame rotating at ω_a introducing, for example a Bloch-Siegert shift [98]. Nevertheless, for this pulse sequence, coupled spin dynamics were analyzed in significant detail by Maryasov after making minor assumptions [104].

In the case of arbitrary pulses, a pulse acting on the anti-phase SQC, $S_{a+}S_{bz}$, may affect either of the two spins. Pulse action on spin A can change coherence order. Selecting the desired coherence pathway is handled by phase-cycling. However, flipping just spin B (i.e., $S_{bz} \rightarrow -S_{bz}$) has no effect on the coherence order of A-spins, but reverses the sense of time-evolution of spin A caused by its dipolar coupling to spin B. Therefore a branching into two signals, different in dipolar evolution (“dipolar pathways”) may occur, i.e., spins A associated with spin B that are flipped and those that are not. This resembles the presence of two terms for a given pathway in DQC. These “dipolar pathways” affect most of the PDS pulse

sequences based on selective pulses. Since branching into two pathways can occur after each selective pulse, for an N -pulse sequence there could be as many as 2^{N-1} distinct terms, different in dipolar evolution. One of them corresponds to unperturbed S_{bz} , while the rest may evolve with respect to their specific timing variables that depend on how the evolution periods are prescribed to vary in the pulse sequence. Although these signal pathways may be very different in their dipolar evolution, they cannot be separated by phase-cycling, since they still correspond to the same coherence pathway of A spins. In the DEER technique this would be the case when there is an overlap of the excitations at the two frequencies or more than one pump pulse is applied. [Single-frequency techniques (SQC sequences) also have such features, because anti-phase SQC may or may not change sign after the pulse. It can be shown that such unwanted dipolar pathways do not contribute to the amplitude of the 6-pulse DQC signal, because in-phase SQC will not evolve into anti-phase SQC during the preparation period or else anti-phase SQC produced after the DQC filter will not evolve into observable in-phase SQC during the mixing period, if only one of the spins is flipped by the π -pulse.] For the 3-pulse sequence there are, thus, four terms representing possible dipolar signals. If dipolar coupling is small compared to the B_1 s, the sequence can be analyzed with a properly tailored product operator technique. Excitation overlap generates all four pathways. This gives us four terms in PELDOR (cf. Appendix).

$$V(\tau, t) = V_0 \langle q_2 q_3 + q_2 p_3 \cos(a\tau) + p_2 q_3 \cos(at) + p_2 p_3 \cos a(\tau - t) \rangle_{\omega_a \omega_b} \quad (40)$$

Here we included some amplitude factors giving echo amplitude for a single spin into V_0 ; p_k is the probability of flipping either S_{az} or S_{bz} by the k th pulse (labeled as given in Fig. 5a), with $q_k = 1 - p_k$ is the probability for them remaining unaffected. When pulse excitations at the two frequencies have only a small overlap, i.e., $\langle p_2 p_3 \rangle \ll \langle q_2 p_2 \rangle$, only the first three terms are significant and one arrives at the following form

$$V(\tau, t)/V_0 \cong (1 - p_3)[1 - p_2(1 - \cos(at))] + p_3 \cos(a\tau) \quad (41)$$

Typically there is only a small effect of pulse 3 on the B-spins, so the fourth term in Eq. (40) is relatively small compared to the others, but it does exist and is a dominant term in “2+1” [38], where excitation overlap is large. Another form of Eq. (41) is

$$V(\tau, t)/V_0 \cong 1 - p_2(1 - \cos(at)) - p_3(1 - \cos(a\tau)) \quad (42)$$

At first glance Eq. (42) appears to contain two similar terms, but they are actually quite different, since the last depends on pseudosecular terms in H_{dd} . However, p_3 is not small compared to p_2 as its main effect is to act on the anti-phase coherence of A spins via S_{az} of the second spin at ω_a . Furthermore, the spin dynamics of A spins is not necessarily in the weak-coupling limit, which could make Eqs. (40) and (41) far more complicated functions of τ than $\cos(a\tau)$ [106], so that Eq. (40) in that case would become unwieldy. To a good approximation one should ignore this entire

nuisance by dropping the second term in Eq. (41) as it dies out for $a\tau \gg 1$, and by including $(1 - p_3)$ into an “initial amplitude,” V_0 . Note that the latter action is not legitimate for more than two spins when one is interested in spin-counting or “instantaneous diffusion.” We do not detail the well-known amplitude factors in V_0 in Eq. (40) (cf. Appendix) that determine spectral excitation of A-spins and the echo amplitude and shape. Since all amplitude factors contained in V_0 of Eq. (41) depend on generally orientationally dependent ω_a and ω_b and are coupled through $a(r, \boldsymbol{\eta})$, the signal in DEER, similar to the DQC case, is expressed as

$$V(t) = V_{12}(t) + V_{21}(t) \quad (43)$$

with each term, after neglecting $p_3 \cos(a\tau)$, having the form:

$$V_{km}(t) = \langle G_k(\omega_k(\boldsymbol{\lambda}_k, \boldsymbol{\eta})) [1 - H_m(\omega_m(\boldsymbol{\lambda}_m, \boldsymbol{\eta})) (1 - \cos(\omega(r, \boldsymbol{\eta})t))] \rangle_{r, \boldsymbol{\lambda}_k, \boldsymbol{\lambda}_m, \boldsymbol{\eta}} \quad (44)$$

where $G_k, H_m, \omega_{k(m)}(\boldsymbol{\lambda}_{k(m)}, \boldsymbol{\eta})$, with k, m (a or b) numbering the spins, have the same meaning as in DQC (cf. Sect. 2.3.5). They are expressed differently (cf. Appendix) due to fewer pulses and the nature of the signal, but as in DQC depend mainly on the factors given by Eq. (31). In an ideal case, when there is no correlation between $\boldsymbol{\lambda}_1$ and $\boldsymbol{\lambda}_2$ as well as with $\boldsymbol{\eta}$, $V_{km}(t)$ becomes

$$V_{km}(t) = \langle V_{0k} [1 - p_m (1 - \cos(a(r, \boldsymbol{\eta})t))] \rangle_{r, \boldsymbol{\eta}} \quad (45)$$

Finally, for like spins, there is only one term of the form given by Eq. (45) which is the well-known form

$$V(t) = \langle V_0 [1 - p (1 - \cos(a(\mathbf{r}, \boldsymbol{\eta})t))] \rangle_{\mathbf{r}} \quad (46)$$

where $a \equiv \omega_d (1 - 3 \cos^2 \theta)$ [30]. In the isotropic case Eq. (46) becomes

$$V(t) = \int_0^\infty P(r) dr \int_0^1 [1 - p (1 - \cos(\omega_d t (1 - 3u^2))] du \quad (47)$$

where $u \equiv \cos \theta$. Equation (47) is quite similar to Eq. (38) for the case of DQC, differing only because $p < 1$, and in Eq. (47) the $V(t)$ is reduced by factors reflecting the fraction of spins irradiated by the selective pulses, ω_{1a} (i.e., the A-spins). As one can notice in Fig. 5b, the signal has a short “dead-time,” since the initial part of the signal is distorted in the beginning and this may interfere with measuring a distance shorter than $\sim 25 \text{ \AA}$, but it should be less of a problem for longer distances. The implementation is helped by using an independent source for the pump pulse, but a single TWTA with enough power operating in the linear regime ($\sim 12 \text{ dB}$ backoff from saturation) also does very well (cf. Fig. 5b), if one uses the receiver with full quadrature to account for “dynamic” phase shifts [98].

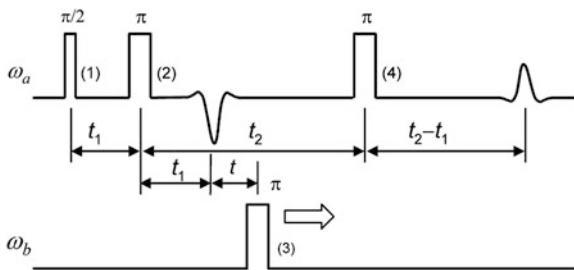


Fig. 6 The 4-pulse form of DEER [107] is a modification of its 3-pulse predecessor. It is based on detecting the refocused primary echo formed by $\pi/2 - t_1 - \pi - (t_1 + t_2) - \pi - t_2 - echo$ pulse sequence at the frequency ω_a of A-spins. The time variable t is referenced to the point where the primary echo from the first two pulses is formed (but is not detected). At $t = 0$ the dipolar phase is zero for all A spins (the precise position of $t = 0$ is limited by the width of the pulses). Shifting the starting point for dipolar evolution away from the second pulse by t_1 makes this pulse sequence dead-time-free with respect to dipolar evolution and eases its technical implementation

2.3.7 Four-Pulse DEER

Four-pulse DEER was introduced in 2000 by the group in the Max-Planck Institute, Mainz [107] to help alleviate issues with the dead-time encountered with setting up 3-pulse PELDOR using a single amplifier that was a limiting factor in accessing a wider range of distances.

This was accomplished by using the pulse sequence based on a refocused primary echo (RPE) $(\pi/2)_a - \tau - \pi_a - t - \pi_b - (2\tau - t) - \pi_a - \tau - echo$ with variable position, t of pump pulse (π_b) in between the second and fourth pulses. The addition of the refocusing pulse modifies the dipolar evolution to shift its initial point to be in the middle of the interval between the two refocusing pulses. Later this sequence was modified as shown in Fig. 6. In this implementation the zero time for the dipolar signal also coincides with the first (primary) echo but one chooses $t_1 \ll t_2$.

This ensures “zero dead-time” since the pump pulse does not need to be close to the detection pulses, thereby permitting easy implementation based on a single high-power mw amplifier, as in a commercial spectrometer. This fact enabled a rapid expansion of this method, known as 4-pulse DEER. Today it is the mainstream technique with several dozen spectrometers in operation worldwide. As a result, the number of studies that use DEER is rapidly increasing.

It should be noted that in the 3-pulse method its “dead-time” is the delay required for the detection pulse 1 (Fig. 5) to create transverse magnetization before the pump pulse flips coupled B-spins (i.e., it is of the order of half the time interval required for the pulses to “pass through each other”). The starting point of the dipolar evolution in the 4-pulse DEER sequence is when the pump pulse is centered on the refocused echo. Therefore, the two sequences are comparable in their capacity

to follow fast dipolar oscillations, due to the main limitation imposed by the width of pulses. However in the single power amplifier Ku-band PELDOR implementation (cf. Sect. 2.3.6) the need to use the linear regime limits the capacity to use a stronger pump pulse and may be not suitable for larger resonators in X-band. Another issue is that pulse interaction often exists in TWT amplifiers depending on the type of TWT and the design of the high-voltage power supply with the effects lasting for several hundred nanoseconds. A dual-amplifier configuration, as we found, is free from such artifacts, but is expensive. In summary, indeed 4-pulse DEER is easier to setup and use than the original PELDOR.

It was shown that the approximate form of 4-pulse DEER signal for two spins has essentially the same form [73] as in 3-pulse PELDOR:

$$V(t_1, t_2, t) = V_0(t_1, t_2)[1 - p(1 - \cos(at))] \quad (48)$$

with the amplitude factors V_0 depend mainly on spectral excitations of observing pulses applied at ω_a , and p is the fraction of spins B flipped by the pump pulse. Equations (42)–(47) from the previous section also apply. These expressions are satisfactory for most practical purposes. As with 3-pulse PELDOR, Eq. (48) is adequate when the pulses at the two frequencies do not overlap. Otherwise, there are eight different dipolar signals, which introduce a moderate level of artifacts (cf. Appendix). It is common to use a ~ 12 ns pump pulse to maximize the dipolar signal while minimizing unwanted signals. However, a moderate increase in signal amplitude could sometimes be offset in the case of typical T_{2S} (~ 1.2 – 2.5 μ s) by the need to discard the latter points of the signal trace and because of nuclear ESEEM effects. The condition of small overlap is substantially satisfied in a typical setup that uses ~ 32 ns observer and pump π -pulses and a frequency separation of ≥ 70 MHz. It also results in much smaller nuclear ESEEM. This setup is standard at ACERT.

A useful feature of DEER is its flexibility. It can be applied to radicals with nonoverlapping spectra and to very broad spectra. Relaxation effects and ESEEM are mostly factored out. The artifacts due to pulse overlap can be kept small for a broad range of pump pulses. Nevertheless, as we noted, there are a number of effects that should be taken into account, when needed.

To this date DEER has been implemented over a broad frequency range from S-band [108] up to E-band (180 GHz) [48]. It was implemented by us at Ku-band as a very high sensitivity DEER spectrometer that was able to rival our DQC in some cases, as we will show later in this chapter. It has operated for 9 years at ACERT and was used for several studies. PDS, represented by 3- or 4-pulse versions of DEER and 6-pulse DQC, allows one to measure distances from ~ 10 Å to nearly 90 Å, with DQC having a wider range due to intense B_{1s} and stronger signals. The main limitation to sensitivity and consequently the long distance range is imposed by phase relaxation, which we discuss next.

2.4 Relaxation

The amplitude of the primary echo V_0 decays during the period 2τ (cf. Fig. 5 for 3-pulse DEER), and during period $2(t_1 + t_2)$ for 4-pulse DEER (cf. Fig. 6), and $2t_m$ for 6-pulse DQC (cf. Fig. 4) due to phase relaxation. Therefore the maximum dipolar evolution time interval, t_{\max} ($=\tau$), available for recording $V(t)$ is ultimately limited by the phase memory time, T_m . In the simplest case, $V(t) = V_0 \exp(-2t/T_m)$. In more general cases several mechanisms contribute to relaxation, some are described by stretched exponentials [109, 110] and some such as instantaneous diffusion [111] are spin concentration dependent. Furthermore, the signal could be the sum of several terms, with each modified by relaxation in its own way. Signal decay due to relaxation is the main factor that limits the maximum distance, r_{\max} , that one can measure, over a reasonable period of signal averaging.

Depending on the signal-to-noise ratio (SNR), t_{\max} is ca. $(1 \text{ to } 3)T_m$ and cannot be extended much further. In DQC (cf. Fig. 4) t_m is essentially taken as t_{\max} and $(t_1 + t_2)$ as t_{\max} in DEER (cf. Fig. 6). The largest measurable distance r_{\max} is proportional to $(t_{\max})^{1/3}$ in order to recover a full dipolar oscillation [32, 35]. Thus only a minor increase in r_{\max} can be made by increasing t_{\max} which would further reduce $V(t_{\max})$, and this would necessarily require a large increase in signal averaging to improve SNR. Clearly, significantly improved sensitivity could also be of considerable value here. In the case of relaxation given by a simple exponential, the maximum time t_{\max} that can provide “acceptable” SNR for distance analysis depends on the spectrometer sensitivity, S , as $\log(S)$, where S gives the SNR for a standard sample. An improvement of S by a factor of 5–20 (as we find for DEER and DQC with the ACERT Ku-band spectrometer) extends t_{\max} by a factor of 1.8–3 increasing r_{\max} typically by 20–50% or else dramatically shortening the data averaging time.

For nitroxide-labeled proteins, T_m is largely determined by the dynamics of the nearby protons [110, 112–114] especially those from rotating methyl groups, leading to simple exponential decay as expressed above with T_m in the range of 1–2 μs for buried or partially buried labels. Such relaxation times are characteristic of hydrophobic environments that are encountered in lipid membranes (including fluctuating methylene protons) [115] and the protein interior [112]. At ACERT’s Ku band level of sensitivity, this typically limits t_{\max} to about 3–6 μs (in the absence of other relaxation mechanisms that could become dominant at larger t_{\max}); thus permitting r_{\max} of ~ 55 –65 \AA .

Such short relaxation times could be significantly improved by protein and (when possible) lipid deuteration, with distances as long as 87 \AA having been reported [116]. However, even in this case a typical limit is about 60–70 \AA , since in such systems the average spin concentrations are often very low (2–20 μM). For water-exposed spin labels in soluble proteins, relaxation times could be considerably longer, ca. 3–4 μs [112] and could be as large as 6–8 μs in a deuterated buffer. Nitroxide probes have T_m s of nearly 100 μs in D_2O /glycerol- d_8 [114]. However, if there are surrounding protons, for example from the protein itself, the relaxation

time becomes much shorter. At longer τ (≥ 3 μs) relaxation is dominated by the nuclear spin diffusion mechanism, leading to relaxation as $\exp(-m\tau^\kappa)$ with $\kappa \sim 1.5$ – 2.5 [110, 117]. We can define the respective phase memory time T_m for such cases by expressing this relaxation term as $\exp[-(2\tau/T_m)^\kappa]$. In water, spin-diffusion typically limits T_m to ~ 4 μs , permitting an r_{max} of ~ 50 \AA (or ~ 65 \AA with lower accuracy).⁶ Using deuterated solvent [35, 58, 59, 109] could extend T_m of spin-labeled proteins to ~ 6.5 μs and t_{max} to ca. 8 μs in favorable cases [114], i.e., less than is possible in completely deuterated systems [116, 118, 119], as there still is a bath of protons of the protein that will enable efficient nuclear spin-diffusion.

Another way to deal with such types of nonlinear ($\kappa > 1$) relaxation is to do multiple refocusing of the spin-echo [120]. This can partially suppress this relaxation, since each subsequent refocusing pulse is applied to the spin-echo produced by just the preceding refocusing pulse, so the total decay is a product of the decays between refocused echoes. For example, 6-pulse DQC has two points of refocusing first-order coherence (i.e., π -pulses 2 and 6 in Fig. 4) that help to extend t_{max} when T_m is dominated by nuclear spin diffusion, so the decay becomes: $\exp[-(2t_p/T_m)^\kappa - (2t_s/T_m)^\kappa]$ rather than $\exp[-(2t_m/T_m)^\kappa]$ (assuming a very short t_{DQ}) [35, 58]. Of course, for $\kappa = 1$ the two expressions are equivalent. This permits a more accurate estimate of r_{max} to ca. 70 \AA .

The longitudinal relaxation time, T_1 , determines how frequently the pulse sequence can be repeated (usually no more than at the rate of $\sim 1.5/T_1$) and consequently the rate at which the data can be averaged. Both T_1 and T_2 are temperature dependent, as is the signal amplitude, which depends on the Boltzmann factor for spins in the static magnetic field. The combined effect of all these factors is such that for proteins in water solution or in membranes the optimal temperature as a rule is in the range of 50–70 K for nitroxide labels. The presence of paramagnetic impurities with short relaxation times shortens both T_1 and T_2 . This requires conducting experiments at even lower temperatures. However, it is difficult to use nearby ions to improve sensitivity, as T_2 can quickly become quite short. The distance between two ions [22, 87] or nitroxide to ion [121] can also be measured and the optimal temperature is usually less than 20 K.

2.5 Distance Ranges

2.5.1 Long Distances

In the previous section we discussed relaxation as the major limitation in the context of long distance measurements. The other limitations arise due to spectrometer sensitivity and sample properties, such as its morphology and heterogeneity [122]. The ability to measure very long distances is thus limited by the phase memory time,

⁶ One could use just a t_{max} of $\sim 1.2T_m$ in this case.

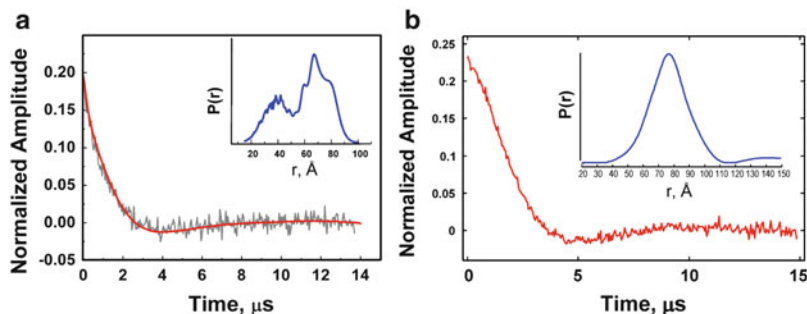


Fig. 7 Time-domain normalized DEER signals after baseline removal and reconstructed distance distributions: (a) 70% deuterated α -synuclein Parkinson’s A30P mutant spin-labeled at sites 24 and 72 and reconstituted in SDS-d₂₅, (40 μ M protein; 3 h of signal averaging); (b) 26 b.p. undeuterated TAR-RNA/TAR-cDNA duplex, DNA spin labeled at 3', 5'. The signal was averaged over an 8 h period. The DNA concentration was 50 μ M and D₂O buffer was used. The signal in (b) represents a distance of 80 Å with a width of \sim 30 Å. [The same sample was recorded using a 20 μ s “oscillation” time in 3 h with S/N about 50% of that shown. This permits one full period of dipolar frequency corresponding to 101 Å distance. (a is adapted from [116]; the sample used in b is courtesy of C. P. Scholes.)]

T_m and for proteins, 65–75 Å is about the upper limit with current technology. Also, distances measured in this range are typically not very accurate because of a lower SNR and reduced fractional period of the dipolar oscillation detected. Modified pulse sequences have been shown to bring some level of improvement [58, 59].

Sometimes just buffer or lipid deuteration suffices to measure distances up to 80 Å (Fig. 7b), but in general further improvement would require much greater effort, such as a dramatic increase of the spectrometer sensitivity and/or improvements in sample preparation, e.g., partial or complete protein deuteration (Fig. 7a) [116, 119], which in itself we estimate may extend r_{\max} to 100–130 Å and make distances ranging up to 80 Å much more accurate. Since such enrichment also benefits high resolution NMR [123–125], one could hope that this technology may become, in the future, an accepted way to improve the accuracy of distances in the 50–80 Å range, which are currently accessible, and to increase the sensitivity dramatically, bringing it to the micromolar level. This is of particular value for the difficult case of membrane proteins. Alternatively, with a good spin labeling strategy, such long distances can often be avoided, but much more double mutants have to be engineered to recover very long distances by triangulation [1, 5, 63, 71].

2.5.2 Short Distances

While measuring short distances is not limited by sample relaxation, this task has its own challenges. The sensitivity to shorter distances decreases significantly because the dipolar (and J) coupling increases and both components of the Pake doublet can no longer be adequately excited [104] in DEER. Also, account must be taken of the strong dipolar coupling that still exists during these long pulses [102, 104].

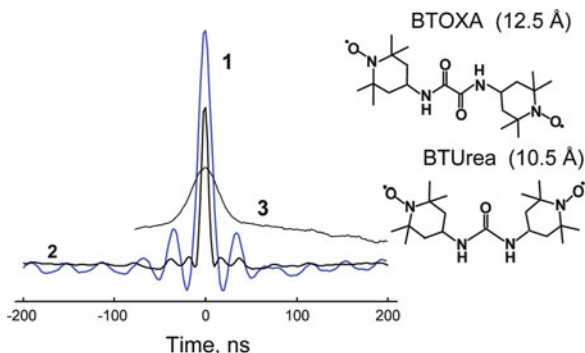


Fig. 8 The challenge of short distances with the example of short biradicals used for DNP. Ku-band (17.3 GHz) DQC (1) and DEER (3) are compared for a rigid ~ 12.5 Å nitroxide biradical, BTOXA. Detection $\pi/2$ and π -pulses in 4-pulse DEER were 16 and 32 ns, respectively; the pumping pulse was 18 ns ($B_1 \sim 10$ G). This is found to be insufficient to properly excite the dipolar spectrum. For DQC $\pi/2$ and π pulses of 2 and 4 ns widths were used ($B_1 \sim 45$ G), developing the oscillations very cleanly. The longer pulses of DEER lead to a spread in the refocusing point of different spin packets and the weaker B_1 does not excite the full dipolar spectrum. Both function as a low-pass filter smearing out the high-frequency dipolar oscillations. (2) Ku-band (17.3 GHz) DQC signal for an even shorter biradical, BTUrea. In these experiments, $\pi/2$ and π pulses were also 2 and 4 ns. The dipolar spectrum has a characteristic frequency ~ 50 MHz and spreads up to ~ 75 MHz. However, it is believed this is in part due to an electron exchange J of 7.8 MHz. (The biradicals is courtesy of R.G. Griffin.)

Below about 18 Å the sensitivity of DEER to short distances reduces significantly and distances shorter than ~ 15 Å are difficult to measure. The π -pulse excites a spectral extent (in Gauss) of about B_1 . It is necessary in DEER to excite both components of the Pake doublet at both pump and detection frequency. DEER normally uses pump π -pulses longer than 20 ns (B_1 of ≤ 9 G) and longer than 32 ns for detection. This imposes a lower limit to DEER of ca. 15–20 Å (cf. Fig. 8). However, π -pulses of 30 ns are typical, since they provide a cleaner implementation of the method, which requires that the pump pulse and observing pulses do not overlap in spectral extent. This tends to limit short distances measurable by DEER to 20 Å. A modification of the 4-pulse DEER sequence for short distance measurement was suggested [60], and may be useful in future applications to biological systems.

DQC uses intense pulses with B_1 of 30 G or greater, hence it can access distances as short as ca. 10 Å [11, 93] (cf. Fig. 8). In this case the pseudosecular part of the dipolar term in the spin-Hamiltonian [i.e., the last term on the right in Eq. (12)] cannot be neglected, but this can be accounted for [35].

Thus, pulse methods could be applied to most practical cases arising in protein distance mapping, i.e., 10–90 Å. The short distance range is more appropriate however for organic biradicals, buried spin labels, or radical cofactors, TOAC, and similar cases, when radicals are substantially immobilized and their geometry is known or can be deduced. This lower range is less relevant for typical nitroxide labels with long tethers, with uncertain geometry.

2.5.3 Optimal (PDS) Range of Distances

In our experience, an optimal range of distances for the purposes of PDS is within 20–50 Å (45 Å for membrane proteins, whose T_m s are 0.8–1.5 μ s), even though larger distances can be and have been measured with a longer period of signal averaging, but usually with reduced accuracy. This is based on our extensive experience at ACERT at Ku band, so the upper range would be smaller at X-band (commercial). Distances shorter than 20 Å introduce a relatively larger uncertainty in estimating the C_α – C_α distances. Measurement of distances in the optimal range are fast and accurate in most cases. The labeling sites and distance network should thus be chosen when possible such that they provide optimal conditions for PDS, by increasing the relative number of optimal distances, as needed.

A good example of this effect is the recent study on structural models of the complex between the cytoplasmic domain of erythrocyte band 3 protein and Ankyrin-R repeats 13–24, where PDS data were supplemented by cw ESR for distances shorter than 15 Å [71].

Optimal conditions are not readily available for oligomeric proteins due to multiple labels and their typically large size [5, 65, 122]. For an unknown structure, a preliminary scanning by several trial measurements may be very helpful.

2.6 Distance Distributions and Extracting Distance Information

Several approaches to determine distance distributions of paramagnetic centers in solids were utilized in the early applications of DEER and related methods [29]. Such methods have been improved [66, 67, 69, 70, 126, 127] and Tikhonov regularization is now a major tool for extracting distance distributions from the raw or preprocessed data.

In PDS the “raw” experimental time-domain signal encoding distance information is not an ideal dipolar signal which is the Fourier-transform of the dipolar frequency spectrum. Depending on the method it can contain a constant or decaying background and be modified by some decaying function. Before any attempt to reconstruct the distances is made, the pure dipolar signal should be separated from these. Without going into the details of the forms and origin of these contributions, which we discuss in Sect. 2.8, we express the time-domain PDS signal (both DQC and DEER) in the following general form consistent with the above signal description.

$$V(t) = \left\langle V_{\text{intra}}(t, \boldsymbol{\mu}) V_{\text{inter}}^{(1)}(t, \boldsymbol{\mu}) + V_{\text{inter}}^{(2)} \right\rangle_{\boldsymbol{\mu}}, \quad (49)$$

where V_{intra} is the “dipolar” signal of interest, produced by a pair of spins in the molecule bearing a pair of spins, while the other terms and factors depend on the PDS method to detect the signal and the sample property, for example the contributions to the intramolecular spin-pair signal from the surrounding spins

(vide infra), denoted by the subscript “inter.” The averaging in Eq. (49) is conducted over parameters $\boldsymbol{\mu} = (\mu_1, \dots, \mu_n)$, some of which may be common for contributing terms. For example, they could depend on the distribution of B_1 over the sample, or there could be a local structure, leading to a MOMD⁷ case [128]. For DEER a widely accepted approximation is to take $V_{\text{inter}}^{(2)}$ as a constant offset modified by $V_{\text{inter}}^{(1)}$ [105].

These terms can have a different origin in DQC and $V_{\text{inter}}^{(2)}$ could originate from the spins on other molecules and does not factor out in a simple way [1]. DQC filtering helps to make $V_{\text{inter}}^{(2)}$ small and it becomes insignificant at very low concentrations when molecules become essentially isolated. $V_{\text{inter}}^{(1)}$ in DEER could also originate from local aggregation effects that will only modify the signal of the aggregated molecules [129]. In all cases, the task is to extract the “dipolar signal” V_{intra} from $V(t)$. It can be helped by any a priori knowledge about the morphology of the sample. We emphasize that this step is one of the major sources of errors in distance reconstruction.

In most cases, the signal in PDS, used to extract the distance is based on the V_{intra} assumed to be given by the “ideal” signal form given by Eqs. (38) and (47). This level of approximation is often adequate, except for the cases when orientational effects (cf. Sect. 5.3) are significant or aggregation effects cannot be neglected. After extraction of V_{intra} , it is subjected to inverse reconstruction by Tikhonov regularization or related methods. The problem can be represented by a Fredholm integral equation of the first kind

$$V_{\text{intra}}(t) = V_0 \int_0^{\infty} P(r)K(r, t) dr \quad (50)$$

with the kernel $K(r, t)$ for an “ideal” isotropic sample is given by

$$K(r, t) = \int_0^1 \cos(\omega_d t(1 - 3u^2)) du. \quad (51)$$

The inversion of the signal V_{intra} given by Eq. (50) to obtain $P(r)$, the distance distribution, is in principle achievable by standard numerical methods, such as by singular value decomposition (SVD), but it is an ill-posed problem which requires regularization methods in order to arrive at a stable solution for $P(r)$. In the practical implementation, the data are discrete and available over a limited time interval, and the actual form of the kernel $K(r, t)$ may differ from the ideal form given by Eq. (51), or could be modified to address a specific issue, such as providing corrections to the reduced sensitivity of DEER to short distances.

⁷ Microscopic order with macroscopic disorder.

Tikhonov regularization [67, 70] recovers the full distribution in distance, $P(r)$. It is based on seeking an optimum, $P(r)$, which tries to minimize the residual norm of the fit to the data while also trying to maximize the stability of $P(r)$ (i.e., to reduce its oscillations). The relative importance of both is determined by the regularization parameter, λ . The L-curve method for optimizing λ is computationally very efficient and the most reliable to date [70]. In the Tikhonov method the regularization removes the contributions of the small singular values, σ_i in the SVD that are corrupted by the noise by introducing the filter function

$$f_i \equiv \frac{\sigma_i^2}{\sigma_i^2 + \lambda^2}, \quad (52)$$

which filters out those contributions for which $\sigma_i^2 \ll \lambda^2$. Further refinement of the $P(r)$ can be performed by means of the maximum entropy method (MEM) [69], although it is computationally more time consuming.

The latest versions of MEM and Tikhonov regularization permit one to simultaneously fit and remove the effects of $V_{\text{inter}}^{(k)}$ while optimizing the $P(r)$ from raw experimental data⁸ [69]. This is important, since any attempt to remove a “prescribed” baseline (assumed to be a linear or a stretched exponential function) in the case of broad distributions usually results in a level of distortion that can render the distribution totally unreasonable. The reconstructed distribution may exhibit, for example, long-distance tails that correspond to distances exceeding the size of the protein.

Experimental artifacts, a multitude of minor effects leading to signal distortions, and residual baseline make the signal recovery somewhat less accurate than what can be achieved with model data generated using the ideal kernel of Eq. (51). The test examples in the literature [69, 70] demonstrate the accuracy of recovery of average distances and distribution widths when the signal is free of artifacts.

The best condition for having the least distorted data is to use a sample with very low concentrations to reduce the baseline practically to a constant in DEER and to a very small (negligible) constant by using DQC. This however requires that one employs a PDS spectrometer with adequate sensitivity. The analysis based on ideal kernel data suggested that the SNR should be not less than 30–50 depending on the reconstruction method [69, 70]. But a low level of distortions is also very important. However, since it is difficult to obtain such high SNR, we commonly find from the literature that distance reconstruction was conducted on data with SNR of ~ 10 or less or highly distorted in the latter points of the record. This practice is very likely to result in very poor or even unphysical reconstructions.

⁸ Available for download through the ACERT web page www.acert.cornell.edu.

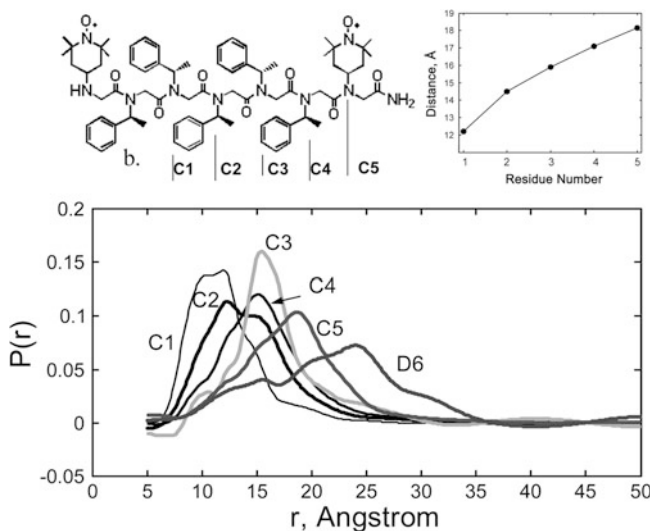


Fig. 9 Distance distributions (*bottom*) obtained from DQC data for double-labeled peptoids C1–C5 (*left top*) as determined by inverse reconstruction by Tikhonov regularization. Distances as a function of inter-residue spacing for C1–C5 (*right top*). Maxima shift from ~ 12 Å to longer distances (~ 18 Å) as the residue spacing between labeled side chains increases. Note that D6 (structure not shown) lacks branched structure-inducing side-chains, so it exhibits a wide distance distribution. (Adapted from [11].)

As an example of the viability of distance reconstruction, using short-range distance DQC data, we show in Fig. 9 the reconstruction of distance distributions for peptoids which are synthetic peptide analogs with side-chains attached to nitrogens.

2.7 Orientational Effects in PDS

The signal in DQC or DEER, given by Eqs. (34), (43), and (44), depends on the orientations of the magnetic and dipolar tensors, leading to a dependence of the dipolar spectrum on the exact position of spectral excitation in DQC and of both frequencies in DEER. On one hand, this can confuse the distance measurements, and on the other hand, it provides the opportunity to determine (to some extent) the orientations of spin labels, thus providing additional structural constraints. In cases of strong magnetic anisotropy and broad spectra, such as for Cu^{2+} – Cu^{2+} spin pairs, this orientation selectivity is already available at X-band [87], whereas for nitroxides W-band may be more suitable.

For spin labels with flexible tethers such as MTSSL, orientational effects are usually small and it is difficult to detect them at Ku band, but the effects are more pronounced for cases of more rigid labels such as TOAC and those developed for labeling oligonucleotides [130, 131], or even for MTSSL in some cases [132].

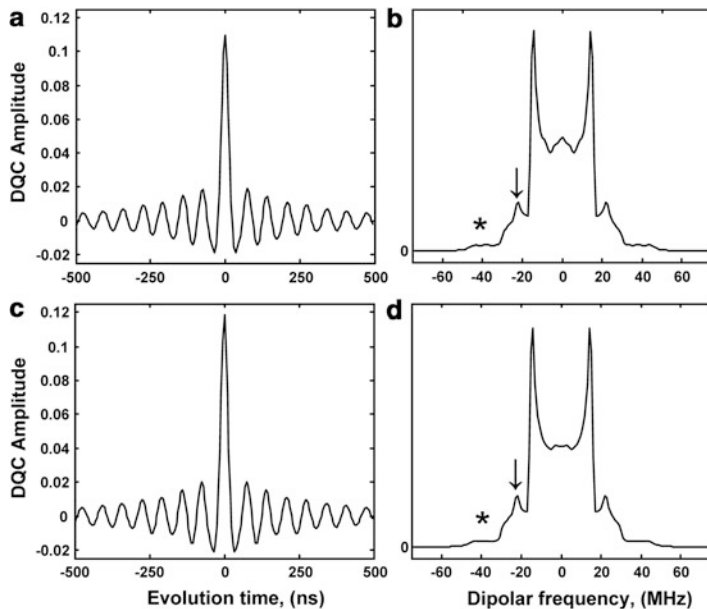


Fig. 10 Time-domain 1D DQC signals and their Fourier transforms for ^{14}N nitroxides with their magnetic tensor axis orientations distributed isotropically in the molecular frame (i.e., referred to as uncorrelated case). (a, b) A computation based on analytical approximation [cf. Eq. (32)] and (c, d) that computed rigorously. $B_0 = 6,200$ G, $B_1 = 30$ G, and dipolar coupling (v_d) is 15 MHz (15.1 Å). This figure shows the time-domain data in dipolar and echo times and its FT. A small peak at $3v_d/2$ (indicated by *downward arrow*) and a weak shoulder (marked by *asterisk*) extending up to $3v_d$ are manifestations of the pseudosecular terms in H_{dd} . The difference between the two cases is quite small, being mostly caused by using simplified amplitude factors in Eq. (32). (Adapted from [93].)

New spin-labels with reduced flexibility [133, 134] may help to achieve stronger orientational effects than what can be achieved with MTSSL.

When a sample containing bilabeled proteins is subjected to a sufficiently strong microwave pulse, as is used in DQC, the nitroxide EPR spectrum is almost uniformly excited by each pulse, and any orientational selection is (largely) suppressed given the excellent Pake doublet predicted for DQC [93] as shown in Fig. 10; that is, it does not modify the echo amplitude (except for the effect of pseudosecular dipolar terms for short distances). Also, in high B_1 -fields, the effect of dipolar coupling during the pulses becomes relatively weak so that the spectral rotation of both components of the Pake doublet is essentially the same as in the absence of coupling. In other words, a strong B_1 decouples the spins. Therefore, for not very short distances and in sufficiently strong excitation fields (B_1 s), the information on orientations of the magnetic tensors of the spin-label moieties is virtually excluded from the time-domain dipolar evolution of the echo amplitude in DQC. However, as shown by Borbat and Freed [35] and later in [93], orientational information is still retained in the spin-echo evolution, and can be retrieved by

recording the 2D time–domain data as a function of both the spin-echo time (t_{echo}) and the dipolar evolution time (t_{dip}); this is discussed later in this chapter (cf. Sect. 5.3). We remind the reader that the spectral extent that contributes to the DQC signal is less than that given by an individual π -pulse, since there are three such π pulses in the DQC sequence. Therefore not all orientations are equally represented in a real DQC signal.

2.8 *Multi-spin Effects*

So far, we have been discussing pulse methods for a system of two spins. These methods have also been applied to systems that contain more than two spins, such as oligomeric proteins [5, 65, 122] and small spin clusters [135]. In principle, all electron spins in a sample interact with the spin-pair in spin labeled molecules, giving rise to an intermolecular contribution that modifies the dipolar signal from that of an isolated spin pair or a small cluster [cf. Eq. (49)]. Such contributions are reasonably well understood in the case of DEER, but they are less tractable for single-frequency techniques, such as DQC. In all cases these effects should be accounted for in order to extract the intramolecular signals that encode the information on the relevant distances. Experimentally, intermolecular contributions should be reduced by using samples as dilute as possible consistent with the distance range and the available SNR. Intermolecular contributions on the other hand can be used to estimate spin concentration and homogeneity of the spin distribution in the sample.

2.8.1 **Multi-spin and Intermolecular Effects, Clusters, Oligomers, and Spin-Counting**

In many cases one has to deal with a protein that may have more than two spin labels, such as an oligomeric protein or a protein binding several spin-labeled substrates. For N spin labels, there could be up to $N(N - 1)/2$ distances. For instance, in our work on CheA/CheW complex [5] there were four spins per complex, with six distances possible, limited to four by symmetry, and up to five distances in our study of binding of the receptor by this complex [65]. Therefore, one might expect that except for a few advantageous cases like this, a broad distribution may be the only result, limiting the opportunity to infer detailed information on distances. The study on the CheA/CheW/Receptor complex used modeling to match several broad distance distributions in order to verify rigid-body docking, based on loosely defined constraints [64, 65].

One important application of PDS is spin-counting that could yield aggregation numbers. This currently is based on a well-tested DEER method. Small spin systems based on rigid polyradicals have been studied to correlate the modulation

depth with the number of spins [136] and to estimate nonlinear effects [137] in cases when the pump pulse is not weak enough, as recommended in early work on spin-counting by DEER [105]. Recently a magnetic dilution method was introduced for cases where the aggregate structure is not well defined [129].

In general, the small spin cluster problem is not as simple as it may appear. All A-spins are coupled and in the subsystem of A-spins one has to deal with the multi-spin dipolar Hamiltonian that contains non-commuting pseudosecular terms [138]; therefore the contributions of spins in the cluster to the echo from a particular spin do not factor out, as they do for B-spins or remote spins on other molecules. Thus, a good approach may be in using weak detection pulses minimizing the A-spins in order to limit the task to the first-order in spin number. The contribution from remote A-spins has no such problem and is treated in the same way as for B-spins, since the pseudosecular dipolar term can be neglected. Even in the case of mono-disperse clusters, due to less than ideal spin labeling efficiency, there is a distribution in number of spins per cluster, therefore the term in $\cos(a\tau)$ in Eq. (41) should be explicitly included in computing the signal from the cluster [105]. The case of several spins can become more complicated if the relaxation times of the spins are significantly different due to different local environments [65].

For an N spin system, e.g., for a spin-labeled oligomer of order N , bearing nitroxide spins $k = 1, \dots, N$, the dipolar signal in DEER can be written as a product according to [105] as:

$$V_{\text{intra}}(t) = V_0 N^{-1} \left\langle \sum_{i=1}^N \prod_{k \neq i} [1 - p_{ik} u_{ik}(\mathbf{r}_{ik}, t)] \right\rangle_{\mathbf{r}_{ik}} \quad (53)$$

Here, $u_{ik}(\mathbf{r}_{ik}, t) \equiv 1 - \cos(a(\mathbf{r}_{ik})t)$ is the dipolar signal detected on spin i when pumping on spin j , p_{ij} is the probability of flipping spin j by the pump pulse; \mathbf{r}_{ij} is the vector connecting spins i and j .

Micro-heterogeneous systems or systems with local order, such as lipid membranes and micelles which have characteristic microscopic order, are usually not amenable to simple analytic solutions, and their signals should be derived based on the appropriate averaging of Eq. (53) for the particular case [135].

The case of a small group of spins (clusters) has been considered in the literature [33, 105, 135]. This case requires numerical treatment based on Eq. (53), typically by the Monte Carlo method, although simplified approaches exist and were used to make crude estimates of the number of spins in a cluster [105]. Actually, an accurate treatment is rarely justified in such cases, since there are too many unknown parameters to fit and the limited data which permit determining one or two parameters at most. In addition one must have a priori knowledge about the system in order to model it properly.

2.8.2 Intermolecular Effects

The spin echo amplitude from an isolated pair of spins in DEER [30, 122, 139] according to Eq. (46) can be written as:

$$V_{\text{intra}}(t) = V_0(1 - p + p\langle \cos(at) \rangle_r) \quad (54)$$

where p is the fraction of B spins flipped by the pump pulse. The angular brackets denote averaging over \mathbf{r} , which is simplified by assuming no orientation selection [32, 131], which usually holds well for flexible tether MTS spin labels. Note also that $V_{\text{intra}}(t)$ in DEER contains a large contribution from spin pairs not flipped by the pump pulse, $V_0(1 - p)$, cf. Eq. (54).

The amplitude of the DEER time-domain signal, $V(t)$, as noted in Sect. 2.6 can usually be factored into an ‘‘intramolecular’’ contribution, V_{intra} [Eq. (54)], which gives the dipolar interaction in a pair of sufficiently isolated spatially correlated spins (i.e., on the same molecule), and a nonspecific ‘‘intermolecular’’ contribution, V_{inter} , from those spins randomly located within a few hundred angstroms from the pair [139].

$$V(t) = V_{\text{intra}}(t)V_{\text{inter}}(t) \quad (55)$$

V_{inter} is a decaying signal that modifies $V(t)$, resulting in a large decaying background (baseline) signal, and term $V_{\text{inter}}^{(2)}$ could also be present (cf. Eq. (49)), e.g. it can be contributed to from other sources, such as free spin-labels. For a spin i the dipolar signal in DEER due to all surrounding spins can be written as a product according to [105] as:

$$V_{i,\text{inter}}(t) = \left\langle \prod_{j \neq i}^{N-1} [1 - p_{ij}(1 - \cos(a(\mathbf{r}_{ij})t))] \right\rangle \quad (56)$$

where angular brackets denote configurational averaging over all spins in the sample. Relaxation may complicate Eq. (56), but is not included, as is appropriate for most practical cases. Equation (56) can be simplified by Markoff configurational averaging [140] over the spin distribution throughout the sample. Protein solutions can generate an isotropic, but not necessarily uniform spin distribution because of spatial correlations through excluded volume or interaction effects [141]. One finds [129] by using the Markoff method:

$$V_{\text{inter}}(t) = \exp(-k_0 p C_0 t - 9\sqrt{3}k_0 p C_0 \int_0^\infty f(r)r^2 dr \int_0^1 dx \sin^2(\omega_d t(1 - 3x^2)/2)) \quad (57)$$

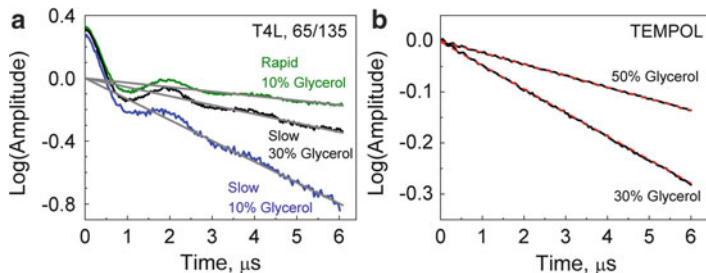


Fig. 11 The effect of the glassing agent and sample freezing method on local concentration. Raw dipolar signals are plotted on semilogarithmic scale for (a) 56 μM 65/135 mutant of T4-lysozyme and (b) 100 μM TEMPOL (1-oxyl-2,2,6,6-tetramethyl-4-hydroxypiperidine). The samples were prepared using a different percentage of glycerol in D_2O buffer by freeze-punch (slow-freeze) and freeze-quench (rapid-freeze). One can see different slopes, indicating variations in C_{loc} , depending on percentage of glycerol and the freezing method. The slopes for the 10% glycerol rapid-freeze sample, and 30% and 10% glycerol slow-freeze samples correspond to C_{loc} of 122, 248 and 578 μM , respectively. For TEMPOL the slopes correspond to 100 and 200 μM , in 50% and 30% glycerol samples, respectively. Only with 50% glycerol the spin probe distribution in the sample is truly uniform. In the case of T4L, a rapid freeze ensures a nearly uniform distribution even in the presence of just 10% of glycerol. (Adapted from [142].)

where $k_0 = 8\pi^2\gamma_e^2\hbar/9\sqrt{3} \approx 10^{-3} \mu\text{M}^{-1} \mu\text{s}^{-1}$ and p is the fraction of spins flipped by the pump pulse; C_0 is the average spin concentration over the sample; and $f(r) \equiv 1 - C(r)/C_0$ represents the effect of variable (local) spin concentration, $C(r)$, in heterogeneous samples, and r is the distance from the spin. It is clear from Eq. (57) that the exponent is nonlinear in t , whose character depends on whether the molecules attract or avoid each other [141].

For a uniform spin distribution when $C(r) = C_0$ and $f(r) = 0$, then Eq. (57) reduces to the well-known form $V_{\text{inter}} = \exp(-pk_0C_0t)$. If one approximates $C(r)$ by a constant local concentration, C_{loc} , then

$$V_{\text{inter}} \cong \exp(-pk_0C_{\text{loc}}t) \quad (58)$$

C_{loc} thus can be estimated from the slope k of the baseline (cf. Fig. 11) in the semi-logarithmic plot of $V(t)$, i.e., from

$$k^{-1} = 1.0027 \frac{10^3}{pC_{\text{loc}}} \quad (59)$$

where C_{loc} is the molar concentration and p is 0.2–0.35 for typical pump pulses [142]. The dipolar signal from the spin pair of interest [cf. Eq. (54)] is then modified by multiplication by this decaying factor (cf. Figs. 11, 12, 13, 14, and 15 for examples). A similar mechanism works amongst A-spins and is referred to as the

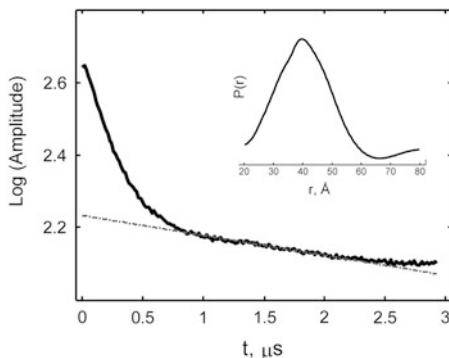


Fig. 12 Time-domain DEER signal for CheW complex with CheA- Δ 289 Q545C spin-labeled cysteine mutant. Inset shows broad distance distribution between pairs of nitroxides in this homodimeric protein [5]. CheA Δ 289 concentration was 25 μ M, signal averaging time was 8 h 20 min due to short T_m . The latter part of the signal deviates from a straight line in the semi-log plot due to the presence of unwanted dipolar signals caused by the overlap of pulse excitation at the two frequencies separated by 65 MHz. DEER was recorded using 20 ns pump pulse in dual amplifier spectrometer configuration, which eliminates the contribution from pulse cross-talk in the TWTA. The signal after subtracting the background has to be truncated or apodized prior to L-curve Tikhonov regularization. This shortens the trace by ~ 0.5 μ s. (Adapted from [122].)

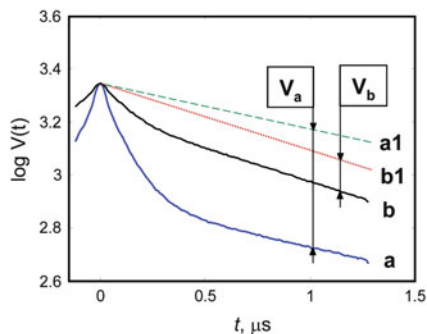


Fig. 13 The DEER data in the case of clusters for spin-labeled alamethicin magnetically diluted (*b*), and without dilution (*a*). (*a1*, *b1*) are *straight line* semi-log fits to the asymptotic parts of (*a*, *b*). (*a*) is typical for a spin cluster; in this case single labeled alamethicin molecules are organized into small clusters with an expected constant number of monomers. The data in (*b*) represent the same spin concentration but magnetically diluted by a factor of 5 with unlabeled peptide, indicating that this signal indeed originates from a spin cluster. The asymptotic DEER amplitudes (V_a , V_b) can be immediately analyzed to yield an estimate of how many peptide molecules, N are in the cluster [105], given that the fraction of peptides in clusters is known. Based on [105] $\log V_a = (N - 1) \log(1 - p)$, where p was 0.2. This yields four peptide molecules per cluster. (Adapted from [122].)

“instantaneous diffusion” mechanism mentioned earlier [34, 111, 117, 138, 143], although it is not a dissipative relaxation mechanism, so it can be partially refocused [95].

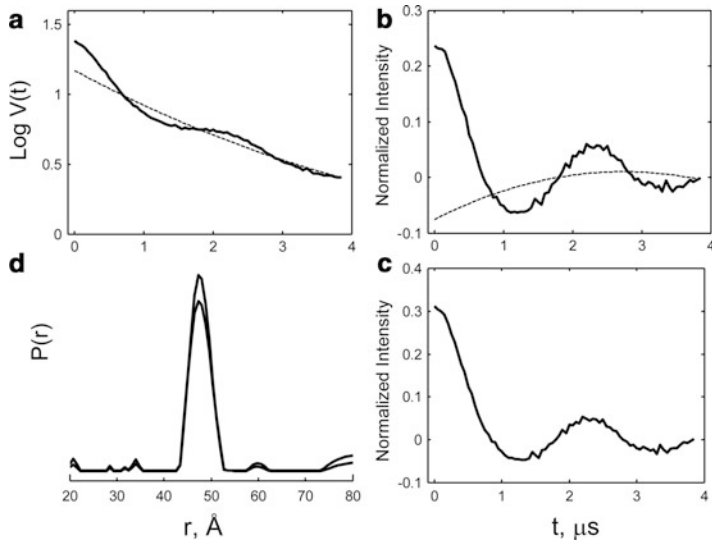


Fig. 14 Data processing of a Ku band time-domain DEER data for monoamine oxidase MAO-B labeled with spin-labeled pargyline substrate and reconstituted in octylglucopyranoside micelles [27]. (a) The intermolecular background is removed by first fitting (inappropriately) the data on the 1–4 μs interval to a second degree polynomial (rather than to a *straight line* as relevant for this case) in the semi-log plot, followed by subtracting it out. (b) Dipolar signal after removal of background. *Dashed line* shows the correction for the background that was generated in the process of MEM reconstruction [69]. (c) Corrected dipolar signal generated by fitting (a) to a linear background signal; it is indistinguishable from (b), after subtracting from (b) the correction, indicating the capability of MEM to adjust the inter-molecular contributions to the dipolar signal, reducing introduced spurious content, without introducing large errors or instability. (d) $P(r)$ produced from data from (b) (*upper curve*) and (c). (Adapted from [122].)

Strictly speaking, Eq. (58) only holds for the primary echo decay in magnetically dilute spin systems. The intermolecular contribution depends on how the multi-pulse sequence manipulates the spins in the surrounding spin bath and all possible dipolar evolution pathways should be considered [38]. In 3-pulse PELDOR the primary echo is the sum of four components that have different time dependencies with respect to the position of the pump pulse (cf. Sect. 2.3.6) [106].

The refocused echo used in 4-pulse DEER is an eight-component signal originating from all dipolar pathways (cf. Appendix). In both cases there is a common intermolecular factor, given by Eq. (58), but the coefficient k may be different from what is given by Eq. (59), if any overlap exists between the excitations at the two frequencies. Even when the overlap is small, it affects the longer time points of the signal and may become comparable to or exceed the dipolar oscillations at these points as illustrated in Fig. 12. This complicates fitting to the baseline. To minimize the distortions of this part of the signal, it is better for the pump pulse to be less than ~ 32 ns in width for nitroxides and virtually all distance measurements at ACERT were made in this mode.

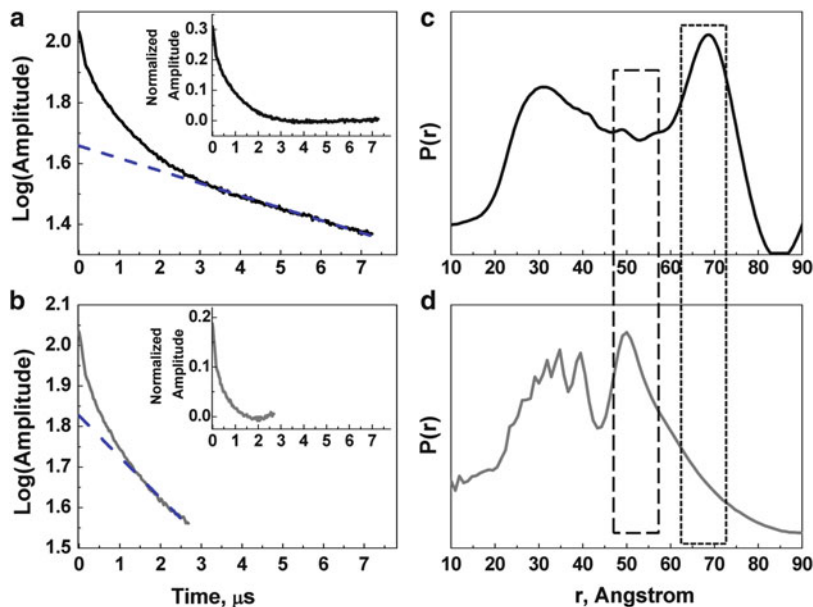


Fig. 15 Distance distribution reconstruction as a function of the evolution time of the dipolar signal. Subplot (a) shows the logarithms of raw time-domain DEER data from Parkinson’s mutant A30P of α -Synuclein with spin labels introduced at positions 24 and 72 [116], total protein concentration (labeled and unlabeled) was 40 μM in 20 mM SDS- d_{25} solutions. The baseline produced by fitting to log-linear background is plotted as *dashed line*. Subplot (b) is otherwise the same as (a), but uses the data in (a) truncated down to 2.5 μs . The insets in (a) and (b) show the data after baseline subtraction. The panels (c, d) show respective $P(r)$ s. A better reconstruction is obtained on original 7 μs data. (This lab, unpublished.)

A similar approach can be applied to an isotropic uniform distribution in space with fractal dimensionality, where a closed-form solution can be written [109]. Practical examples of lower dimension are the 2D case of unilamellar lipid membranes or the 1D case of self-avoiding polymer chains.

We note that a generalization of DQC methods to provide multiple-quantum coherence pulses that select the order of coherence is, in principle, possible [35]. Such a methodology would be very useful for spin counting, but it has not yet been developed for practical use in ESR.

For the sophisticated pulse sequence of DQC, there is no rigorous theory yet for the intermolecular dipolar effects in DQC. To first order, it is a linear contribution, which is modified by instantaneous and nuclear spin diffusion effects such as to provide a monotonically decaying nonlinear background, which should be fit to a polynomial or obtained by conducting reference measurements on singly labeled molecules. After correcting for damping as described in [1], MEM with baseline fit [69] can be applied and usually works well.

As either evolution time or concentration increases, higher order coherences will play a further role in reducing the signal. This has been analyzed for a simplified

Many-Spin Hamiltonian by Nevzorov and Freed [138]. Therefore at low concentrations, DQC has the advantages of better sensitivity due to all or nearly all the spins participating and to the weaker effects of the surrounding spins. But in cases of high local concentration (lipid vesicles, protein oligomers, or peptide clusters), DEER is able to produce the same (or sometimes even better) sensitivity than DQC, because of reduced instantaneous diffusion resulting from the weaker DEER pulses.

From the standpoint of PDS the intermolecular term is usually an unwanted complication, requiring that the intramolecular signal of interest be separated from the intermolecular contribution to the signal. Clearly, the best approach is to minimize the latter by sample dilution, whenever it is an option and sensitivity permits, as we continue to point out.

For clusters, controlled magnetic dilution proved useful to detect aggregation [129, 144] and evaluate the size of the clusters and the number of spins [145]. We illustrate in Fig. 13, the practical implementation of the method, with some additional details given in [105].

2.8.3 Data Processing in DQC and DEER

Before the data from a PDS experiment is processed into a distance distribution, it should be separated from the offset and intermolecular contribution, as discussed in Sect. 2.6. As can be seen in the literature, in many (or maybe most) cases the task of extracting the pure intramolecular dipolar signal from the data record is a difficult one, as there is no truly accurate and reliable theory that can describe all the intermolecular contributions. It has been accepted that a benefit of DEER is the multiplicative nature of the background, as it permits one to fit the background to, e.g., a simple (or stretched) exponent and then simply factor it out. However, this is not necessarily true.

In fact, the multiplicative nature of the DEER signal is often not the case and intermolecular and intramolecular signals can be convoluted. Some obvious reasons are: local heterogeneity, excluded volume, and spatial correlation lead to distributions in local concentrations, relaxation times are different, B_1 is not uniform over the sample, fractal distributions are often encountered in anisotropic environment, etc. Nevertheless, our (unpublished) analysis showed that in most of the above cases the assumption of a signal of the form $V_{\text{intra}}V_{\text{inter}}$ does not result in large errors.

But generally speaking, in most cases baseline removal still is a highly empirical procedure, as it can be highly nonlinear. The best solution would be to have it constant or nonexistent, e.g., to use highly dilute samples and when possible, DQC. However, membrane proteins are usually locally too concentrated even for DEER, even though the average (or bulk) spin concentrations are usually much less than 100 μM . So, this recipe would require a level of sensitivity that is beyond the current state of the art. For DQC, one may work with very dilute solutions

(ca. 10 μM) so the small intermolecular background signal is readily removed by means of least squares polynomial fitting in the time-domain of the latter part of the signal with sufficiently decayed oscillations; then this is extrapolated back to the earlier points of the signal and subtracted out. A correction to (quadratic) relaxation decay may be needed for not very small backgrounds [1].

In the case of DEER the removal of (multiplicative) background signal often is performed by fitting the latter part of the signal to a straight line in a log plot under the assumption of an exponent that is linear in time as in Eq. (58). This model often is not the case for the following reasons: fast-relaxing ions, charges on the protein [141], and excluded volume. All these produce a concave baseline on a logarithmic scale, whereas aggregation [cf. Eq. (57)] and fractal dimension [109] lead to the opposite or convex baseline. In these (typical) cases a low-degree polynomial can be used if a reasonable model for V_{inter} cannot accurately reproduce the intermolecular contributions. Referencing using singly labeled protein has proved to be useful for DEER.

When V_{intra} is oscillatory and does not significantly decay, more of the earlier points should be used to determine V_{inter} , sometimes all the way back to $T_d/2$ (T_d is the period of dipolar oscillations). This approach to baseline subtraction could be highly inaccurate; therefore it may be necessary to supplement it by MEM regularization to reduce the error in subtraction (cf. Fig. 14).

In the opposite case of broadly distributed distances the signal makes a gradual transition into the baseline and their separation becomes problematic, especially if the baseline is not expected to be described by a simple exponent, as is typical for membrane proteins reconstituted into liposomes. In the case of broad distributions a very shallow negative oscillation may last for more than one period of dipolar oscillations and cannot be recovered by straightforward log-linear fitting. But it is more successful to use MEM with an integrated baseline fit.

An example of such broad distributions is shown in Fig. 15. The approach is to use as long an evolution time as possible and as low a concentration as possible. This requires very high sensitivity. In Fig. 15 Panels (c) and (d) show the outcome of distance reconstruction, from (a) and (b), respectively, based on L-curve Tikhonov regularization followed by MEM refinement. The long-distance component in (c) (in dashed box) was lost and the peak with a long-distance “tail” (the dot-dashed box) at ~ 5 nm appears instead from the truncated (b) data set.

As we mentioned above, one way of accounting for the intermolecular background is to use methods of signal reconstruction with simultaneous baseline fitting [69], which separates out the part of the signal governed by the intramolecular kernel. When possible a more dilute sample is recommended, as it reduces background and also helps to make it more linear, ultimately just a constant offset. A related approach for membrane-associated proteins is to modify the sample preparation by using detergents, bicelles, and nanodisks [27, 116, 118, 146], but this may not always be possible or acceptable.

3 Technical Aspects

3.1 Spectrometers

Due to the complexity associated with construction and maintenance of a high-quality (pulse) ESR spectrometer, “home-built” designs have become increasingly uncommon. This could have become a bottleneck for PDS development, confining this method to a few research laboratories, which, over a period of two decades, have developed the adequate technology needed and even state-of-the-art performance in unique designs. PDS gained wide acceptance, however, as a result of the availability of DEER-capable commercial X-band spectrometers (and recently its Q-band extension).

However, several key aspects of PDS continue to be developed using home-built spectrometers, such as ACERT’s Ku-band PDS spectrometer and several others [46–50]. The most important feature of our pulse spectrometer is that intense microwave pulses of 1–8 kW are produced, depending on the working frequency, in order to optimize such methods as DQC (and also to satisfy the requirements of 2D-FT ESR). The Ku-band spectrometer used in the PDS work carried out at ACERT is based on a highly successful implementation of X/Ku band 2D-FT ESR [147].

This (upgraded) spectrometer provides accurate pulse widths, with pulses that can be as short as 0.5–0.8 ns, efficient signal capture in up to 1 GHz bandwidth, averaging at the rate of hundreds of kilohertz, generation of accurate phases in quadrature, and complex phase cycling schemes to greatly suppress unwanted signals including DQ filtering. Stability is essential, so the phase drift from all destabilizing factors is less than $\pm 4^\circ$ over a period of several days. The Ku band operation is supported by 2 and 4 kW amplifiers, wherein the latter is capable of providing a $B_1 \sim 45$ G in a 15 μL sample volume, which is highly beneficial for DQC. Importantly, DQC is more immune to pulse distortions typically produced by TWTAs than DEER. However, the 4 kW TWT life span has proved to be shorter than that for 2 kW amplifiers. This is an important consideration, given that the actively used spectrometer operates for nearly 8,000 h per year. Solid-state power amplifiers (SSPA) are commonly used at Q-band and above, with the output power level gradually increasing. But they are not a match to TWTAs and EIKs at least in the foreseeable future. There is also a problem with blanking the output noise of SSPA, the problem is virtually nonexistent for a TWTa.

PELDOR with an independent pumping source (magnetron) has been in use by the Novosibirsk group, who carried out several key studies on PDS methodology and applied it extensively to study aggregation of lipopeptaibols and some biological systems. Magnetrons cannot generate stable pulses shorter than ~ 30 ns, but this is not a disadvantage for DEER.

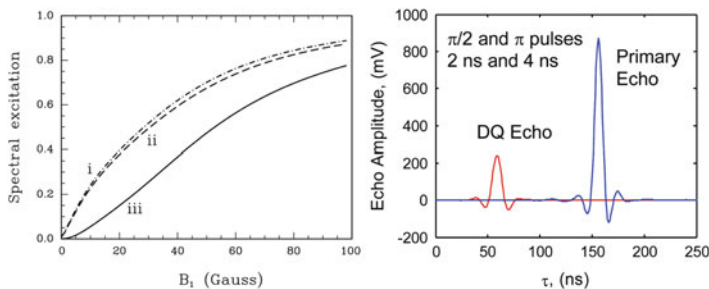


Fig. 16 (Left) Amplitude factors in the 6-pulse DQC sequence as a function of B_1 calculated for an uncorrelated pair of ^{14}N nitroxides excited at the center of the ESR spectrum for rectangular pulses. (i) G^{AV} , (ii) H^{AV} , and (iii) their product $M^{\text{AV}} \equiv H^{\text{AV}}G^{\text{AV}}$, which determines the amplitude of the DQC signal for the 6-pulse sequence given by Eq. (35). Note that as $B_1 \rightarrow \infty$ one obtains $H_6(\infty) = G_6(\infty) = 1$. These results were calculated for 9.3 GHz. At 17.3 GHz differences from 9.3 GHz are small, so the results are approximately valid at this frequency as well. (Adapted from [35].) (Right) A comparison of the primary echo and a “standard” (6-pulse) DQC-filtered echo (“DQ Echo”) from 40 μM T4L 8C/44C mutant labeled with MTSSL. $\pi/2$ and π pulses were 2 and 4 ns, respectively, corresponding to B_1 of 45 G. Data were taken at 60 K. The primary echo and DQC echo are plotted to scale. The distance from the first pulse to echo was 0.6 μs in both cases. The DQ echo is $\sim 52\%$ of its theoretical maximum that is 26% of the primary echo

3.1.1 Intense Pulses

Spectral excitation by a sequence of finite pulses⁹ depends on the available $\omega_1 = \gamma_c B_1$ and the type of signal, i.e., number of pulses and flip angles. The major factor limiting spectral excitation in DQC arises from the products of “narrow-band” terms in Eq. (30) such as $S_2(\pi)$ [cf. discussion of Eq. (31)]. In Fig. 16 we plot the amplitude factors G^{AV} and H^{AV} of Eq. (35), and their product M^{AV} calculated for an uncorrelated pair of ^{14}N nitroxides at X-band. At Ku-band there is almost no difference. The product of three $S_2(\pi)$ functions arising from the three π pulses in the 6-pulse sequence yields very reasonable values of about 0.5 for the amplitude factors given by G^{AV} or H^{AV} for a B_1 of 30 G, for which the overall amplitude factor, M^{AV} , is about 0.25. It is useful to note that the width of the spectral excitation predicted for a product of N $S_2(\pi)$ terms depends on N as $\sim N^{-1/2}$. For B_1 under 20 G the growth of M^{AV} is faster than linear, and achieving $B_1 \geq 30$ G is essential for producing strong DQC signals.

In the case of short distances (under 15 \AA) the distortions of the Pake pattern caused by the pseudo-secular term are less significant at large B_1 . For nitroxides whose orientations are correlated, we have shown [93] that by increasing B_1 to ca. 60 G and consequently H to 0.75 would greatly decrease the correlation effects (cf. Sect. 5.3). Further increases in B_1 are not very helpful as the asymptotic value of unity for H is only slowly approached with increasing B_1 . The spectral excitation that has been achieved so far at ACERT, based on π -pulses of 4 ns, corresponds to

⁹That is the fraction of spins contributing to the signal of interest.

$B_1 \cong 45$ G, and this is sufficient for producing strong DQC signals even in samples with a small number of spins. With $B_1 \cong 30$ G the amplitude of the DQC signal at $t_\xi = 0$ is about ~ 0.15 of the primary echo. We show in Fig. 16 that it approaches ~ 0.26 of the primary echo for $B_1 \cong 45$ G (the theoretical maximum is 0.5). This is somewhat better coverage than expected from Fig. 16 (left), which we attribute to instrumental phase modulation of such short pulses (cf. Sect. 3.1.3).

3.1.2 Phase Cycling

Phase cycling is a powerful method for suppressing unwanted coherence pathways by alternating the phases of the microwave pulses and then combining the detected signals appropriately. It was introduced in NMR and has become widely employed for the selection of desired coherence pathways in numerous types of 1D and 2D experiments [94]. This method was brought into the ESR field [148, 149] in order to select desired signals in 1D and 2D pulsed electron spin-echo experiments.

The general rule for the selection of a particular coherence pathway is based on the fact that if a unitary pulse propagator U acting on the density matrix according to

$$\rho(t) = e^{iUt} \rho(0) e^{-iUt} \quad (60)$$

produces a change in the given coherence order p by Δp , then the same pulse propagator, but with the phase shifted by φ , i.e., $U(\varphi)$, will multiply $\rho(t)$ by $e^{-i\Delta p\varphi}$. Consequently, a sequence of pulse propagators ($U_1(\varphi_1)$, $U_2(\varphi_2)$, \dots , $U_N(\varphi_n)$) will multiply the density matrix and hence the signal produced by a particular coherence pathway $\mathbf{p} = (p_1, p_2, \dots, p_n)$ by:

$$\exp(-i \sum_k \Delta p_k \phi_k) \quad (61)$$

Stepping the phase φ_k for the k th pulse in increments $2\pi L/N$ ($L = 0, 1, \dots, N - 1$) and combining the detected signals having weighting factors $e^{i\Delta p_k \varphi_l}$, where the subscript l refers to the L in the incremented phase, selects signals with a change in the coherence order equal to $\Delta p_k \pm Nm$ ($m = 0, 1, \dots$) [94]. For phase increments of $\pi/2$ one has $N = 4$. Hence a phase cycle that selects $\Delta p_k = \pm 2$ also selects pathways $\Delta p_k = (\pm 6, \pm 10, \dots)$ and suppresses the others.

For phase increments of π , N is 2. Thus $\Delta p_k = (0, \pm 2, \pm 4, \dots)$ are selected. We see that $\Delta p_k = 2$ and $\Delta p_k = 0$ are both selected. Therefore a phase cycle based on just the π increment cannot separate DQC from ZQC. The more pathways there are, containing a given Δp_k that can interfere with the desired signal, the more pulse propagators should be included in the phase cycling scheme. It is well known that a series of pulse propagators (which represents unitary transformations) can be replaced by a single propagator representing the cumulative effect of the series. This also applies to a series of pulse propagators interspersed by free evolution

propagators representing the effect of the spin Hamiltonian, Eq. (12). Such a cumulative propagator is referred to as a composite propagator or rotation in NMR [99].

For example, the 2- and 3-pulse sequences for the preparation of DQC (cf. Sect. 2.3.4) can be replaced by a single composite propagator which produces changes in the order of coherence of $\Delta p = 0, \pm 1, \pm 2$. It is the last value that corresponds to DQC. Thus a phase cycle that selects $\Delta p = \pm 2$ is required. The virtue of using the composite propagator is that it is sufficient to consider just its phase shifts in constructing the phase cycling. Then for a given phase shift φ for the composite propagator each pulse in its sequence must be given the identical phase shift, φ .

Consider as an example the 6-pulse DQC sequence. The first three pulses may be considered as a composite propagator that produces DQC. The change in the coherence order Δp is ± 2 . We should select all four pathways depicted in Fig. 4 with this change. Using $N = 4$, with the understanding that the phases of the three pulses should be incremented simultaneously, we arrive at a 4-step phase sequence with the phases of these 3 pulses changing as follows $(0, 0, 0)$, $(\pi/2, \pi/2, \pi/2)$, (π, π, π) , $(3\pi/2, 3\pi/2, 3\pi/2)$ and each of the four pathways are weighed by factors $(1, -1, 1, -1)$, when they are added in order to combine the signals from the selected pathway(s) constructively. This phase cycle is, in principle, sufficient (for nonselective pulses) because it suppresses all of the pathways that yield SQ or ZQ coherence.

This phase cycle for the 6-pulse sequence is satisfactory if the phases are very accurate, which is hard to achieve in practice. Therefore, it is usually necessary to cycle the phases of the other pulses in order to attain an improved suppression of unwanted signals. Additionally, the phase cycle should be combined with the CYCLOPS (CYClically Ordered Phase Sequence) [150] for suppression of signals at the image frequency. This increases the number of phase steps by a factor of four. The typical phase cycling that we employ for the 6-pulse sequence consists of 64 steps, which combined with CYCLOPS yields 256 steps, although we do find that a nearly comparable level of performance is achieved with only a 64-step phase cycle [35, 63, 151]. With these phase cycles we can suppress unwanted echoes by a factor of 300–3,000 depending on the sharpness of the echoes. The smaller value is more typical for nitroxides.

3.1.3 Composite Pulses

We discussed above some technical aspects of PDS instrumentation hardware that are required for generation of intense mw pulses that benefit DQC (cf. Sects. 3.1 and 3.1.1). It was noted that high-power mw amplifiers, which enable generation of hard pulses, have a shorter life and they are also more expensive. Therefore in order to achieve even better spectral coverage, it would be desirable to utilize a different approach.

Years ago, when we faced the problem of insufficient spectral coverage due to a power-limited source, we showed that the method of Composite Pulses, which is

common in NMR and MRI for a variety of applications, can be applied successfully to the ESR case [152], which requires much shorter pulse widths than NMR (i.e., much shorter than the ESR T_2 s, typically in the (sub) microsecond domain). However, the technology available to us at that time was still insufficient to usefully carry out short enough composite pulses, so instead we developed our technology of improving the microwave B_1 field strength at the sample, with much success. However, hardware suitable to effectively accomplish efficient composite pulse generation has become available. Furthermore, widespread use of relatively low-power solid-state power amplifiers (SSPAs) at mm-waves, as well as the desire to utilize smaller more robust TWTAs, provide additional motivation to revisit the theme of composite pulses that has been extensively developed in NMR for more than two decades [153–155]. Broadband (nonselective) spectral excitation, achieved for example by a “hard” RF pulse, formally corresponds to uniform spectral rotation of the spins, by the required rotation angle, θ . This goal can also be achieved by means of a finite shaped pulse. For a well-designed nonselective pulse, the uniformly rotated spectral range, $\pm\omega_0$, usually corresponds to $\omega_0 \geq \omega_1$, with $\omega_1 = \gamma_e B_1$ [154–158]. In our case, we are primarily concerned with rotations by $\pi/2$ and π , where the latter provides the main challenge to broadband excitation.

It is tempting to utilize one of many types of composite rotations, which were developed in NMR [154, 156, 158–163]. Our current need is primarily to provide pulses with broadband excitation for DQC since our best π pulses of 4 ns width are insufficient for uniform excitation (cf. Fig. 25). There are different kinds of uniform rotation that the pulse can provide, namely excitation ($S_z \rightarrow S_{\pm}$), refocusing ($S_+ \leftrightarrow S_-$), and population inversion ($S_z \leftrightarrow -S_z$) [159]. The rotation of spins by the oscillating mw field can be represented by a density matrix transformation [77, 94, 95, 99]. We have applied such a relevant formalism [35] in our analysis of DQC and SQC sequences. This formalism can also be applied to the general case of shaped pulses generating rotations by Suzuki-Trotter theory [164–166]. It can be shown that phase effects do not contribute a major problem for refocusing, and if Q is adequately lowered to provide sufficient bandwidth to accommodate broadband excitation at the expense of B_1 magnitude, a very uniform population inversion can be achieved.

Another issue concerns pulse sequences based on selective pulses, such as DEER. The demands of PDS applications for structural biology require their further development in order to realize the full potential of ESR. For example, in the study of RNA, which can be large in size, and of large water-soluble proteins and their complexes, long distances ≥ 60 Å need to be measured. Long relaxation times are necessary to determine such distances, and relaxation processes caused by protons in the system, in particular those of the protein, such as nuclear spin diffusion become important, especially due to their exponent obeying a quadratic to cubic law in time [113, 114]. Suppression of this type of diffusion requires multiple spin refocusing. To increase the upper range of distances, in addition to the DQ-filtered refocused primary echo (DQF-RPE) method [58], we designed a novel 5-pulse sequence for DEER (cf. Sect. 5.1, Fig. 18) intended to provide suppression of nuclear spin diffusion (as in DQF-RPE), but with the advantage of canceling the

effects of relaxation decay in the signal record as in the 3- or 4-pulse DEER sequence. But since this pulse sequence generates a sum of two types of dipolar signals (cf. Sect. 5.1, Figs. 18 and 19), it requires the means to suppress the unwanted signal. A good solution to this would be to employ selective pulse with more uniform spectral excitation. Composite selective pulses have also been successfully developed in ESR for imaging [167], suggesting that this technology could also benefit 5-pulse DEER.

4 Sensitivity Considerations

4.1 Sensitivity in PDS Experiment

The sensitivity of pulse ESR spectroscopy is more difficult to characterize than for cw ESR, wherein strict criteria were established. In pulse ESR, similar criteria are harder to set, because relaxation times, which are the major determinants of the outcome of a pulse experiment, vary over a wide range amongst the systems studied. For this reason, often the single-shot SNR for a standard sample (e.g., gamma-irradiated vitreous silica) can be used [147, 168] to calibrate sensitivity. Due to variations in pulse ESR techniques and samples, the capacity for a meaningful experiment based on considerations of its sensitivity should be decided on a case-by-case basis [47, 147] with all relevant parameters considered.

The sensitivity of PDS techniques, specifically DQC and DEER, has been discussed in [35, 101, 122], where the main criterion for sensitivity was based on the ability to perform a successful experiment (i.e., of reliably measuring a distance) in a reasonable period of time. It was chosen to correspond to a minimum acceptable SNR, nominally taken as a S_{acc} of 10 (S_{acc} is the minimum acceptable SNR), which has to be attained in the time of experiment nominally taken as 8 h of signal averaging. Such an SNR would make it possible to obtain the distance, given a sufficient length of t_{max} (cf. Sect. 2.4), which, conservatively, should be at least one period of the dipolar oscillation, $T_d \equiv 2\pi/\omega_d$. [A relaxed criterion, based on a shorter $t_{\text{max}} = T_d/2$, would still enable a less accurate estimate of the distance, depending on the specifics of the signal and given a higher SNR than 10 [122]. This may include a priori knowledge of spin concentration and labeling efficiency or whether the distance is distributed over a narrow or broad range. However, an S_{acc} of 10 is just a bare minimum, and we usually require an SNR of at least 50, but preferably 100–200 to enable reliable distance distribution analysis [69, 70]. [It should be noted that a very high SNR can be undesirable for signal analysis due to the presence of a number of signal distortions that exceed the noise but cannot be adequately accounted for and corrected in the Tikhonov or MEM analysis, thereby leading to instability in the analysis. This is of particular concern regarding the errors introduced in baseline subtraction].

Even though it is possible to estimate sensitivity from first principles [168], we prefer to use an experimental calibration in the spirit of [35], so the following approach has been chosen to give estimates of sensitivity in distance measurements. First of all, a simple and standard experiment, such as a single-shot amplitude measurement of the primary echo, is performed under conditions when relaxation and other complications can be ignored. Then the sensitivity of the single-shot experiment of a more complex pulse sequence is deduced from this, based on the known theory of the method. Within such an approach, it suffices to measure the spin-echo amplitude at a selected point of the nitroxide ESR spectrum with a 2-pulse primary echo sequence, applied at a low repetition rate and with a short inter-pulse spacing. Such an experiment provides the SNR for a single-shot, $S_{1,PE}$, which we give as per unit of concentration (1 μM) or per the number of spins (1 pmol), whichever is needed. Subsequently, the S_1 for the more complex experiment is estimated by comparison to the S_1 of the primary echo, $S_{1,PE}$. Due to the limited capacity of simulating the outcome of a complex pulse sequence, such an estimate has limited accuracy, but it should be a reasonable predictor of the actual SNR. Finally, all the other major factors that influence the outcome of the actual experiment, such as relaxation, temperature dependence of the signal, instantaneous diffusion, pulse sequence repetition rate, and noise bandwidth, must be determined and their values used to estimate their effect on the SNR for a given distance and its range of uncertainty.

The calibration of DQC and DEER has been conducted for our pulse ESR spectrometer [5] at the working frequency of 17.35 GHz on a nitroxide sample of 4-hydroxy TEMPO in a vitrified solution of 50% w/v glycerol in H_2O with a 20 μM spin concentration in a 10 μL sample volume at 70 K, at which most PDS measurements are performed. The DEER calibration used a primary echo [169] generated by $\pi/2 - \pi$ pulses (π pulse of 32 ns) separated by 80 ns, with the pulses applied at the low-field edge of the nitroxide spectrum, typical of a DEER pulse setup at centimeter wavelength. The classic analysis of the SNR of a primary echo has been given by Mims [169], and the sensitivity in all PDS is directly related to that of a primary echo. A similar DQC calibration was based on $\pi/2 - \pi$ pulses with a 6 ns π pulse, and the same separation as in DEER, but pulses were applied in the middle of the spectrum. For the two measurements, the ratio of the echo amplitudes (DQC vs. DEER) was ca. 6.5 and the ratio of SNRs of the single-shot signals at the condition of optimal signal acquisition (i.e., given by the integration of the spin echo in the time window defined by the time points corresponding to 0.7 of the echo amplitude) was ca. 3.0, i.e., $S_1 \approx 0.42 \mu\text{M}^{-1}$ (DEER) and $S_1 \approx 1.25 \mu\text{M}^{-1}$ (DQC).

Based on these numbers, the estimates of the dipolar signals for the two methods (using the ACERT spectrometer) according to the analyses given in [35, 122] are summarized as follows. For 4-pulse DEER with 16/32/32 ns pulses in the detection sequence and a 32 ns pump pulse, S_1 is $0.084 \mu\text{M}^{-1}$, and for DQC based on a 3/6/3/6/3/6 ns pulse sequence, S_1 is $0.3 \mu\text{M}^{-1}$, i.e., it is greater for DQC by a factor of 3.6. It is possible to use a shorter pulse of 12–16 ns in DEER and to increase the signal

by the factor of 1.5, but the resulting distortions and large increase of ESEEM outweigh a small signal increase, generally discouraging this practice. Also the use of 2 and 4 ns pulses in DQC enhances the DQC SNR by a factor of 1.6 (cf. Fig. 16 left). This ratio is supported by our experimental observations (cf. Figs. 10, 16 right). Using the sensitivity analysis of [35] we estimate the SNR of the raw data of the full PDS experiment as

$$\text{SNR} = 2S_1 x^2 C \eta_c K(f, T_1) \left(\frac{ft_{\text{exp}}}{N} \right)^{1/2} \exp \left(-\frac{2t_{\text{max}}}{T_m} - 2\kappa x C G_d t_{\text{max}} \right) \quad (62)$$

Here, t_{exp} is the duration of the experimental data acquisition; f is the pulse sequence repetition frequency; N is the number of data points in the record; C is the doubly labeled protein concentration (in μM); η_c is the ratio of the sample volume ($\leq 15 \mu\text{L}$) to that used in the calibration (i.e., $10 \mu\text{L}$). The terms in the exponent are consistent with those given in [35], namely the first accounts for the phase relaxation [but we use $\kappa = 1$ in Eq. (62)] and the second for instantaneous diffusion. G_d is method-specific [35] and for the pulse sequences defined above it is ca. 0.14 in DEER and ca. 0.52 in DQC. We also include the spin-labeling efficiency, x , which modifies the fraction of both spins that need to be flipped in PDS, showing its strong effect on the outcome of an experiment. Below we assume complete labeling for convenience in the discussion ($x = 1$). $K(f, T_1) = 1 - \exp(-1/fT_1)$ gives the effect of incomplete spin–lattice relaxation for a given relaxation time, T_1 and repetition rate, f (K is 0.72 for the optimal repetition rate, when $fT_1 = 0.79$ and is unity when $fT_1 \ll 1$). The maximum of the SNR as a function of f is broad, so selection of f is not critical. Typically f is 0.5–2 kHz for Ku band. As an illustration of the capability of PDS in various regimes, we give the following estimates based on our experience at ACERT at 17.3 GHz.

4.2 Short Distances, Low Concentrations

In the case of short distances, sensitivity is rarely a concern, but it is the capacity of the method to measure this distance, that matters. Assuming a short distance of 20 \AA ($T_d = 154 \text{ ns}$), which is within the DEER capacity and setting $t_{\text{max}} = 0.48 \mu\text{s} \approx 3T_d$ in order to provide very good resolution of distance; T_m is taken as $1.0 \mu\text{s}$, i.e., about the shortest within its typical range; 8 ns steps in t yielding 60 data points are taken as producing the signal record; a pulse repetition frequency f of 1 kHz should be optimal for a spin-labeled protein at 70 K. One finds from Eq. (62) that just $t_{\text{exp}} \cong 4 \text{ min}$ of signal averaging of the DQC signal provides an SNR of 10 for a C of $1 \mu\text{M}$. DEER will require nearly 1 h (50 min) for achieving this result. Note that this concentration corresponds to just 10 picomoles of protein in a typical $10 \mu\text{L}$ Ku-band sample. A high SNR of 100 for DQC could be attained in 6.5 h for the same amount of protein.

4.3 Long Distances

We assume $t_{\max} = 4 \mu\text{s}$, which is certainly a challenge using H_2O buffer; a typical T_m for partly buried label [113] of ca. $2 \mu\text{s}$, and the steps in t are taken to be 16 ns . Then an SNR of 10 will be reached in 8 h for a C of $3.7 \mu\text{M}$ for DQC (while for DEER it would be 104 h). By using one period of T_d we find $R_{\max} = 59 \text{ \AA}$; for half of the period, R_{\max} is 75 \AA . Longer distances cannot be estimated reliably with this SNR. An accurate analysis of the distance distribution requires a higher concentration of at least $18 \mu\text{M}$ in order to provide an SNR of at least 50 [69, 70], under otherwise similar conditions. For t_{\max} of $4 \mu\text{s}$ one should also account for nuclear spin diffusion, which will make this case more difficult, requiring one to increase concentration up to $10\text{--}50 \mu\text{M}$ in practice. Note that standard DQC provides some degree of suppression of spin diffusion [1]. The improvements that can be achieved by deuteration are discussed in the following references [116, 119].

4.4 Distances in the Optimal PDS Range

We consider 50 \AA to be an upper limit for the “optimal” PDS distance range [122]; T_d is then $2.4 \mu\text{s}$, so a t_{\max} of $2.4 \mu\text{s}$ suffices to provide the distance sufficiently accurate for a structure constraint. However, let us assume the rather challenging case of $T_m = 1.5 \mu\text{s}$; steps in t are taken to be of 32 ns ; f is 1 kHz , C is taken as $25 \mu\text{M}$; but here we require a good SNR of 50. Such an SNR is achieved in 16 min by DQC. DEER requires nearly 3.5 h for the same result, or else the concentration must be increased (by a factor 2–4). Shorter distances of $20\text{--}45 \text{ \AA}$ are measured faster, or else yield a better SNR or improves distance resolution. This is the case for the ACERT 17 GHz spectrometer. Most published work based on a commercial X-band DEER spectrometer use this range. As a rule t_{\max} is around $2\text{--}2.5 \mu\text{s}$ providing good enough resolution in this distance range. Typical data collection time reported is on average $12\text{--}24 \text{ h}$ per measurement. This may be adequate to characterize a protein in about 2–3 months, unlike the situation at ACERT requiring at least an order of magnitude less time.

4.5 Examples

We conducted Ku-band DEER sensitivity test experiments at ACERT on model systems that include organic biradicals R-I and R-II [35] in perdeuterated *o*-terphenyl glass and spin-labeled T4-Lysozyme, with the results shown in Fig. 17 along with the data on the membrane protein α -Synuclein [116, 118]. These measurements are in good agreement with the estimates given above.

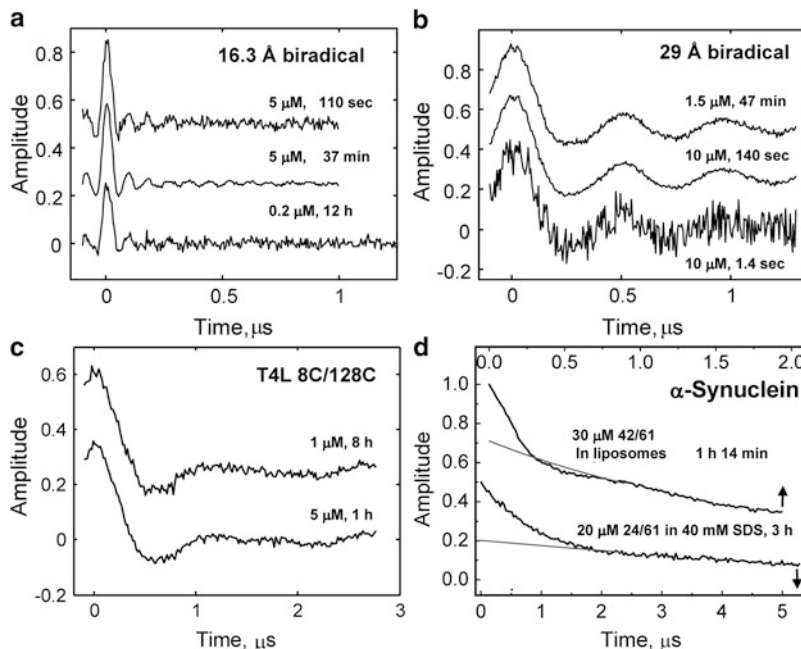


Fig. 17 Sensitivity test of ACERT Ku-band DEER performed on: (a, b) rigid biradicals (R-I and R-II, [35]) in orthoterphenyl- d_{24} glass prepared in different concentrations and recorded using several signal averaging periods. T_2 -relaxation decay can be neglected in this case. Pump pulse was 16 ns, dwell time was 5 ns, pulse repetition rate was 500 Hz for (a) and 2 kHz for (b); (c) T4-Lysozyme double-labeled mutant 8C/128C in D_2O buffer (40 Å interspin distance). The refocused echo decayed by a T_2 -mechanism to ~ 0.35 of its value taken at a short evolution time. (d) Liposome and detergent data for wild-type α -Synuclein, labeled at different positions, are plotted with their background fits using different horizontal scales (*top scale*: 42/61 mutant 36 Å distance; *bottom scale*: 24/61 mutant 55 Å distance). The visible slope in the case of detergent (SDS- d_{25} in D_2O buffer) is due to a low content of glycerol, so water freezes out. Repetition rates were 1 kHz for (c) and (d); pump pulse was 16 ns (in a–c) and 32 ns (in d), temperature was 60 K in all cases. All signals are raw, normalized to unity at zero time and plotted shifted vertically for convenience. Based on these sensitivity calibration data, concentration sensitivity can be estimated for other systems, where relaxation times may be shorter and spin labeling efficiency is less. (Ref. [171] for a and b; data from [116, 118] for d; c unpublished.)

Absolute spin sensitivity is closely related to the concentration sensitivity; however, it does increase rapidly with an increase in the working frequency due to the smaller volume of a resonator used at a higher frequency, for example, at Ku band 25–250 picomoles of protein are routinely used in the optimal distance range.

The smaller amounts are better suited for DQC. These amounts can be reduced by about an order of magnitude by using smaller resonators than we currently employ, but by an even greater factor at a higher working frequency [46, 49].

We remind the reader that the previous estimates relate to our 17.3 GHz spectrometer. Lower estimates of sensitivity, in particular absolute sensitivity, would apply to the typical pulse spectrometers that operate at 9 GHz

5 Newer Aspects

5.1 5-Pulse DEER

In order to increase the SNR, and to access longer distances, both DQC and DEER pulse sequences were subsequently tested in the forms of double-quantum filtered RPE (DQF-RPE) [58, 170] and variable time DEER [59], respectively. Both pulse sequences increase SNR by using a variable time. DQF-RPE can be used to measure longer distances due to partial suppression of nuclear spin diffusion by means of multiple refocusing; variable-time DEER improves SNR just because of the variable time. DQF-RPE has finite dead-time and is not immune to ESEEM, which may interfere with the signal when caused by deuterium nuclei. The signals from both pulse sequences are used in conjunction with a suitable recorded reference signal to account for signal decay caused by phase relaxation, however, the referencing is not perfect, since in some cases relaxation does not necessarily factor out and instantaneous diffusion is not the same in the reference signal. In both cases referencing causes a residual background that should be removed in data processing in the manner similar to how it is done in standard DQC or DEER (cf. Sect. 2.6).

It thus was very desirable to construct a constant-time pulse sequence (i.e., using fixed positions of all detection pulses) in order to minimize the impact of relaxation and nuclear ESEEM, to ensure zero dead-time, and to avoid other unwanted effects. A 5-pulse DEER sequence that substantially satisfies these requirements was described by Borbat, Georgieva, and Freed in context of a more general approach [171]. This new pulse sequence is shown in Fig. 18.

The suppression of nuclear spin diffusion by this pulse sequence is essentially based on the same principle that is used in DQF-RPE [58], i.e., by creating a refocusing point in the middle of the detection pulse sequence between the first $\pi/2$ pulse and the echo separated by the time interval $2t_m$, thus minimizing the time interval available for “quadratic” relaxation to develop. The original version of 4-pulse DEER [107] satisfies this criterion; however, it is not optimal with respect to evolving dipolar modulation, which is recorded over one quarter of the time interval between the first pulse and detected echo, i.e., by using only half of the time interval $2t_m$ to evolve dipolar coupling; the rest was wasted. For this reason, this pulse sequence was modified into its current asymmetrical form [59].

In 5-pulse DEER (DEER-5) this task is accomplished by applying an additional pump pulse, which reverses the effect of one of the refocusing pulses, thereby shifting the time-reversal (refocusing) point of the dipolar evolution from the middle of the second interval to the position of the second (for 5') or the third (for 5) of the detection pulses. However, there is a small problem. This pulse sequence (cf. Appendix) does develop the desired new dipolar pathway, but the original one survives as well, although it is substantially attenuated. Since the same coherence pathway is involved, phase cycling cannot separate them, because it holds for all dipolar signals in a multi-pulse sequence based on selective pulses (cf. Sec. 2.3.6). One immediate solution is to reference this pulse sequence by using

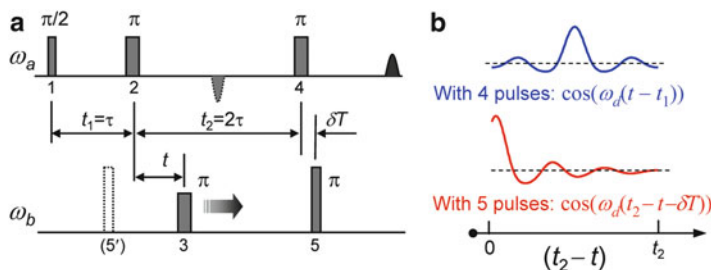


Fig. 18 A 5-pulse DEER pulse sequence uses 3 pulses for signal detection applied at ω_a and the signal is recorded as in the standard 4-pulse DEER by varying the timing of the pump pulse 3, applied at ω_b . Time interval t_2 is set to $2t_1$ to minimize the phase relaxation caused by the nuclear spin diffusion from the surrounding proton bath by refocusing the primary echo exactly in the middle of the interval made by the first $\pi/2$ pulse and the refocused primary echo. In order to utilize all the time from the first pulse to the spin echo for dipolar evolution, an additional pump pulse is applied, with its position fixed. Two essentially equivalent positions (5 or 5') of the additional π -pulse are possible, that is position 5 following pulse 4 or 5' before the pulse 2, as shown in the figure. As result, a minor dipolar pathway, which could be formed due to excitation overlap in the 4-pulse sequence (cf. Appendix), becomes the major pathway, while the standard 4-pulse DEER dipolar signal becomes attenuated. On the *right*, these two dipolar signals are shown: the standard (in *blue*) which is symmetrical about the center of the interval $(0, t_2)$ is recorded in the absence of the additional pulse; a new signal (in *red*) appears, starting from time $t = t_2$, in the presence of the fifth pulse at position 5. Using position 5' instead of 5 will reverse the time changing the signal to $\cos(\omega_d t)$ (cf. Table 1 in Appendix). Shifting pulse 5 (or 5') as shown by a small amount, $\delta T \sim 100$ ns, results in zero dead-time. The time interval δT is much smaller than t_1 and does not affect the performance. Both cases were tested, the results are shown for preferred position 5, after pulse 4, since for position 5' a small excursion due to an unwanted primary echo from pulses 5' and 2 may be visible on the signal

the 4-pulse sequence which generates the signal that should be removed. The subtraction (Fig. 19) is performed as detailed in [171]. Of course, the amplitude of the unwanted signal should be minimized in order to keep the residuals of the unwanted signal pathway at a very low level (Fig. 19) permitting one to use only a small percentage of experimental time to record the reference. This is achieved by making the pulse 5 (or 5') less selective than the standard pump pulse 3. However, complete suppression has not yet been achieved using this approach and future efforts should be directed toward engineering selective pulses with a more uniform spectral excitation profile.

It should be noted that the subtraction cannot be made perfect because of orientational effects, nonlinear effects caused by intermolecular dipolar coupling, and by nonuniform B_1 over the sample. However, baseline removal in DEER or DQC signals is also never perfect, and orientational correlation effects inevitably result in reconstruction artifacts, which are greater at high concentrations. For not too high concentrations, and in the absence of strong orientational effects, subtraction leaves behind a low level of distortion [171], which does not exceed the typical level of unwanted signals, distortions, and artifacts present in other known pulse sequences. It would be desirable to improve the suppression by another factor of 3.

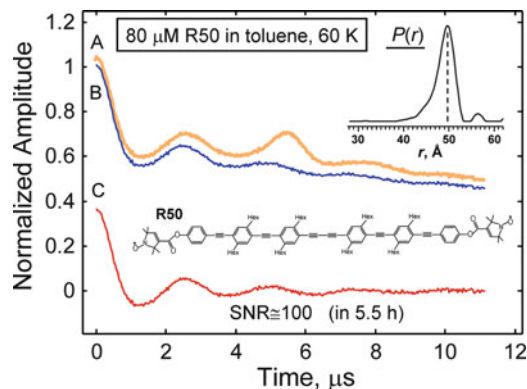


Fig. 19 The raw signal in 5-pulse DEER (A, top curve) contains the desired signal, (B, middle curve) and the unwanted contribution of the type shown in Fig. 18b top, which is visible as a small hump in the middle. The unwanted signal is partially suppressed by using a stronger fifth pumping pulse in Fig. 18. The residual contribution is removed by subtracting out a 4-pulse DEER reference signal of the type shown in Fig. 18b, recorded in the absence of this pulse [171]. This does not noticeably increase the duration of the experiment, nor does it degrade the SNR. This is because this signal is scaled down by a factor 3–6 in making the subtraction. C (bottom curve) is B after removing homogeneous background. Inset shows the distance distribution produced from C by Tikhonov regularization [69, 70]. The data were recorded at 17.3 GHz and 60 K on $\sim 80 \mu\text{M}$ long biradical [59]. The detection pulse sequence used 32 ns π -pulses and was applied at the high-frequency edge (low field) of the ^{14}N spectrum. Pump pulses (12 ns, pulse 5' and 29 ns, pulse 3) were applied at 70 MHz lower frequency corresponding to the central peak of the spectrum. (Unpublished data. The biradical is courtesy of Gunnar Jeschke.)

Such improvements could include the following. The size of the sample can be adjusted to achieve more uniform B_1 and better resonators can be employed [56].

Although composite pulses [152] have not yet found routine use in pulse ESR, this could be reconsidered (cf. Sect. 3.1.3), based on current progress with high-speed signal generation in bandwidths wider than 100 MHz, which seems adequate for fine-tuning spectral excitation in 5-pulse DEER, cf. [171].

Intermolecular contributions to the signal do not factor out perfectly, e.g., by dividing the two signals, as they are different in the 4- and 5-pulse DEER sequences [171]. Therefore, high concentrations should be avoided in order to stay practically in the linear regime so that the exponent of the intermolecular contribution should be small, which holds well for spin concentrations less than $100 \mu\text{M}$. This however is true for any PDS technique. Strong intermolecular effects are highly undesirable. The removal of such an unwanted signal is more accurate when the intermolecular contribution is in the linear regime (i.e., exponent is $\ll 1$). Finally, in Fig. 20 we show the improvement in the distance range by comparing echo amplitudes, recorded as a function of pulse separation in the standard 4-pulse and 5-pulse DEER sequences. We found the evolution time was expanded by a factor of ~ 1.94 in this case, whereas only a factor of $2^{1/2} = 1.41$ was expected [58]. The maximum time, t_{max} , was taken

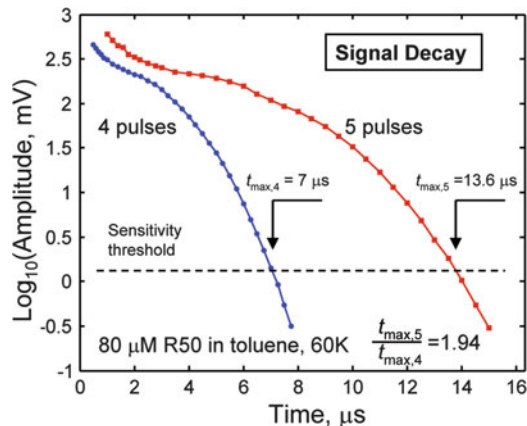


Fig. 20 A comparison of 4- and 5-pulse DEER amplitudes as a function of separation between the two π -pulses of the detection sequence. The 5-pulse DEER signal decays much slower, leading to nearly a factor of 2 increase of the time period, t_m , available for recording a dipolar signal. The data were recorded on $\sim 80 \mu\text{M}$ of biradical R50 (cf. Fig. 19) at 17.3 GHz and 60 K using the 5-pulse sequence of Fig. 18 and the standard 4-pulse DEER sequence. Since the signal at the sensitivity threshold is only ~ 0.003 of its value for $t_m < 1 \mu\text{s}$, the presence of slowly relaxing free spin label may offset the measurements, taken at large values of t_m [27]. Therefore, the control DEER experiment was conducted to test the DEER modulation depth, which was found to be the same as for short t_m values where such a contribution is negligible

at the signal level that corresponds to a SNR ~ 10 (in background-subtracted dipolar signal) after ~ 3 h of data averaging both for the standard 4-pulse DEER and DEER-5.

5.2 More on Sensitivity: Method Comparison

So far, the two distance measurement techniques of DEER and DQC detailed above have proven to be very successful. DEER in its 4-pulse form has received wide acceptance due to the availability of commercial spectrometers operating at X-band and permitting easier implementation with a single high-power mw amplifier. However, a Q-band extension has also become commercially available, and it provides significant sensitivity increase [146, 172] compared to the commercial X-band spectrometer.

DQC, for its optimal performance, requires more powerful mw amplifiers than those typically employed in X-band because at this frequency range optimal sample size for maximizing concentration sensitivity could be impractically large, that is ~ 1 – 2 ml. At a higher working frequency in Ku- or Ka-band a 1–2 kW amplifier is adequate and the optimal sample sizes can be small (10–80 μL). We employ at Ku-band a 4 kW amplifier for DQC. Ultra-fast MESFET (metal semiconductor field effect transistor) switches allow us to generate pulses as short as 0.8 ns and to achieve B_1 s of at least 45 G in a dielectric resonator. This corresponds to 4 ns π -pulses, producing strong signals.

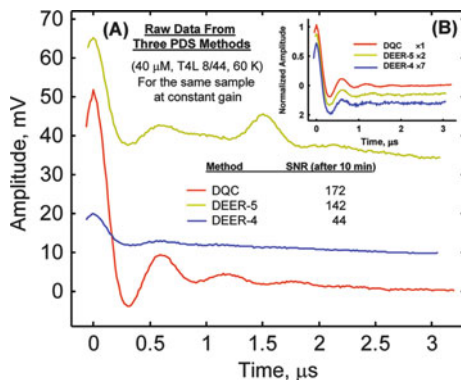


Fig. 21 (A) Raw data from 4-pulse DEER (*middle*), 6-pulse DQC (*bottom*), and 5-pulse DEER (*top*), taken on the same sample with the same receiver settings. The measurements were conducted on a 10 μL sample of 40 μM T4L MTSSL-labeled 8/44 cysteine mutant (31 \AA avg. distance). The sample was prepared in H_2O buffer containing $\sim 30\%$ (w/v) glycerol. Data were collected at 60 K using Ku-band (17.3 GHz). Both DEER sequences used a 29 ns main pump pulse, and the additional pump pulse in the 5-pulse sequence was 12 ns. DQC used 2 ns $\pi/2$ and 4 ns π pulses, corresponding to a B_1 of ~ 45 G. Signal averaging times were 40 min (4-pulse DEER), 50 min (DQC), and 10 min (5-pulse DEER). The DQC signal is about a factor of 7 greater than the dipolar signal (i.e., the modulated part) in 4-pulse DEER. The ratio of SNRs of DQC to 4-pulse DEER is a factor of ~ 4.0 due to a wider signal bandwidth used to record the DQC signal. Unprocessed DEER-5 contains an unwanted signal pathway (cf. previous section), (B) The same data are shown after removing baselines and unwanted signal in DEER-5. All data were normalized to unity at zero time and distributed vertically for clarity

In Fig. 21 we show a comparison of all three methods using the ACERT Ku band spectrometer, where we already have very high spin sensitivity illustrated for 4-pulse DEER in Fig. 17. At $t_m = 3 \mu\text{s}$, nuclear spin diffusion begins to be important and it dominates the phase relaxation for larger t_m . As one can see, S/N in 5-pulse DEER is already almost on a par with DQC and well above 4-pulse DEER. We cannot detect a useful signal beyond $\sim 5 \mu\text{s}$ with standard DEER and, for slightly longer t_m , by DQC. (DQC-RPE was not conducted, as it is better suited for longer distances, due to its dead-time) [58]. With the DQC method of PDS, we can achieve a wider distance range and better sensitivity than with 4-pulse DEER for many biological systems. Usually an order-of-magnitude improvement in data averaging time was achieved. However, measurement of long-distances still has limits imposed by the phase relaxation. When it is possible to select solvent-exposed labeling sites, nuclear spin diffusion becomes the dominant mechanism. This can be partly offset by using deuterated solvents, and in some cases (Fig. 7) distances as long as 80 \AA can be measured. 5-pulse DEER, that we described above, helps to extend this distance range and/or improve the quality of distance data by suppressing effects of nuclear spin diffusion. It allows a significant extension of the distance range without using deuteration. However, with solvent deuteration we often find substantial improvement [171]. Consequently, a time-consuming and often unfeasible measurement of a 80 \AA distance becomes a routine 1-h experiment.

DQC provides the best value in the low concentration range, for not very long distances (~ 50 Å) as a result of higher sensitivity, and the most accurate dipolar signals. For very long distances (≥ 60 Å) DEER-5 seems to surpass DQC (at present) but DQC should again provide the higher sensitivity by deuteration of the entire system including the biomolecules. In some cases, deuterated solvent will suffice. For example, for oligonucleotides with highly solvent-exposed spin-labels (cf. Fig. 7b), nuclear spin diffusion is not a dominant relaxation mechanism on the 15–20 μs time-scale used. This is not the case for spin labeled proteins tested in D_2O (T4L and α -Synuclein), where nuclear spin diffusion dominates after ~ 6 μs .

As is true for DQC, using 5-pulse DEER requires optimizing the spectrometer and resonators in order to maximize the suppression of the unwanted signal, but it is achieved with a smaller, and therefore less expensive and more reliable, high-power mw amplifier, since it uses pulses typical for standard implementation of DEER. Clearly, this pulse sequence adds capability to the two already proven techniques.

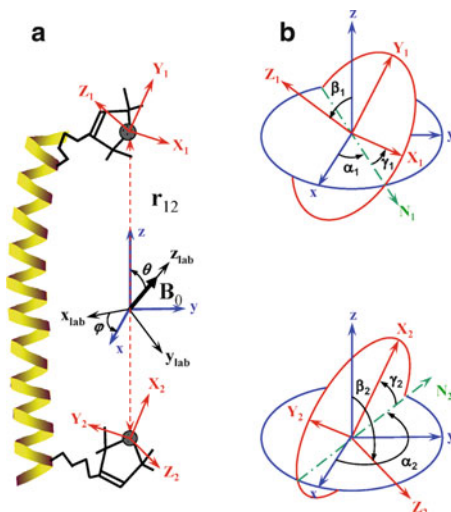
5.3 2D-DQC: Orientations

When a sample containing bilabeled proteins is subjected to sufficiently strong microwave pulses, the nitroxide ESR spectrum is almost uniformly excited, so that any dependence of the signal on spectral position (frequency) including orientational effects is largely suppressed. That is, the echo amplitude results from (nearly) all the spins (except for the effect of pseudosecular dipolar terms, important for short distances). Also, as we discussed in Sect. 2.3.5, in high B_1 -fields ($\gamma_e B_1 \geq \omega_d$), the effect of the dipolar coupling during the action of the pulses becomes very weak.

Therefore, for not very short distances and in sufficiently strong B_1 s, the information on orientations of the magnetic tensors of the spin-label moieties (cf. Fig. 22) is virtually excluded from the time-domain dipolar evolution of the echo amplitude, taken at its maximum. Nevertheless, as we showed [35, 93], it is still retained in the spin-echo signal and can be retrieved by recording the 2D time-domain data as a function of the spin-echo time (t_{echo}) in addition to the dipolar evolution time ($t_{\text{dip}} \equiv t_{\xi}$) and then converting this data into a 2D-FT spectrum. Then by making a “shearing” transformation [128] one achieves two orthogonal dimensions: the nitroxide spectral dimension and the dipolar dimension (i.e., the x and y axes in the “2D” plot). Rigorous computations of 1D and 2D signals have been carried out [93].

In the 2D-DQC experiment the pulse sequence of Fig. 4 is used and pulses are stepped out in the same manner as in 1D-DQC. However, the following is noted. The echo shape is recorded in a window $t_w \sim 80$ –160 ns, centered at a time $2t_m + 2t_{\text{DQ}}$ after the first pulse, i.e., at $t_6 (=t_m)$ after the sixth pulse. Note that the width of the echo sampling window limits the minimal values of t_6 and t_p by about $t_w/2$ and their maximum values to $(t_m - t_w)/2$. As in the 1D format the dipolar evolution is recorded as a symmetric signal with respect to $t_{\text{dip}} \equiv t_{\xi}$ but over the whole range of $\pm t_m$. In practice t_p starts with a larger t_{p0} , than in the 1D implementation, selected

Fig. 22 The set of Euler angles $\lambda_k = (\alpha_k, \beta_k, \gamma_k)$, ($k = 1, 2$), which define the orientations of the hf and g -tensor tensor principal axes for nitroxides 1 and 2 in the dipolar (molecular) frame of reference. In this frame the z -axis is chosen to coincide with the vector \mathbf{r} , connecting the magnetic dipoles of the nitroxides. The orientation of the dipolar frame in the laboratory frame (with z -axis parallel to the external magnetic field \mathbf{B}_0) is defined by the Euler angles $\eta = (0, \theta, \varphi)$. Adapted from [93]



such that the last pulse (including the dead-time after the pulse) and the echo window do not overlap.

Therefore, the signal in the 2D DQC experiment is recorded over $\pm (t_m - t_{p0})$ with t_{p0} always slightly greater than $t_w/2$. Figure 23 shows an example of a 2D DQC time-domain signal. Note the tilt of spin-echo which is due to the fact that a shift by Δt in the spin echo time t_{echo} corresponds to a shift by $\Delta t/2$ in the position of the dipolar coupling refocusing point. This coupling between t_{echo} and t_{dip} is removed at the signal processing stage by the shearing transformation conducted for convenience in the frequency domain as $f_{\text{echo}} \rightarrow f_{\text{echo}} + f_{\text{dip}} (\Delta t_{\text{echo}}/2\Delta t_{\text{dip}})$. This is easier to accomplish on the smoother 2D frequency spectrum with better S/N compared to the oscillatory signal in the time-domain. Also, the 2D signal background is first removed from the time-domain signal by fitting it to a surface, which is extrapolated to small t_{dip} , in a manner similar to 1D DQC before the Fourier Transform.

Figure 24 illustrates the main concept of 2D-FT-DQC. Results for uncorrelated (a) and correlated (b) ^{14}N nitroxide pairs with 2 MHz dipolar coupling (corresponding to ca. 30 Å) are shown in the upper row with a fixed rigid arrangement with $\lambda_{1,2} = (0^\circ, 90^\circ, 0^\circ), (0^\circ, 90^\circ, 0^\circ)$ (cf. Fig. 22 caption) shown in (b). The B_1 was made infinite by using $H_p \propto S_x$ and the pseudosecular term in H_{dd} was set to zero. The 2D FT spectrum may be summed over the range of ESR frequencies to produce a 1D dipolar spectrum (Pake doublet shown) on the right side of the 2D plot. When summed over the range of dipolar frequencies one produces a 1D ESR spectrum at the top of each 2D plot. Note that there is virtually no difference in the 1D dipolar spectra from uncorrelated and correlated cases, as one would expect for the strong pulses, which uniformly excite all orientations. However, this information, hidden in 1D, is developed in the 2D representation, wherein the uncorrelated

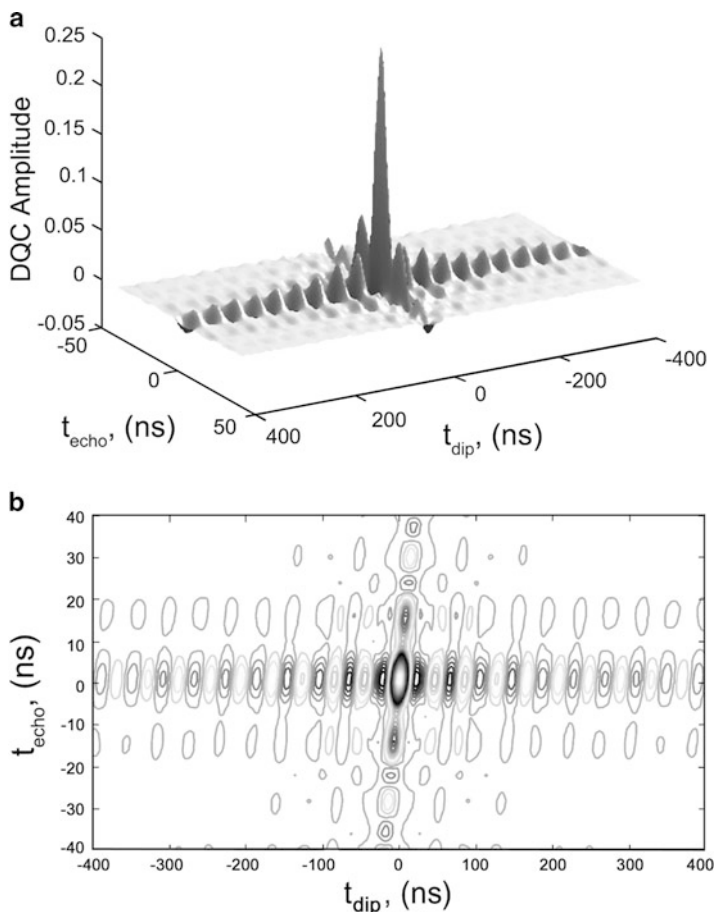


Fig. 23 Time-domain 2D DQC signal is shown as a 3D stack plot (a) and contour plot (b). The simulation was carried out rigorously for $B_0 = 6,200$ G, $B_1 = 60$ G, $\nu_d = 25$ MHz and uncorrelated ^{14}N nitroxides. The tilt of the spin-echo-refocusing line is clearly visible. The reason is due to the fact that the spin-echo envelope is recorded over the time period where only one point corresponds to the dipolar interaction refocusing. A shift by Δt in the spin echo time corresponds to a shift by $\Delta t/2$ in the position of the dipolar coupling refocusing point. (Adapted from [93].)

case shows no variation of the dipolar spectrum along the ESR dimension, whereas in the correlated case there is clearly a distinct pattern of such variations.

Figure 24c–d shows the correlated and the uncorrelated case for $\lambda_{1,2} = (0^\circ, 0^\circ, 0^\circ)$, $(0^\circ, 90^\circ, 0^\circ)$ and $\nu_d = 25$ MHz. The simulation corresponds to a realistic case of a large but finite B_1 of 60 G, which could be produced with our spectrometers if we use a somewhat smaller volume resonator. We observe only small features caused by the pseudosecular terms dipolar coupling. They become more pronounced in the case of stronger correlation effects, for example for β angles both either 0° or 90° . A small distribution in distances washes them out in 1D, leading to

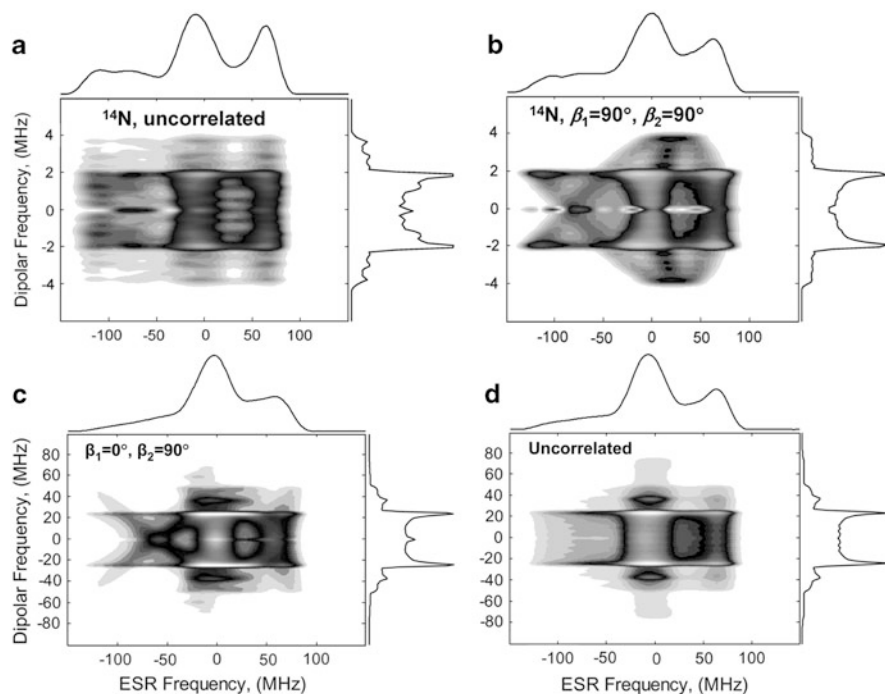


Fig. 24 2D DQC magnitude filled contour plots obtained by 2D FT with respect to t_{dip} and t_{echo} . The magnitude 2D signal is summed along both dimensions and is shown as the 1D ESR absorption spectrum (at the *top*) or Pake doublet (on the *rhs*). *Top row* – uncorrelated (**a**) and correlated (**b**) case. $B_0 = 6,200$ G, $\nu_d = 2$ MHz ($r = 29.6$ Å). B_1 was set to infinity (i.e., perfect delta-function pulses), pseudosecular terms were neglected. In (**b**) angles beta were $(90^\circ, 90^\circ)$ corresponding to strong correlations. The other Euler angles were set to zero. Note the similarity of the 1D dipolar spectra obtained by integration along the ESR frequency. They all are classic Pake doublets. But in the 2D representation the differences are striking. For the uncorrelated cases the dipolar spectrum is uniform for different slices along the ESR frequency axis, whereas for the correlated case they show a distinct “fingerprint” of this type of correlation. Since pseudosecular terms are neglected, the results are applicable to long distances, such as the present case. *Bottom row* – Examples of 2D FT magnitude contour plots for another case of orientational correlation: angles beta in (**c**) are $(0^\circ, 90^\circ)$. The other four Euler angles were set to zero. Case (**d**) is the uncorrelated case. Plots (**c**) and (**d**) are very similar in their 1D projection, but still distinct in 2D plots. In both cases $B_0 = 6,200$ G, $B_1 = 60$ G, $\nu_d = 25$ MHz (12.7 Å). (Adapted by combining two figures from [93].)

a broadened dipolar spectrum, which gives no clue that there are in fact strong correlations between nitroxide orientations. In the 2D map however this information is clearly seen [93].

Finally, we show an experimental example of 2D DQC conducted on 15 μM solution of rigid biradical [35] in *o*-terphenyl- d_{24} glass. Since B_1 of 45 G is insufficient to provide uniform spectral coverage of the whole nitroxide spectrum, two data collections were made using mw pulse sequences applied at the low-field and high-field part of the spectrum.

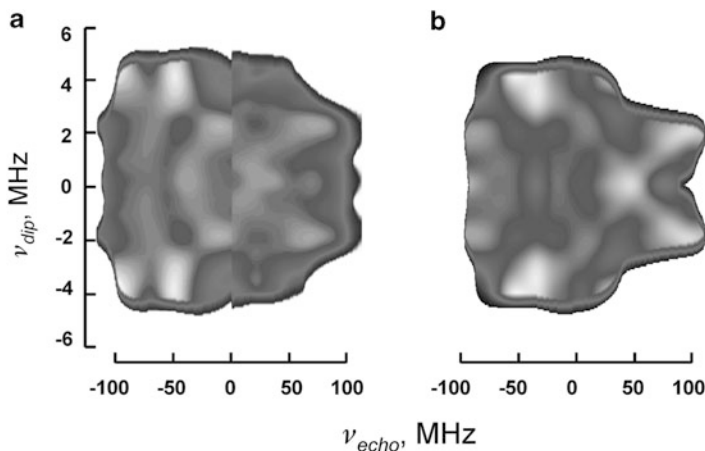


Fig. 25 Experimental (a) and calculated (b) correlation maps from 17.25 GHz 2D DQC data. 2D correlation map (a) is a composite plot made of two correlation plots obtained from 2D data acquired for mw pulses applied at -10 and 20 G field offsets from the center of the ^{14}N nitroxide ESR spectrum. The respective low- and high-field side of these two spectra was used to make a composite plot according to the following procedure. The time-domain signals were first 2D Fourier transformed in the manner used in Fig. 24. Then each resulting contour plot was normalized by dividing it by the 2D spectrum constructed as a product of two 1D spectra, taken as sums along spectral and dipolar frequencies, respectively, as shown in Fig. 24. The low-field and high-field parts of these contour plots were then combined into a single 2D plot (a), with the cut-out line set at the field offset of 15 G. The plot in (b) was computed using for adequate spectral coverage B_1 of 80 G, $r_{12} = 28.9$ Å, and the set of Euler angles $\lambda_1 = (0^\circ, 75^\circ, 0^\circ)$, $\lambda_2 = (90^\circ, 111^\circ, 0^\circ)$ from molecular modeling [35]. The following experimental conditions were used: Sample temperature was 60 K; $\pi/2$ and π pulse widths were 2 and 4 ns, corresponding to B_1 of 45 G. Pulse repetition frequency was 2 kHz; 2D data sets corresponded to ± 4 μs in t_{dip} and ± 100 ns in t_{echo} for total of 500×200 data points. Data collection time was 9.5 h for the -10 G offset and 19 h for the 20 G offset for very high SNR, although satisfactory data were obtained already in 2 and 4 h, respectively. A 64 -step phase cycle [35, 63] was used to get a clean DQC signal. There was no need to suppress ESEEM and a small baseline could simply be ignored for the 15 μM concentration used. (This lab, unpublished.)

For this linear biradical one expects nitroxide moieties to be oriented with their beta angles, $\beta_{1(2)}$ about 90° , the remaining angles are less important. Molecular modeling [35] yielded $r_{12} = 28.9$ Å for the distance measured between the points located at 0.75 of NO bond length to the nitrogens; and for the Euler angles the following values were obtained $\lambda_1 = (0^\circ, 75^\circ, 0^\circ)$, $\lambda_2 = (90^\circ, 111^\circ, 0^\circ)$. In Fig. 25 we compare correlation maps for experimental and calculated data. The maps are built as normalized contour plots. It is clear that the plots are similar, i.e., nitroxides' orientations are of the expected type, but there are some differences that could be addressed after developing a faster computational procedure than is currently available.

In summary, we note that acquiring orientational information necessitates recording several DEER traces [132] whereas 2D DQC can do it in a single pass, if mw pulses can excite the whole spectrum. The advantage of DEER is that it can

be applied to infer orientational information from very broad orientationally well-resolved spectra.

5.4 Multifrequency

High absolute spin sensitivity and potentially improved concentration sensitivity at a higher frequency strongly motivated the development of PDS ESR measurement technology in the mm-wave frequency range. In an important development at St Andrews University, a 1 kW mm-wave amplifier was employed at W-band, providing 12 ns π -pulses in a circular waveguide-based nonresonant induction probe that has a relatively high conversion factor ($\sim 0.6 \text{ G/W}^{1/2}$) [46], (even shorter π -pulse widths of ~ 10 ns were achieved at 95 GHz [47] at ACERT with the Fabry–Perot resonator setup developed for aqueous samples). It admits samples as large as at X-band, whereas the high conversion factor and frequency scaling of spin sensitivity as ω^2 (for constant sample volume [147]) have resulted in very high sensitivity comparable to that of our ACERT Ku-band spectrometer [46, 171].

Orientalional selectivity is another common argument in favor of the mm-wave range [21]. In the case of rigidly attached spin-labels, determining their orientation provides valuable structural information. The sensitivity to orientations increases at high fields, where the ESR spectrum of nitroxides is dominated by g -tensor anisotropy. In order to infer orientations, the DEER signal is recorded using several field positions of the pump and detection pulses [21, 173, 174]. A modification to the signal acquisition scheme was shown [173] that allowed simultaneous recording at several field points, thereby helping to shorten the duration of the experiment. Given sufficiently broad spectral excitation, 2D-DQC may provide significant improvement in this area, by recording the whole correlation map in a single pass or maybe by using just 2 or 3 field points (cf. Sect. 5.3). High power amplifiers available at W-band [46, 47] and resonators designed to maximize B_1 could make such a plan realistic. However, DQC is not yet an option for these spectrometers, but it seems it is just a matter of time. In Fig. 26 we show a simulated 2D DQC correlation spectrum at Ku- and W-band for ^{14}N nitroxides. The correlation map is richer in detail at W-band. The results for Ka band (35 GHz) look similar to Ku band but are not shown. The uncorrelated case for W-band (not shown) has a similar appearance to the Ku and Ka bands shown in Fig. 24a, d, indicating only the presence of spectral features aligned parallel to the v_{echo} spectral axis. In all cases, the high-field (low frequency) side of the 2D spectrum is more sensitive to orientations, as expected. Therefore, even with limited B_1 it could be possible to test orientations in this spectral region. At W-band the g_y part of the spectrum is also sensitive and exhibits the effects of pseudosecular terms, which in general are weaker at this frequency due to its wider spectral extent.

It thus seems to be useful to conduct PDS experiments in lower fields, where orientational correlation effects are weaker and more accurate distance reconstruction can be made. This distance information could be combined with orientation-dependent data from the high-field experiment to be used in structure modeling.

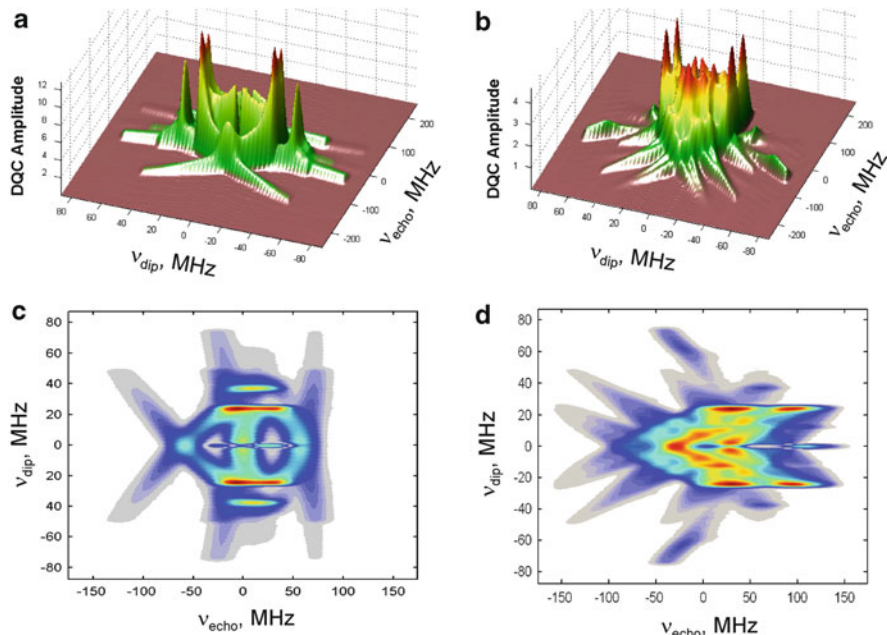


Fig. 26 Frequency dependence of 2D-DQC orientation correlation map. (a) 2D spectrum calculated for Ku band and (b) for W-band are shown as stack plots. (c, d) Filled contour plots representation of the above stack plots. The following simulation parameters were used: $B_1 = 60$ G, $v_d = 25$ MHz; magnetic tensor frame orientations, $\lambda_1 = (\alpha_1, \beta_1, \gamma_1)$, $\lambda_2 = (\alpha_2, \beta_2, \gamma_2)$ were taken as $(0^\circ, 0^\circ, 0^\circ)$ and $(90^\circ, 0^\circ, 0^\circ)$

While orientations can be difficult to infer for MTSSL, due to its very substantial side-chain flexibility usually exhibiting multiple rotamers, sometimes spin-labels can become occluded as is the case for MsbA when in the ADP-Vi trapped state the spin-label is buried inside the closed transporter [175]. Recent development of conformationally restricted nitroxide labels [133, 134] may be useful in this regard even for conventional working frequencies. Thus, nitroxides may ultimately fit well into such a multifrequency study. Of course, there are systems that are already orientationally well resolved in the centimeter frequency range but become too broad in W-band and higher, but they may benefit from the slightly higher frequency of Ku or Ka band. For example, DEER was successfully applied at X-band to determine orientational information in a Cu^{2+} - Cu^{2+} biradical and also to a protein-protein complex with NO^\bullet and a [2Fe-2S] cluster [87]. In contrast, the $\text{Gd}^{3+} -1/2 \leftrightarrow 1/2$ transition becomes very narrow in Ka band and above and carries no significant orientational dependence. These (and some other) properties allow one to use pairs of Gd^{3+} spin labels for distance measurements, free from orientational effects and with spin sensitivity comparable to that generally achieved with nitroxide labels, or else they can be used in combination with nitroxides to even higher sensitivity [121]. Nitroxide labels, however, have the relative advantage of being smaller and least perturbing. They are also easy to attach and use with a

variety of systems and sample types. Another issue with Gd^{3+} labels is that they currently require more expensive operation at 5–10 K and the modulation depth is typically small (ca. 0.01–0.05), thus considerably elevating technical requirements of the pulse spectrometer, which for example become very relaxed for DQC applied to nitroxides or Cu^{2+} . A benefit of Gd^{3+} labels is that their positions are better defined, potentially providing more useful constraints for structure modeling. It is believed [178] that ultimately a higher sensitivity may be achieved than is currently possible with nitroxides using typical X-band DEER spectrometers; naturally one could expect that 5-pulse DEER could benefit distance measurements based on Gadolinium labels, if the challenges with small modulation depth could be overcome. Thus, ongoing development of spectrometers operating at different frequencies, methods, spin-labels, and other aspects continues to make PDS an increasingly more powerful technique for studying biomolecular structure and function.

6 Summary and Perspectives

We have shown that there are currently two pulse ESR methods that are most beneficial for biological pulse dipolar spectroscopy. They are DQC and DEER (PELDOR). In dilute systems DQC is considerably more sensitive in most cases, *shortening the time of the experiment by at least an order of magnitude*. DQC is uniquely applicable to relatively narrow spectra such as nitroxides, which promise the greatest sensitivity improvement, but we also find it (at Ku-band) more sensitive for wide spectra such as for the Cu^{2+} – Cu^{2+} system (unpublished, ACERT), since the concentration sensitivity for this case scales as $(B_1)^\alpha$ with α ranging from 1 to 1.5 (cf. Sect. 4.1) [101]. Its double quantum coherence filter suppresses background signals. It has a broader distance range and is substantially free from orientational selection effects in its 1D mode, but reveals them in its 2D mode. DEER on the other hand is very useful for a wide range of systems and uniquely suitable for nonoverlapping spectra. For pairs of spins, it provides very good separation from relaxation effects and is less sensitive to ESEEM. It can be applied to more concentrated spin systems than DQC, thereby extending the concentration range. Also, since it is based on selective pulses and automatically references to the signal at zero time, it helps to study the presence of small spin clusters and in some cases provides an estimate for aggregation numbers.

These two methods actually are quite complex with respect to the underlying spin dynamics; but fortuitously they happen to exhibit minimal artifacts throughout the wide region of dipolar couplings for distances of about 15 Å and greater, so that the ideal kernel (cf. Sect. 2.6) can be used in many cases to reconstruct the distance distributions.

In DEER, unless the pulses are sufficiently selective and the dipolar coupling is small, a more complicated spin dynamics is observed than with the DQC technique. In the latter, pseudosecular terms in dipolar coupling do play a role, but are easy to account for. As we have shown, DQC is typically in the regime of weak coupling,

where its spin dynamics is quite simple. On the other hand in the case of strong correlation effects, a special 2D mode of DQC is a potent technique to yield a correlation map in a single experiment. Furthermore, at low concentrations, where DQC excels, the background is greatly suppressed, aiding its removal, and it can often be ignored altogether in 2D DQC.

Suffice it to say that in all cases, cultivating both DQC and DEER and selecting the most appropriate PDS pulse sequence for the system studied are good strategies.

We conclude that quite remarkable progress has been achieved in pulsed dipolar ESR spectroscopy. This includes continuing progress with instrumentation, pulse sequences, spin-labels, data processing with structure modeling, and system preparation protocols. We see that the number of potential biological applications is growing, and it may be only “the tip of the iceberg.”

For more rapidly relaxing spin-labels, such as nitroxides in hydrophobic environments of proteins and in lipid membranes, further spectrometer sensitivity improvement would be highly desirable, especially for proteins from higher organisms, which are difficult or impossible to deuterate. More water-exposed labels would benefit most from solvent deuteration and using new methods such as 5-pulse DEER.

At Ku-band (at ACERT) and higher working frequencies the sensitivity is currently at the low micromolar level of concentration for proteins and nucleotides. This was achieved without compromising the distance range and resolution. Distances can be measured at least to 90 Å, which helps to characterize large objects such as protein complexes and RNA. We anticipate that progress in method development and sensitivity improvement will continue.

Acknowledgments The authors acknowledge Elka R. Georgieva for her help with model systems and figures. This work was supported by NIH grants NIH/NIGMS P41GM103521 and NIH/NCRR P41RR016292.

Appendix

Signals in 3,4,5-Pulse DEER Sequences

Here, we derive the expression given by Eq. (40) for PELDOR/DEER (cf. Fig. 5a), using the spin Hamiltonian given by Eqs. (13) and (14) (which neglects pseudosecular terms), in the absence of pulses. We express H_0 in the frame of reference doubly rotating with frequencies ω_1 and ω_2 of mw pulses applied, respectively, to spins A and B, having their Larmor frequencies at Ω_a and Ω_b (cf. Slichter, p. 279, and assumptions therein [95]). Note that Eqs. (13) and (14) use spins 1 and 2, but for DEER pulse sequences we number spins by the subscripts a and b . In this frame of reference H_0 becomes

$$H_0 = \omega_a S_{az} + \omega_b S_{bz} + a S_{az} S_{bz} \quad (63)$$

In Eq. (63) a is as in Eq. (14), ω_a and ω_b are the Larmor frequency offsets from ω_1 and ω_2 respectively. We further assume the following set of inequalities $a \ll \gamma_e \mathcal{B}_{1a(b)} \ll |\omega_1 - \omega_2|$. The first inequality allows us to neglect the dipolar coupling during the pulse, the second ensures that there may be only a small overlap of pulse excitations at the two frequencies, but we will retain related terms that may be produced in the course of calculations of the signal. (The first inequality, as related to A-spins, makes it easier for one to consider pseudosecular terms in conducting a more detailed analysis). Note that for a pair of spins, depending on angle θ , one of or both spins may contribute to the echo. We can assume that the first spin is always an A spin, but the second spin can be either A or B spin. To simplify this matter, we use when needed the subscripts numbering spins as 1 or 2.

The amplitude $V(t)$ of the echo signal that we are interested in computing is given by the trace, $\text{Tr}(S_{a+\rho(t)})/\text{Tr}(S_{a+}S_{a-})$, where $\rho(t)$ is the density matrix measured at time t after the first pulse in the sequence. Therefore in the end we retain in ρ only the terms in S_{a-} . We will follow the evolution of single-quantum in-phase coherences of spin 1, $S_{1a\pm}$ created by the first $\pi/2$ pulse. They evolve due to the dipolar coupling $aS_{1z}S_{2z}$ into anti-phase coherences $S_{1a\pm}S_{2z}$ and vice versa; the process thus interconverts these coherences leading to their modulation by the dipolar frequency $a/2$ as described in Sect. 2.3.1. These coherences under the action of pulses and free evolution periods will turn out as detectable S_{a-} carrying this dipolar modulation.

The pulse sequences for 3-pulse PELDOR and 4-pulse DEER can be expressed in arrow representation respectively as:

$$\begin{aligned} & P_{1a}(\pi/2) \xrightarrow{H_0(t_1-t)} P_{2b}(\pi) \xrightarrow{H_0(t)} P_{3a}(\pi) \xrightarrow{H_0(t_1+t_e)} \text{echo} \\ & P_{1a}(\pi/2) \xrightarrow{H_0(t_1)} P_{2a}(\pi) \xrightarrow{H_0(t)} P_{3b}(\pi) \xrightarrow{H_0(t_2-t)} P_{4a}(\pi) \xrightarrow{H_0(t_2-t_1+t_e)} \text{echo}, \end{aligned} \quad (64)$$

where $H_0(t)$ denotes free evolution for the duration of t due to H_0 and $P_{ka(b)}$ is the pulse propagator for k th pulse applied nominally at the frequency ω_a or ω_b . The primary echo produced by pulses 1 and 3 in 3-pulse PELDOR corresponds to a coherence pathway, $\mathbf{p} = (+1, -1)$. In 4-pulse DEER based on the refocused echo created by pulses 1, 2, and 4 coherences pass through a $\mathbf{p} = (-1, +1, -1)$ pathway. We describe the action of π -pulses by introducing probability p_{ka} or p_{kb} for the spin at ω_a or ω_b , respectively, to be flipped by the k th pulse. (We may drop the subscript a (or b), when unimportant.) The probability not to be flipped, q_{kc} , is then $1 - p_{kc}$ (where c is a or b). We denote the amount of $S_{1a\pm}$ produced by the first $\pi/2$ pulse as h_{1a} . Note that q , p , and h correspond to standard amplitude factors for the action of selective pulses, for example, as defined in the literature [35]. For a spin at a resonant frequency offset ω from the frequency of the RF pulse, the probabilities p and q to be flipped or not flipped by the pulse with nominal flip angle β is given by

$$p = \sin^2(\beta u/2)/u^2, \quad q = 1 - p \quad (65)$$

Here, $u^2 = 1 + \omega^2/\omega_{\text{mw}}^2$ and $\omega_{\text{mw}} = \gamma_e \mathcal{B}_1$.

To manage free evolution, we introduce operators $H_z \equiv \omega_a S_{1z}$ and $\Omega_{12} \equiv a S_{1z} S_{2z}$. Then the free evolution propagator is $\exp[-i(H_z + \Omega_{12})]$. Note that H_z and Ω_{12} commute and we can consider them separately and write for the free evolution of shift operators $S_{1a\pm}$ due to H_z or Ω_{12} the following:

$$\begin{aligned} S_{1a\pm} &\xrightarrow{H_z t} S_{1a\pm} e^{\mp i \omega_a t} \\ S_{1a\pm} &\xrightarrow{\Omega_{12} t} S_{1a\pm} (\cos(at/2) \mp 2i S_{2z} \sin(at/2)) \equiv S_{1a\pm} D_{\pm t} \end{aligned} \quad (66)$$

We numbered the spins in Eq. (66). Note that S_z may correspond to spin 2 at ω_a or ω_b , since pseudosecular terms are neglected and the evolution due to weak dipolar coupling is then given by Eq. (15). Since first-order coherences of A-spins pass through the prescribed pathway and all pulses applied during the evolution are nominally π -pulses, we need to consider only the following actions of the pulses:

$$\begin{aligned} S_{1a\pm} &\xrightarrow{P_{kb}} q_{kb} S_{1a\pm}, & S_{1a\pm} &\xrightarrow{P_{ka}} p_{ka} S_{1a\mp} \\ S_{2z} &\xrightarrow{P_{kc}} (q_{kc} - p_{kc}) S_{2z} \end{aligned} \quad (67)$$

Here, P_k represents the action of pulse k and subscript a or b is added to indicate at what frequency the pulse is applied. Other spin manipulations lead to pathways that do not contribute to the echo of interest. In the following, we drop the subscripts numbering spins. Since pulse excitations at the two frequencies have only small overlap, Eq. (67) is good approximation. We will disregard unessential phase shifts [98] introduced into $S_{a\pm}$ by the pulses applied at ω_b . From Eqs. (66) and (67) we find that D_t has the following properties:

$$D_t \xrightarrow{H_{kc}} q_{kc} D_t + p_{kc} D_t^*, \quad D_t^* = D_{-t}, \quad D_{t_1+t_2} = D_{t_1} D_{t_2} \quad (68)$$

We first compute the final density operator ρ_f for 3-pulse PELDOR by tracking the coherence pathway that lead to S_{a-} . We thus start from S_{a+} produced by the first $\pi/2$ pulse. Equations 67 and 68 reduce our task to merely writing all ensuing ‘‘dipolar trajectories’’. By repeatedly applying Eqs. (67) and (68) to S_{a+} , the following sequence of transformations defines the detectable density matrix element in PELDOR:

$$\begin{aligned} \rho_0 &= S_{az} \xrightarrow{P_{1a}} h_{1a} S_{a+} \xrightarrow{H_0(t)} h_{1a} S_{a+} D_t e^{-i \omega_a t} \\ &\xrightarrow{P_{2b}} h_{1a} q_{2a} S_{a+} (q_2 D_t + p_2 D_{-t}) e^{-i \omega_a t} \xrightarrow{H_0(\tau-t)} h_{1a} q_{2a} S_{a+} (q_2 D_\tau + p_2 D_{\tau-2t}) e^{-i \omega_a \tau} \\ &\xrightarrow{P_{3a}} S_{a-} h_{1a} q_{2a} p_{3a} (q_2 q_3 D_\tau + q_2 p_3 D_{-\tau} + p_2 q_3 D_{\tau-2t} + p_2 p_3 D_{2t-\tau}) e^{-i \omega_a \tau} \\ &\xrightarrow{H_0(\tau+\delta t_c)} S_{a-} h_{1a} q_{2a} p_{3a} (q_2 q_3 D_0 + q_2 p_3 D_{-2\tau} + p_2 q_3 D_{-2t} + p_2 p_3 D_{2t-2\tau}) e^{i \omega_a \delta t_c} \end{aligned} \quad (69)$$

Table 1 t -Dependent dipolar pathways in four-pulse sequence

k	B_k	Standard asymmetric 4-pulse DEER ($t_1 \ll t_2$) t_k	“Symmetric” form 4-pulse DEER ($t_2 = 2t_1 \equiv 2\tau$) t_k	Different definition of time variable, t_k ($t \rightarrow t_1 + t$) t_k
(1)	$q_4 p_3 q_2$	$t - t_1$	$t - \tau$	t
(2)	$q_4 p_3 p_2$	t	t	$t + t_1$
(3)	$p_4 p_3 p_2$	$t + t_1 - t_2$	$\tau - t$	$2t_1 + t - t_2$
(4)	$p_4 p_3 q_2$	$t - t_2$	$2\tau - t$	$t + t_1 - t_2$

Coefficients p_k and q_k inside the brackets refer to spin 2, which may be at ω_b or ω_a . The spin echo amplitude, V at time $2\tau + \delta t_e$ is then taken as the trace: $Tr(S_{a+} S_{a-}(2\tau + \delta t_e)) / Tr(S_{a+} S_{a-})$. For simplicity, we neglect dipolar evolution during δt_e and after retaining detectable in-phase coherences by substituting D_{2t} with their real parts, $\cos(at)$, we arrive at the expression for the echo signal

$$V(\tau, t, \delta t_e) = \langle h_{1a} q_{2a} p_{3a} [q_2 q_3 + q_2 p_3 \cos(a\tau) + p_2 q_3 \cos(at) + p_2 p_3 \cos(a(t - \tau))] e^{i\omega_a \delta t_e} \rangle_{a,b} \quad (70)$$

The term in $\exp(i\omega_a \delta t_e)$ together with all other frequency-dependent factors (p, q, h) after averaging over $\omega_{a,b}$ produces the spin echo shape, $V(\delta t_e)$ so that Eq. (70) becomes equivalent to Eq. (40). The dipolar modulation in Eq. (70) is represented by the two terms: $\sim q_3 [1 - p_2 (1 - \cos(at))]$ and $\sim p_3 p_2 \cos(a(t - \tau))$. The first term is the well-known formula for the PELDOR/DEER signal [30, 73]. The second “back-in-time” signal is relatively small if $\langle p_3 p_2 \rangle_{a,b} \ll \langle p_2 \rangle_{a,b}$. Usually, this is the case for DEER (but in the single-frequency DEER analog, “2 + 1,” both signals are comparable [38]). In Eq. (70), there are two more terms that are constant in t : one, which is time independent, corresponds to unaffected spin B; whereas another term in $\cos(a\tau)$ corresponds to the dipolar signal between A spins in the limit of very small a (when pseudosecular term can be neglected). To fully account for their effects more detailed calculations have to be carried out, for example ones based on a modified product operator method as described by Borbat and Freed [35]. Then Eq. (70) becomes at first somewhat unwieldy (e.g., such as an approximate expression given by Raitsimring [106]), but it will simplify practically to Eq. (70) when the “+1” pumping pulse has only a small overlap with the rest of the pulses.

Derivation of the expression analogues to Eq. (70), but for 4-pulse DEER adds one more step to Eq. (69) doubling the number of terms in dipolar signals to a total of eight,

$$V(t) \propto B_a \sum_{k=1}^8 B_{bk} \cos(at_k) \quad (71)$$

where $B_a = h_{1a}p_{2a}q_{3a}p_{4a}$. Only four terms in Eq. (71) have a dependence on the position t of the pump pulse. Table 1 compiles B_{bk} and respective time variables, t_k defined in different ways for these terms.

The dipolar pathways in the 5-pulse DEER sequence were studied in [171] by employing a similar approach. We can describe them qualitatively using the data from Table 1. Signal (1) is the standard 4-pulse DEER signal whereas signals 2–4 are relatively weak. In the 5-pulse DEER sequence, (2) or (4) are no longer weak, since the extra pulse 5 following pulse 4 makes p_4 greater than p_3 , thereby suppressing (1) and developing the 5-pulse dipolar signal (2). Alternatively, the extra pulse may have position $5'$ right before pulse 2 and develops (4) due to increased p_2 and suppresses (1).

References

1. Borbat PP, Mchaourab HS, Freed JH (2002) Protein structure determination using long-distance constraints from double-quantum coherence ESR: study of T4-lysozyme. *J Am Chem Soc* 124(19):5304–5314
2. Jeschke G, Wegener C, Nietschke M, Jung H, Steinhoff H-J (2004) Interresidual distance determination by four-pulse double electron–electron resonance in an integral membrane protein: the Na⁺/proline transporter PutP of *Escherichia coli*. *Biophys J* 86(4):2551–2557
3. Zhou Z, DeSensi SC, Stein RA, Brandon S, Dixit M, McArdle EJ, Warren EM, Kroh HK, Song L, Cobb CE, Hustedt EJ, Beth AH (2005) Solution structure of the cytoplasmic domain of erythrocyte membrane band 3 determined by site-directed spin labeling. *Biochemistry* 44(46):15115–15128
4. McNulty JC, Silapie JL, Carnevali M, Farrar CT, Griffin RG, Formaggio F, Crisma M, Toniolo C, Millhauser GL (2001) Electron spin resonance of TOAC labeled peptides: folding transitions and high frequency spectroscopy. *Biopolymers* 55(6):479–485
5. Park S-Y, Borbat PP, Gonzalez-Bonet G, Bhatnagar J, Pollard AM, Freed JH, Bilwes AM, Crane BR (2006) Reconstruction of the chemotaxis receptor-kinase assembly. *Nat Struct Mol Biol* 13(5):400–407
6. Hilger D, Jung H, Padan E, Wegener C, Vogel K-P, Steinhoff H-J, Jeschke G (2005) Assessing oligomerization of membrane proteins by four-pulse DEER: pH-dependent dimerization of NhaA Na⁺/H⁺ antiporter of *E. coli*. *Biophys J* 89(2):1328–1338
7. Milov AD, Erilov DA, Salnikov ES, Tsvetkov YD, Formaggio F, Toniolo C, Raap J (2005) Structure and spatial distribution of the spin-labelled lipopeptide trichogin GA IV in a phospholipid membrane studied by pulsed electron–electron double resonance (PELDOR). *Phys Chem Chem Phys* 7(8):1794–1799
8. Hubbell WL, Cafiso DS, Altenbach CA (2000) Identifying conformational changes with site-directed spin labeling. *Nat Struct Biol* 7(9):735–739
9. Hustedt EJ, Smirnov AI, Laub CF, Cobb CE, Beth AH (1997) Molecular distances from dipolar coupled spin-labels: the global analysis of multifrequency continuous wave electron paramagnetic resonance data. *Biophys J* 72(4):1861–1877
10. Bennati M, Robblee JH, Mugnaini V, Stubbe J, Freed JH, Borbat PP (2005) EPR distance measurements support a model for long-range radical initiation in *E. coli* ribonucleotide reductase. *J Am Chem Soc* 127(43):15014–15015
11. Fafarman AT, Borbat PP, Freed JH, Kirshenbaum K (2007) Characterizing the structure and dynamics of folded oligomers: pulsed ESR studies of peptoid helices. *Chem Commun* (4):377–379

12. Borbat PP, Ramlall TF, Freed JH, Eliezer D (2006) Inter-helix distances in lysophospholipid micelle-bound α -synuclein from pulsed ESR measurements. *J Am Chem Soc* 128 (31):10004–10005
13. Dzikovski BG, Borbat PP, Freed JH (2004) Spin-labeled gramicidin a: channel formation and dissociation. *Biophys J* 87(5):3504–3517
14. Banham JE, Timmel CR, Abbott RJM, Lea SM, Jeschke G (2006) The characterization of weak protein-protein interactions: evidence from DEER for the trimerization of a von willebrand factor A domain in solution. *Angew Chem Int Ed* 45(7):1058–1061
15. Borbat PP, Freed JH (1999) Multiple-quantum ESR and distance measurements. *Chem Phys Lett* 313(1,2):145–154
16. Borbat PP, da Costa-Filho AJ, Earle KA, Moscicki JK, Freed JH (2001) Electron spin resonance in studies of membranes and proteins. *Science* 291(5502):266–269
17. Freed JH (2000) New technologies in electron spin resonance. *Annu Rev Phys Chem* 51:655–689
18. Fanucci GE, Cafiso DS (2006) Recent advances and applications of site-directed spin labeling. *Curr Opin Struct Biol* 16(5):644–653
19. Columbus L, Hubbell WL (2002) A new spin on protein dynamics. *Trends Biochem Sci* 27(6):288–295
20. Milov AD, Tsvetkov YD, Formaggio F, Crisma M, Toniolo C, Raap J (2003) Self-assembling and membrane modifying properties of a lipopeptaibol studied by CW-ESR and PELDOR spectroscopies. *J Pept Sci* 9(11–12):690–700
21. Denysenkov VP, Prisner TF, Stubbe J, Bennati M (2006) High-field pulsed electron–electron double resonance spectroscopy to determine the orientation of the tyrosyl radicals in ribonucleotide reductase. *Proc Natl Acad Sci USA* 103(36):13386–13390
22. Becker JS, Saxena S (2005) Double quantum coherence electron spin resonance on coupled Cu(II)–Cu(II) electron spins. *Chem Phys Lett* 414(1–3):248–252
23. Biglino D, Schmidt PP, Reijerse EJ, Lubitz W (2006) PELDOR study on the tyrosyl radicals in the R2 protein of mouse ribonucleotide reductase. *Chemphyschem* 8(1):58–62
24. Narr E, Godt A, Jeschke G (2002) Selective measurements of a nitroxide-nitroxide separation of 5 nm and a nitroxide-copper separation of 2.5 nm in a terpyridine-based copper(II) complex by pulse EPR spectroscopy. *Angew Chem Int Ed* 41(20):3907–3910
25. Codd R, Astashkin AV, Pacheco A, Raitsimring AM, Enemark JH (2002) Pulsed ELDOR spectroscopy of the Mo(V)/Fe(III) state of sulfite oxidase prepared by one-electron reduction with Ti(III) citrate. *J Biol Inorg Chem* 7(3):338–350
26. Elsaesser C, Brecht M, Bittl R (2002) Pulsed electron–electron double resonance on multi-nuclear metal clusters: assignment of spin projection factors based on the dipolar interaction. *J Am Chem Soc* 124(42):12606–12611
27. Upadhyay AK, Borbat PP, Wang J, Freed JH, Edmondson DE (2008) Determination of the oligomeric states of human and rat monoamine oxidases in the outer mitochondrial membrane and octyl beta-D-glucopyranoside micelles using pulsed dipolar electron spin resonance spectroscopy. *Biochemistry* 47(6):1554–1566
28. Astashkin AV, Kodera Y, Kawamori A (1994) Distance between tyrosines Z⁺ and D⁺ in plant photosystem II as determined by pulsed EPR. *Biochim Biophys Acta* 1187(1):89–93
29. Milov AD, Salikhov KM, Shirov MD (1981) Application of the double resonance method to electron spin echo in a study of the spatial distribution of paramagnetic centers in solids. *Soviet Phys-Solid State* 23:565–569
30. Milov AD, Maryasov AG, Tsvetkov YD (1998) Pulsed electron double resonance (PELDOR) and its applications in free-radicals research. *Appl Magn Reson* 15(1):107–143
31. Martin RE, Pannier M, Diederich F, Gramlich V, Hubrich M, Spiess HW (1998) Determination of end-to-end distances in a series of TEMPO diradicals with a new four-pulse double electron electron resonance experiment. *Angew Chem Int Ed* 37(20):2834–2837
32. Larsen RG, Singel DJ (1993) Double electron–electron resonance spin-echo modulation: spectroscopic measurement of electron spin pair separations in orientationally disordered solids. *J Chem Phys* 98(7):5134–5146

33. Raitsimring AM, Salikhov KM (1985) Electron spin echo method as used to analyze the spatial distribution of paramagnetic centers. *Bull Magn Reson* 7(4):184–217
34. Salikhov KM, Dzyuba SA, Raitsimring A (1981) The theory of electron spin-echo signal decay resulting from dipole-dipole interactions between paramagnetic centers in solids. *J Magn Reson* 42(2):255–276
35. Borbat PP, Freed JH (2000) Distance measurements in biological systems by EPR. In: Berliner LJ, Eaton GR, Eaton SS (eds) *Biological magnetic resonance*, vol 19. Academic/Plenum, New York, pp 385–459
36. Jeschke G, Pannier M, Godt A, Spiess HW (2000) Dipolar spectroscopy and spin alignment in electron paramagnetic resonance. *Chem Phys Lett* 331(2,3,4):243–252
37. Kulik LV, Dzyuba SA, Grigoryev IA, Tsvetkov YD (2001) Electron dipole-dipole interaction in ESEEM of nitroxide biradicals. *Chem Phys Lett* 343(3,4):315–324
38. Kurshev VV, Raitsimring AM, Tsvetkov YD (1989) Selection of dipolar interaction by the “2 +1” pulse train ESE (1969–1992). *J Magn Reson* 81(3):441–454
39. Schiemann O, Piton N, Mu Y, Stock G, Engels JW, Prisner TF (2004) A PELDOR-based nanometer distance ruler for oligonucleotides. *J Am Chem Soc* 126(18):5722–5729
40. Steinhoff H-J (2004) Inter- and intra-molecular distances determined by EPR spectroscopy and site-directed spin labeling reveal protein-protein and protein-oligonucleotide interaction. *Biol Chem* 385(10):913–920
41. Fajer PG (2005) Site directed spin labelling and pulsed dipolar electron paramagnetic resonance (double electron–electron resonance) of force activation in muscle. *J Phys Condens Matter* 17(18):S1459–S1469
42. Cai Q, Kusnetzow AK, Hubbell WL, Haworth IS, Gacho GPC, Van Eps N, Hideg K, Chambers EJ, Qin PZ (2006) Site-directed spin labeling measurements of nanometer distances in nucleic acids using a sequence-independent nitroxide probe. *Nucleic Acids Res* 34(17):4722–4730
43. Freed JH (1967) Theory of saturation and double resonance effects in electron spin resonance spectra. 2. Exchange vs dipolar mechanisms. *J Phys Chem* 71(1):38–51
44. Freed JH (1966) Theory of spin relaxation via quantum-molecular systems – resonance effects. *J Chem Phys* 45(4):1251–1257
45. Freed JH (1965) Theory of saturation and double-resonance effects in ESR spectra. *J Chem Phys* 43(7):2312–2332
46. Cruickshank PAS, Bolton DR, Robertson DA, Hunter RI, Wylde RJ, Smith GM (2009) A kilowatt pulsed 94 GHz electron paramagnetic resonance spectrometer with high concentration sensitivity, high instantaneous bandwidth, and low dead time. *Rev Sci Instrum* 80(10):103102–103115
47. Hofbauer W, Earle KA, Dunnam CR, Moscicki JK, Freed JH (2004) High-power 95 GHz pulsed electron spin resonance spectrometer. *Rev Sci Instrum* 75(5):1194–1208
48. Denysenkov VP, Prisner TF, Stubbe J, Bennati M (2005) High-frequency 180 GHz PELDOR. *Appl Magn Reson* 29(2):375–384
49. Goldfarb D, Lipkin Y, Potapov A, Gorodetsky Y, Epel B, Raitsimring AM, Radoul M, Kaminker I (2008) HYSCORE and DEER with an upgraded 95 GHz pulse EPR spectrometer. *J Magn Reson* 194(1):8–15
50. Astashkin AV, Enemark JH, Raitsimring A (2006) 26.5–40 GHz K-a-band pulsed EPR spectrometer. *Concepts Magn Reson Part B* 29(3):125–136
51. Forrer J, Garcia-Rubio I, Schuhmam R, Tschaggelar R, Harmer J (2008) Cryogenic Q-band (35 GHz) probehead featuring large excitation microwave fields for pulse and continuous wave electron paramagnetic resonance spectroscopy: performance and applications. *J Magn Reson* 190(2):280–291
52. Gromov I, Forrer J, Schweiger A (2006) Probehead operating at 35 GHz for continuous wave and pulse electron paramagnetic resonance applications. *Rev Sci Instrum* 77(6), Article Number: 064704

53. Simovic B, Studerus P, Gustavsson S, Leturcq R, Ensslin K, Schuhmann R, Forrer J, Schweiger A (2006) Design of Q-band loop-gap resonators at frequencies of 34–36 GHz for single electron spin spectroscopy in semiconductor nanostructures. *Rev Sci Instrum* 77(6), Article Number: 064702
54. Tschaggelar R, Kasumaj B, Santangelo MG, Forrer J, Leger P, Dube H, Diederich F, Harmer J, Schuhmann R, Garcia-Rubio I, Jeschke G (2009) Cryogenic 35 GHz pulse ENDOR probehead accommodating large sample sizes: performance and applications. *J Magn Reson* 200(1):81–87
55. Mett RR, Sidabras JW, Golovina IS, Hyde JS (2008) Dielectric microwave resonators in TE (011) cavities for electron paramagnetic resonance spectroscopy. *Rev Sci Instrum* 79(9), Article Number: 094702
56. Mett RR, Sidabras JW, Hyde JS (2007) Uniform radio frequency fields in loop-gap resonators for EPR spectroscopy. *Appl Magn Reson* 31(3–4):573–589
57. Tkach I, Sicoli G, Hobartner C, Bennati M (2011) A dual-mode microwave resonator for double electron–electron spin resonance spectroscopy at W-band microwave frequencies. *J Magn Reson* 209(2):341–346
58. Borbat PP, Davis JH, Butcher SE, Freed JH (2004) Measurement of large distances in biomolecules using double-quantum filtered refocused electron spin-echoes. *J Am Chem Soc* 126(25):7746–7747
59. Jeschke G, Bender A, Paulsen H, Zimmermann H, Godt A (2004) Sensitivity enhancement in pulse EPR distance measurements. *J Magn Reson* 169(1):1–12
60. Milikisyants S, Groenen EJJ, Huber M (2008) Observer-selective double electron–electron-spin resonance, a pulse sequence to improve orientation selection. *J Magn Reson* 192(2): 275–279
61. Milikisyants S, Scarpelli F, Finiguerra MG, Ubbink M, Huber M (2009) A pulsed EPR method to determine distances between paramagnetic centers with strong spectral anisotropy and radicals: the dead-time free RIDME sequence. *J Magn Reson* 201(1):48–56
62. Hirst SJ, Alexander N, Mchaourab HS, Meiler J (2011) RosettaEPR: an integrated tool for protein structure determination from sparse EPR data. *J Struct Biol* 173(3):506–514
63. Gaffney BJ, Bradshaw MD, Frausto SD, Wu F, Freed JH, Borbat P (2012) Locating a Lipid at the Portal to the Lipoxygenase Active Site. *Biophys J* 103(10):2134–2144
64. Bhatnagar J, Freed JH, Crane BR (2007) Rigid body refinement of protein complexes with long-range distance restraints from pulsed dipolar ESR. Two-component signaling systems. *Methods Enzymol B* 423:117–133
65. Bhatnagar J, Borbat PP, Pollard AM, Bilwes AM, Freed JH, Crane BR (2010) Structure of the ternary complex formed by a chemotaxis receptor signaling domain, the CheA histidine kinase, and the coupling protein CheW As determined by pulsed dipolar ESR spectroscopy. *Biochemistry* 49(18):3824–3841
66. Jeschke G, Chechik V, Ionita P, Godt A, Zimmermann H, Banham J, Timmel CR, Hilger D, Jung H (2006) DeerAnalysis2006 – a comprehensive software package for analyzing pulsed ELDOR data. *Appl Magn Reson* 30(3–4):473–498
67. Jeschke G, Panek G, Godt A, Bender A, Paulsen H (2004) Data analysis procedures for pulse ELDOR measurements of broad distance distributions. *Appl Magn Reson* 26(1–2):223–244
68. Polyhach Y, Bordignon E, Jeschke G (2011) Rotamer libraries of spin labelled cysteines for protein studies. *Phys Chem Chem Phys* 13(6):2356–2366
69. Chiang Y-W, Borbat PP, Freed JH (2005) Maximum entropy: a complement to Tikhonov regularization for determination of pair distance distributions by pulsed ESR. *J Magn Reson* 177(2):184–196
70. Chiang Y-W, Borbat PP, Freed JH (2005) The determination of pair distance distributions by pulsed ESR using Tikhonov regularization. *J Magn Reson* 172(2):279–295
71. Kim S, Brandon S, Zhou Z, Cobb CE, Edwards SJ, Moth CW, Parry CS, Smith JA, Lybrand TP, Hustedt EJ, Beth AH (2011) Determination of structural models of the complex between the

- cytoplasmic domain of erythrocyte band 3 and ankyrin-R repeats 13–24. *J Biol Chem* 286 (23):20746–20757
72. Berliner LJ, Eaton GR, Eaton SS (2000) Distance measurements in biological systems by EPR, vol 19, Biological magnetic resonance. Kluwer, New York
 73. Jeschke G (2002) Distance measurements in the nanometer range by pulse EPR. *Chemphyschem* 3(11):927–932
 74. Dzuba SA (2005) Pulsed EPR structural studies in the nanometer range of distances. *Russian Chem Rev* 74(7):619–637
 75. Prisner T, Rohrer M, MacMillan F (2001) Pulsed EPR spectroscopy: biological applications. *Annu Rev Phys Chem* 52:279–313
 76. Borbat PP, Freed JH (2000) In: Berliner LJ, Eaton GR, Eaton SS (eds) Biological magnetic resonance. New York, Kluwer Academic
 77. Abragam A (1961) The principles of nuclear magnetism, vol 386. Clarendon, Oxford, pp 442–451
 78. Jeschke G, Spiess HW (2006) Distance measurements in solid-state NMR and EPR spectroscopy. In: Dolinsek J, Vilfan M, Zumer S (eds) Novel NMR and EPR techniques. Springer, Berlin, pp 21–63
 79. Pake GE (1948) Nuclear resonance absorption in hydrated crystals: fine structure of the proton line. *J Chem Phys* 16:327–336
 80. Rabenstein MD, Shin Y-K (1995) Determination of the distance between two spin labels attached to a macromolecule. *Proc Natl Acad Sci USA* 92(18):8239–8243
 81. Hu KN, Song C, Yu HH, Swager TM, Griffin RG (2008) High-frequency dynamic nuclear polarization using biradicals: a multifrequency EPR lineshape analysis. *J Chem Phys* 128(5), Article Number: 052302
 82. Persson M, Harbridge JR, Hammarstrom P, Mitri R, Martensson L-G, Carlsson U, Eaton GR, Eaton SS (2001) Comparison of electron paramagnetic resonance methods to determine distances between spin labels on human carbonic anhydrase II. *Biophys J* 80(6):2886–2897
 83. Koteiche HA, Mchaourab HS (1999) Folding pattern of the α -crystallin domain in α A-crystallin determined by site-directed spin labeling. *J Mol Biol* 294(2):561–577
 84. Hanson P, Anderson DJ, Martinez G, Millhauser G, Formaggio F, Crisma M, Toniolo C, Vita C (1998) Electron spin resonance and structural analysis of water soluble, alanine-rich peptides incorporating TOAC. *Mol Phys* 95(5):957–966
 85. Xiao W, Poirier MA, Bennett MK, Shin Y-K (2001) The neuronal t-SNARE complex is a parallel four-helix bundle. *Nat Struct Biol* 8(4):308–311
 86. Banham JE, Baker CM, Ceola S, Day IJ, Grant GH, Groenen EJJ, Rodgers CT, Jeschke G, Timmel CR (2008) Distance measurements in the borderline region of applicability of CW EPR and DEER: a model study on a homologous series of spin-labelled peptides. *J Magn Reson* 191(2):202–218
 87. Lovett JE, Bowen AM, Timmel CR, Jones MW, Dilworth JR, Caprotti D, Bell SG, Wong LL, Harmer J (2009) Structural information from orientationally selective DEER spectroscopy. *Phys Chem Chem Phys* 11(31):6840–6848
 88. Hahn EL (1950) Spin echoes. *Phys Rev* 80(4):580–594
 89. Mims WB (1972) Envelope modulation in spin-echo experiments. *Phys Rev B-Solid State* 5(7):2409–2419
 90. Mims WB, Peisach J (1978) Nuclear modulation effect in electron-spin echoes for complexes of Cu²⁺ and imidazole with N-14 and N-15. *J Chem Phys* 69(11):4921–4930
 91. Schweiger A, Jeschke G (2001) Principles of pulse electron paramagnetic resonance. Oxford University Press, Oxford
 92. Dikanov SA, Tsvetkov YD (1992) Electron spin echo envelope modulation (ESEEM) spectroscopy. CRC Press, Boca Raton
 93. Misra SK, Borbat PP, Freed JH (2009) Calculation of double-quantum-coherence two-dimensional spectra: distance measurements and orientational correlations. *Appl Magn Reson* 36(2–4):237–258

94. Ernst RR, Bodenhausen G, Wokaun A (1987) Principles of nuclear magnetic resonance in one and two dimensions. The international series of monographs on chemistry. Clarendon, Oxford
95. Slichter CP (1990) Principles of magnetic resonance, 3rd edn. Springer, Berlin
96. Cavanagh J, Fairbrother WJ, Palmer AG III, Skelton NJ (1996) Protein NMR spectroscopy: principles and practice. Protein NMR spectroscopy: principles and practice. Academic, San Diego
97. Corio PL (1966) Structure of high-resolution NMR spectra. Academic, New York
98. Bowman MK, Maryasov AG (2007) Dynamic phase shifts in nanoscale distance measurements by double electron electron resonance (DEER). *J Magn Reson* 185 (2):270–282
99. Sorensen OW, Eich GW, Levitt MH, Bodenhausen G, Ernst RR (1983) Product operator-formalism for the description of NMR pulse experiments. *Prog Nucl Magn Reson Spectrosc* 16:163–192
100. Saxena S, Freed JH (1996) Double quantum two-dimensional Fourier transform electron spin resonance: distance measurements. *Chem Phys Lett* 251(1):102–110
101. Borbat PP, Freed JH (2007) Pro's and con's of pulse dipolar ESR: DQC and DEER. *EPR Newslett* 17(2–3):21–33
102. Saxena S, Freed JH (1997) Theory of double quantum two-dimensional electron spin resonance with application to distance measurements. *J Chem Phys* 107(5):1317–1340
103. Libertini LJ, Griffith OH (1970) Orientation dependence of electron spin resonance spectrum of di tert butyl nitroxide. *J Chem Phys* 53(4):1359–1367
104. Maryasov AG, Tsvetkov YD (2000) Formation of the pulsed electron–electron double resonance signal in the case of a finite amplitude of microwave fields. *Appl Magn Reson* 18(4):583–605
105. Milov AD, Ponomarev AB, Tsvetkov YD (1984) Electron–electron double resonance in electron spin echo: model biradical systems and the sensitized photolysis of decalin. *Chem Phys Lett* 110(1):67–72
106. Raitsimring A (2000) Distance measurements in biological systems by EPR. In: Berliner LJ, Eaton GR, Eaton SS (eds) Biological magnetic resonance, vol 19. Kluwer, New York, pp 385–459
107. Pannier M, Veit S, Godt A, Jeschke G, Spiess HW (2000) Dead-time free measurement of dipole-dipole interactions between electron spins. *J Magn Reson* 142(2):331–340
108. Weber A, Schiemann O, Bode B, Prisner TF (2002) PELDOR at S- and X-band frequencies and the separation of exchange coupling from dipolar coupling. *J Magn Reson* 157(2):277–285
109. Milov AD, Tsvetkov YD (1997) Double electron–electron resonance in electron spin echo. Conformations of spin-labeled poly-4-vinylpyridine in glassy solutions. *Appl Magn Reson* 12(4):495–504
110. Milov AD, Salikhov KM, Tsvetkov YD (1973) Phase relaxation of hydrogen atoms stabilized in an amorphous matrix. *Soviet Phys-Solid State* 15:802–806
111. Raitsimring AM, Salikhov KM, Umanskii BA, Tsvetkov YD (1974) Instantaneous diffusion in the electron spin echo of paramagnetic centers stabilized in solid matrixes. *Fizika Tverdogo Tela (Sankt-Peterburg)* 16(3):756–766
112. Lindgren M, Eaton GR, Eaton SS, Jonsson B-H, Hammarstrom P, Svensson M, Carlsson U (1997) Electron spin echo decay as a probe of aminoxyl environment in spin-labeled mutants of human carbonic anhydrase II. *J Chem Soc Perkin Trans* 2(12):2549–2554
113. Zecevic A, Eaton GR, Eaton SS, Lindgren M (1998) Dephasing of electron spin echoes for nitroxyl radicals in glassy solvents by non-methyl and methyl protons. *Mol Phys* 95 (6):1255–1263
114. Huber M, Lindgren M, Hammarstrom P, Martensson L-G, Carlsson U, Eaton GR, Eaton SS (2001) Phase memory relaxation times of spin labels in human carbonic anhydrase II: pulsed EPR to determine spin label location. *Biophys Chem* 94(3):245–256

115. Bartucci R, Erilov DA, Guzzi R, Sportelli L, Dzuba SA, Marsh D (2006) Time-resolved electron spin resonance studies of spin-labelled lipids in membranes. *Chem Phys Lipids* 141 (1–2):142–157
116. Georgieva ER, Ramlall TF, Borbat PP, Freed JH, Eliezer D (2010) The lipid-binding domain of wild type and mutant alpha-synuclein: compactness and interconversion between the broken and extended helix forms. *J Biol Chem* 285(36):28261–28274
117. Nevzorov AA, Freed JH (2001) A many-body analysis of the effects of the matrix protons and their diffusional motion on electron spin resonance line shapes and electron spin echoes. *J Chem Phys* 115(6):2416–2429
118. Georgieva ER, Ramlall TF, Borbat PP, Freed JH, Eliezer D (2008) Membrane-bound alpha-synuclein forms an extended helix: long-distance pulsed ESR measurements using vesicles, bicelles, and rodlike micelles. *J Am Chem Soc* 130(39):12856–12857
119. Ward R, Bowman A, Sozudogru E, El-Mkami H, Owen-Hughes T, Norman DG (2010) EPR distance measurements in deuterated proteins. *J Magn Reson* 207(1):164–167
120. Carr HY, Purcell EM (1954) Effects of diffusion on free precession in nuclear magnetic resonance experiments. *Phys Rev* 94(3):630–638
121. Lueders P, Jeschke G, Yulikov M (2011) Double electron–electron resonance measured between Gd(3+) ions and nitroxide radicals. *J Phys Chem Lett* 2(6):604–609
122. Borbat PP, Freed JH (2007) Measuring distances by pulsed dipolar ESR spectroscopy: spin-labeled histidine kinases. In: Simon MI, Crane BR, Crane A (eds) Two-component signaling systems, Pt B, vol. 423. *Methods in enzymology*. Elsevier, San Diego, pp 52–116
123. Venters RA, Farmer BT II, Fierke CA, Spicer LD (1996) Characterizing the use of perdeuteration in NMR studies of large proteins: ¹³C, ¹⁵N and ¹H assignments of human carbonic anhydrase II. *J Mol Biol* 264(5):1101–1116
124. Horst R, Bertelsen EB, Fiaux J, Wider G, Horwich AL, Wuthrich K (2005) Direct NMR observation of a substrate protein bound to the chaperonin GroEL. *Proc Natl Acad Sci USA* 102(36):12748–12753
125. Hamel DJ, Dahlquist FW (2005) The contact interface of a 120 kD CheA–CheW complex by methyl TROSY interaction spectroscopy. *J Am Chem Soc* 127(27):9676–9677
126. Jeschke G, Koch A, Jonas U, Godt A (2002) Direct conversion of EPR dipolar time evolution data to distance distributions. *J Magn Reson* 155(1):72–82
127. Bowman MK, Maryasov AG, Kim N, DeRose VJ (2004) Visualization of distance distribution from pulsed double electron–electron resonance data. *Appl Magn Reson* 26(1–2):23–39
128. Lee S, Budil DE, Freed JH (1994) Theory of two-dimensional Fourier transform electron spin resonance for ordered and viscous fluids. *J Chem Phys* 101(7):5529–5558
129. Bhatnagar J, Sircar R, Borbat PP, Freed JH, Crane BR (2012) Self-association of the histidine kinase CheA as studied by pulsed dipolar ESR spectroscopy. *Biophys J* 102(9):2192–2201
130. Marko A, Margraf D, Cekan P, Sigurdsson ST, Schiemann O, Prisner TF (2010) Analytical method to determine the orientation of rigid spin labels in DNA. *Phys Rev E* 81(2), Article Number: 021911
131. Schiemann O, Cekan P, Margraf D, Prisner TF, Sigurdsson ST (2009) Relative orientation of rigid nitroxides by PELDOR: beyond distance measurements in nucleic acids. *Angew Chem Int Ed* 48(18):3292–3295
132. Endeward B, Butterwick JA, MacKinnon R, Prisner TF (2009) Pulsed electron–electron double-resonance determination of spin-label distances and orientations on the tetrameric potassium ion channel KcsA. *J Am Chem Soc* 131(42):15246–15250
133. Fawzi NL, Fleissner MR, Anthis NJ, Kalai T, Hideg K, Hubbell WL, Clore GM (2011) A rigid disulfide-linked nitroxide side chain simplifies the quantitative analysis of PRE data. *J Biomol NMR* 51(1–2):105–114
134. Fleissner MR, Bridges MD, Brooks EK, Cascio D, Kalai T, Hideg K, Hubbell WL (2011) Structure and dynamics of a conformationally constrained nitroxide side chain and applications in EPR spectroscopy. *Proc Natl Acad Sci USA* 108(39):16241–16246

135. Ruthstein S, Potapov A, Raitsimring AM, Goldfarb D (2005) Double electron electron resonance as a method for characterization of micelles. *J Phys Chem B* 109(48):22843–22851
136. Bode BE, Margraf D, Plackmeyer J, Durner G, Prisner TF, Schiemann O (2007) Counting the monomers in nanometer-sized oligomers by pulsed electron – electron double resonance. *J Am Chem Soc* 129(21):6736–6745
137. Jeschke G, Sajid M, Schulte M, Godt A (2009) Three-spin correlations in double electron–electron resonance. *Phys Chem Chem Phys* 11(31):6580–6591
138. Nevzorov AA, Freed JH (2001) Direct-product formalism for calculating magnetic resonance signals in many-body systems of interacting spins. *J Chem Phys* 115(6):2401–2415
139. Jeschke G, Polyhach Y (2007) Distance measurements on spin-labelled biomacromolecules by pulsed electron paramagnetic resonance. *Phys Chem Chem Phys* 9(16):1895–1910
140. Chandrasekhar S (1943) Stochastic problems in physics and astronomy. *Rev Mod Phys* 15(1):1–89
141. Milov AD, Tsvetkov YD (2000) Charge effect on relative distance distribution of Frey’s radical ions in frozen glassy solution studied by PELDOR. *Appl Magn Reson* 18(2):217–226
142. Georgieva ER, Roy AS, Grigoryants VM, Borbat PP, Earle KA, Scholes CP, Freed JH (2012) Effect of freezing conditions on distances and their distributions derived from double electron electron resonance (DEER): a study of doubly-spin-labeled T4 lysozyme. *J Magn Reson* 216:69–77
143. Klauder JR, Anderson PW (1962) Spectral diffusion decay in spin resonance experiments. *Phys Rev* 125:912–932
144. Dzikovski BG, Borbat PP, Freed JH (2011) Channel and nonchannel forms of spin-labeled gramicidin in membranes and their equilibria. *J Phys Chem B* 115(1):176–185
145. Milov AD, Maryasov AG, Tsvetkov YD, Raap J (1999) Pulsed ELDOR in spin-labeled polypeptides. *Chem Phys Lett* 303(1, 2):135–143
146. Zou P, Mchaourab HS (2010) Increased sensitivity and extended range of distance measurements in spin-labeled membrane proteins: Q-band double electron–electron resonance and nanoscale bilayers. *Biophys J* 98(6):L18–L20
147. Borbat PP, Crepeau RH, Freed JH (1997) Multifrequency two-dimensional Fourier transform ESR: an X/Ku-band spectrometer. *J Magn Reson* 127(2):155–167
148. Gorcester J, Freed JH (1986) Two-dimensional Fourier transform ESR spectroscopy. *J Chem Phys* 85(9):5375–5377
149. Fauth JM, Schweiger A, Braunschweiler L, Forrer J, Ernst RR (1986) Elimination of unwanted echoes and reduction of dead time in 3-pulse electron spin-echo spectroscopy. *J Magn Reson* 66(1):74–85
150. Hoult DI, Richards RE (1975) Critical factors in design of sensitive high-resolution nuclear magnetic-resonance spectrometers. *Proc R Soc Lond Ser A-Math Phys Eng Sci* 344 (1638):311–340
151. Yang ZY, Liu YP, Borbat P, Zweier JL, Freed JH, Hubbell WL (2012) Pulsed ESR dipolar spectroscopy for distance measurements in immobilized spin labeled proteins in liquid solution. *J Am Chem Soc* 134(24):9950–9952
152. Crepeau RH, Dulcic A, Gorcester J, Saarinen TR, Freed JH (1989) Composite pulses in time-domain ESR. *J Magn Reson* 84(1):184–190
153. Levitt MH (1982) Symmetrical composite pulse sequences for NMR population-inversion 1. Compensation of radiofrequency field inhomogeneity. *J Magn Reson* 48(2):234–264
154. Levitt MH (1986) Composite pulses. *Prog Nucl Magn Reson Spectrosc* 18:61–122
155. Levitt MH, Freeman R (1979) NMR population-inversion using a composite pulse. *J Magn Reson* 33(2):473–476
156. Shaka AJ, Pines A (1987) Symmetrical phase-alternating composite pulses. *J Magn Reson* 71 (3):495–503
157. Zax DB, Goelman G, Vega S (1988) Amplitude-modulated composite pulses. *J Magn Reson* 80(2):375–382

158. Zax DB, Vega S (1989) Broad-band excitation pulses of arbitrary flip angle. *Phys Rev Lett* 62(16):1840–1843
159. Baum J, Tycko R, Pines A (1985) Broad-band and adiabatic inversion of a 2-level system by phase-modulated pulses. *Phys Rev A* 32(6):3435–3447
160. Geen H, Freeman R (1991) Band-selective radiofrequency pulses. *J Magn Reson* 93(1):93–141
161. Murdoch JB, Lent AH, Kritzer MR (1987) Computer-optimized narrow-band pulses for multislice imaging. *J Magn Reson* 74(2):226–263
162. Silver MS, Joseph RI, Hoult DI (1985) Selective spin inversion in nuclear magnetic-resonance and coherent optics through an exact solution of the Bloch-Riccati equation. *Phys Rev A* 31(4):2753–2755
163. Warren WS (1984) Effects of arbitrary laser or NMR pulse shapes on population-inversion and coherence. *J Chem Phys* 81(12):5437–5448
164. Salikhov KM, Schneider DJ, Saxena S, Freed JH (1996) A theoretical approach to the analysis of arbitrary pulses in magnetic resonance. *Chem Phys Lett* 262(1, 2):17–26
165. Suzuki M (1985) Decomposition formulas of exponential operators and lie exponentials with some applications to quantum mechanics and statistical physics. *J Math Phys* 26:601–612
166. Trotter HF (1959) On the product of semi-groups of operators. *Proc Am Math Soc* 10(4):545–551
167. Devasahayam N, Murugesan R, Matsumoto K, Mitchell JB, Cook JA, Subramanian S, Krishna MC (2004) Tailored sinc pulses for uniform excitation and artifact-free radio frequency time-domain EPR imaging. *J Magn Reson* 168(1):110–117
168. Rinard GA, Quine RW, Song R, Eaton GR, Eaton SS (1999) Absolute EPR spin echo and noise intensities. *J Magn Reson* 140(1):69–83
169. Mims WB (1965) Electron echo methods in spin resonance spectrometry. *Rev Sci Instrum* 36(10):1472–1479
170. Hara H, Tenno T, Shirakawa M (2007) Distance determination in human ubiquitin by pulsed double electron–electron resonance and double quantum coherence ESR methods. *J Magn Reson* 184(1):78–84
171. Borbat PP, Georgieva ER, Freed JH (2012) Improved sensitivity for long-distance measurements in biomolecules: five-pulse double electron-electron resonance. *J Phys Chem Lett*. doi: [10.1021/jz301788n](https://doi.org/10.1021/jz301788n)
172. Ghimire H, McCarrick RM, Budil DE, Lorigan GA (2009) Significantly improved sensitivity of Q-band PELDOR/DEER experiments relative to X-band is observed in measuring the intercoil distance of a leucine zipper motif peptide (GCN4-LZ). *Biochemistry* 48(25):5782–5784
173. Kaminker I, Florent M, Epel B, Goldfarb D (2011) Simultaneous acquisition of pulse EPR orientation selective spectra. *J Magn Reson* 208(1):95–102
174. Reginsson GW, Hunter RI, Cruickshank PAS, Bolton DR, Sigurdsson ST, Smith GM, Schiemann O (2012) W-band PELDOR with 1 kW microwave power: molecular geometry, flexibility and exchange coupling. *J Magn Reson* 216:175–182
175. Borbat PP, Surendhran K, Bortolus M, Zou P, Freed JH, Mchaourab HS (2007) Conformational motion of the ABC transporter MsbA induced by ATP hydrolysis. *PLoS Biol* 5(10):2211–2219
176. Yagi H, Banerjee D, Graham B, Huber T, Goldfarb D, Otting G (2011) Gadolinium tagging for high-precision measurements of 6 nm distances in protein assemblies by EPR. *J Am Chem Soc* 133(27):10418–10421
177. Potapov A, Song Y, Meade TJ, Goldfarb D, Astashkin AV, Raitsimring A (2010) Distance measurements in model bis-Gd(III) complexes with flexible “bridge”. Emulation of biological molecules having flexible structure with Gd(III) labels attached. *J Magn Reson* 205(1):38–49
178. Song Y, Meade TJ, Astashkin AV, Klein EL, Enemark JH, Raitsimring A (2011) Pulsed dipolar spectroscopy distance measurements in biomacromolecules labeled with Gd(III) markers. *J Magn Reson* 210(1):59–68